Final Technical Report

External Grant Award Number:
G11AP20022

Recipient:
Optim SDS

Principal Investigators:
Aasha Pancha
Optim SDS, 200 South Virginia Street, Suite 560, Reno, NV, 89501
Telephone (775) 236-5869 Fax:(775) 324-5662 aashap@optimsds.com
Satish Pullammanappallil
Optim SDS, 200 South Virginia Street, Suite 560, Reno, NV, 89501
Telephone.: (775) 236-5891 Fax:(775) 324-5662 satish@optimsoftware.com
John N. Louie
University of Nevada Seismological Laboratory, Reno, NV 89557
Telephone: (775) 784-4219 Fax: (775) 784-4165 louie@seismo.unr.edu

Title:
Assessment of site conditions and empirical site response at stations recording near-field extreme ground motions during the 2008 Mogul, Nevada earthquake swarm

NEHRP Elements(s)
Element I: National and regional earthquake hazards assessments
Element III: Research on earthquake occurrence, physics, and effects
Keywords: Site effects, Basin effects, Ground motions, Seismic Zonation, Engineering seismology

Start date: January 2011
End Date: December 2011

Research supported by the U.S. Geological Survey (USGS), Department of the Interior, under USGS award number **G11AP20022**. The views and conclusions contained in this document are those of the authors and should not be interpreted as necessarily representing the official policies, either expressed or implied, of the U.S. Government.

External Grant Award Number **G11AP20022**

Assessment of site conditions and empirical site response at stations recording near-field extreme ground motions during the 2008 Mogul, Nevada earthquake swarm

Aasha Pancha
Optim SDS, 200 South Virginia Street, Suite 560, Reno, NV, 89501
Telephone (775) 236-5869 Fax:(775) 324-5662 aashap@optimsds.com
Satish Pullammanappallil
Optim SDS, 200 South Virginia Street, Suite 560, Reno, NV, 89501
Telephone.: (775) 236-5891 Fax:(775) 324-5662 satish@optimsoftware.com

John N. Louie
University of Nevada Seismological Laboratory, Reno, NV 89557
Telephone: (775) 784-4219 Fax: (775) 784-4165 louie@seismo.unr.edu

ABSTRACT

Vs30 and 2D shear-velocity sections together with 2D P-wave refraction tomography are obtained at twelve seismic stations in the near-source region of the 26th April 2008 Mw 5.0 Mogul, Nevada earthquake. These S-wave and P-wave velocity sections show complex site conditions beneath these stations. These results assessing the site conditions at these near-filed sites will contribute towards quantification of local site response and understanding the high peak ground motions recorded during this mainshock event.

We also empirically evaluate spectral amplification, relative to a rock site, at each of the ANSS strong motion stations within the basin containing the urban areas of Reno and Sparks, Nevada using ground motions from foreshocks and aftershocks of the 2008 Mogul earthquake. All of the site response functions are amplified relative to the rock site. Many are relatively flat, but some sites show strong amplification peaks. Comparison with response spectra calculated at these sites using regional events show strong similarity. These empirically derived site effects are compared with average shallow-shear wave velocities to 30 m and 100 m depth (Vs30 and Vs100) beneath the ANSS sites. Statistical analysis show amplification tends to be smaller as Vs30 and Vs100 increase, showing a dependence of ground motion on site conditions.

External Grant Award Number **G11AP20022**

Assessment of site conditions and empirical site response at stations recording near-field extreme ground motions during the 2008 Mogul, Nevada earthquake swarm

Aasha Pancha
Optim SDS, 200 South Virginia Street, Suite 560, Reno, NV, 89501
Telephone (775) 236-5869 Fax:(775) 324-5662 aashap@optimsds.com
Satish Pullammanappallil
Optim SDS, 200 South Virginia Street, Suite 560, Reno, NV, 89501
Telephone.: (775) 236-5891 Fax:(775) 324-5662 satish@optimsoftware.com

John N. Louie
University of Nevada Seismological Laboratory, Reno, NV 89557
Telephone: (775) 784-4219 Fax: (775) 784-4165 louie@seismo.unr.edu

NEHRP Elements(s)
Element I: National and regional earthquake hazards assessments
Element III: Research on earthquake occurrence, physics, and effects
Keywords: Site effects, Basin effects, Ground motions, Seismic zonation, Engineering seismology

Introduction

Objectives:

This project will obtain Vs30 and 2D shear-velocity sections together with 2D P-wave refraction tomography at twelve seismic stations in the near-source region of the 26th April 2008 Mw 5.0 Mogul, Nevada earthquake (Figure 1). These shallow shear-wave velocities will be combined with those already obtained at the Advanced National Seismic System (ANSS) stations within the Reno area. We propose to use these site measurements to empirically derive relations between spectral response and Vs30 for ground motions from the Mogul swarm. This project will contribute toward the reduction of earthquake losses in the US by providing a thorough characterization of the near-surface conditions of sites at which earthquake shaking has been measured. The results of this project will allow a more knowledgeable assessment of the role that near-surface shear velocities play in amplifying ground motions.

Background:

The 26 April 2008 Mw 5.0 Mogul, Nevada earthquake, located at a shallow depth of 3.1 km, was the largest event during a shallow earthquake swarm that began in February 2008 and persisted for several months (Smith *et al.*, 2008; Anderson, 2009). The largest peak acceleration vector during this mainshock event was recorded at station MOGL (1.19g; 1164 cm/s2), which is among the 25 largest recorded earthquake accelerations worldwide (Anderson, 2010). Strong ground motions observed at the four closest stations installed at the time of the mainshock event,

exceed accelerations of 300 cm/s^2 and velocities of 14 cm/s. Comparison of ground motions during the event with recently developed ground motion prediction equations as part of the Next Generation Attenuation project is presented by Anderson *et al*. (2009) using an assumed Vs30 of 400m/s. This comparison showed that peak accelerations at the four closest stations are much higher than median predictions, while peak accelerations at the distant ANSS stations located in the Reno area basin are greatly over-predicted.

A further eight temporary deployment stations were installed after the 26 April 2008 event, around the aftershock region. These 12 stations (Figure 1), combined with the existing ANSS stations in the Reno area recorded nearly 300 M>2 earthquakes, capturing previously un-recorded ground motions within the aftershock region and the Reno-area basin.

Site conditions using the ReMi technique have previously been evaluated at the twenty-one ANSS strong motion stations within the basin containing the urban areas of Reno and Sparks, Nevada (Pancha *et al*., 2007). The fault-controlled basin is about 13 km wide and 21 km long, and at most 1.1 km deep (Abbott and Louie, 2000). The small basin size and the growing accelerograph network within it makes this basin a very attractive location for improving modeling techniques to explain the relationship between basin structure, near-surface geology, and ground motions. This project will expand efforts toward these goals. Our efforts in this project will allow detailed site characterization at seismic recording stations close to the rupture area of the Mogul mainshock event and swarm region. In "**Part One**" of this project we measure shallow velocities at the 12 recording stations in the near-field region. The shear-velocity profile to 100 m depth is determined along with 2D structural representation of the shear-wave velocities and 2D P-wave refraction tomography beneath each site. These 2D representations of the velocity profile will enhance the understanding of site conditions at each of these recording stations. In "**Part Two**" of the project empirical site amplification are determined, using the ground motions from the Mogul earthquakes recorded at the ANSS stations within the Reno Area Basin. These empirical site effects will then be compared to average shallow shear-wave velocities to ascertain any dependence of ground motion on site conditions. Although influenced by near-source and path effects, we also look at empirical site response at the Mogul recording stations.

PART ONE: Characterization of Site Conditions

We assessed shallow site conditions at the twelve sites of near-source ground motions from the 2008 Mogul, Nevada, earthquake swarm. The locations of these twelve sites are shown in Figure 1.

Figure 1a. Google map showing the location of the ANSS sites (blue) at which site conditions and empirical site response has previously been characterized (Pancha *et al*., 2007). Also shown are the twelve temporary stations (yellow) deployed to record the Mogul swarm events, with the 26th April 2008 Mw 5.0 mainshock epicenter labeled as a red pushpin. At the time of the event WYRD was no longer operational.

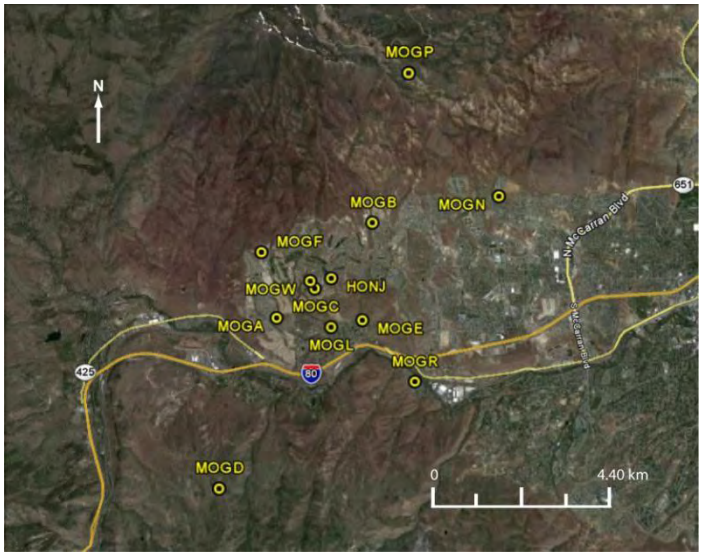

Figure 1b. Google map showing the location of the seismic stations deployed during the Mogul earthquake swarm.

Both shear-wave and P-wave geophysical techniques are used to characterize and map lateral velocity heterogeneity near each of these sites. Twenty-four cabled seismograph recorders attached to vertical-component 4.5 Hz geophones were planted along each array with 8m spacing between each instrument. The arrays were within 100 m of the recording stations. An example of field deployment of these arrays is given in Figure 2 for the seismic station MOGR. Both passive microtremor and active hammer sources were recorded by these arrays. Hammer shot records off each end of the arrays as well as along the array line were recorded for both the microtremor and refraction tomography analyses. Shot locations and line geometry were determined using high precision GPS acquisition equipment. These seismic recordings were then used to obtain shallow shear-wave and P-wave estimates beneath each site. This was achieved using the refraction microtremor (ReMi) technology Louie (2001) (owned by the State of Nevada and commercially available as SeisOpt®ReMiTM, ©Optim 2001-2008) and standard P-wave refraction tomography respectively.

Figure 2: Refraction geophones (red sensors in picture) placed along the sidewalk near station MOGR to record ambient noise generated by traffic, people walking or any other energy generated by active, as well as passive hammer sources.

The ReMi analysis provides a 1D velocity-depth sounding from which average shear-wave values to specified depths can be computed. The vertically averaged 30-meter shear velocity (Vs30) is used to define a "NEHRP" soil hazard classification for earthquake shaking as outlined by the NEHRP-UBC provisions (BSSC, 1998), and is thus adopted here to characterize average site conditions. Refraction microtremor is a volume-averaging surface-wave measurement, averaging velocities where geology is laterally variable, thus differing from the single-point data obtained from downhole logs. In this method, microtremor noise from sources such as traffic on streets and freeways excites Rayleigh waves, which are recorded by a linear array of vertical geophones. The Rayleigh waves contained in the recorded microtremors (ambient noise) are separated from other wave arrivals using a two dimensional slowness–frequency (p–f) transform of the noise records. The fundamental-mode phase-velocity Rayleigh wave dispersion curve is picked along the minimum velocity of the energy envelope within the slowness–frequency spectral image. The spectrum is normalized as the ratio of the power spectrum at a particular frequency and slowness (inverse velocity) over the average value for all slowness values at that frequency. Modeling of the dispersion curve produces a depth–velocity sounding that can be vertically averaged to the single Vs30 value used by the NEHRP-UBC code. Validation of the ReMi technique through comparison with shear wave measurements from boreholes and multichannel analysis of surface waves (MASW) is discussed by Louie (2001), Thelen *et al*. (2006), and Stephenson *et al.* (2005). To depths of up to 100 m, average uncertainties from these comparisons are at most ±20%. The depth-velocity sounding can be evaluated in other ways such as the computation of the average velocity to 100 meters depth ("Vs100"). After analysis of the data from each site we computed summary values such as Vs30 and Vs100 by arithmetic slowness averaging.

To map the lateral velocity heterogeneity beneath each of the arrays, subsets of geophone groups along the microtremor array were used to obtain a series of 1D soundings that were then interpolated to obtain a 2D structural representation of shear-wave velocities and combined with 2D P-wave refraction tomography. The refraction data was processed using SeisOpt® @2D™ (© Optim, Inc., 1997-2011). It uses a proprietary simulated annealing algorithm to invert for velocities within the subsurface from refraction picks. The method is based on Simulated Annealing Optimization, and is used to tackle some of the most complex subsurface imaging problems in the geotechnical and oil & gas industries. Simulated Annealing is a Monte-Carlo estimation process that can match arrival times (P and/or S-wave) to a velocity model even where sophisticated non-linear inversion methods may fail (Pullammanappallil and Louie, 1993; Pullammanappallil and Louie, 1994). The algorithm works by randomly perturbing an arbitrary starting model until the synthetic seismic wave travel times computed through it match the travel times picked from the new data. New models producing less travel time error are accepted for further enhancements, and models having increased error can be accepted conditionally based on their total error. As annealing proceeds, conditional acceptance becomes less and less likely. Unlike linear, iterative inversions, simulated annealing optimization will find the global velocity solution while avoiding local error minimums. It is also completely insensitive to the starting velocity model, removing the interpreter bias that may be involved in a prospect or project. The fact that SeisOpt @2D makes no assumption of the direction of the subsurface velocity gradient, unlike other more conventional seismic refraction methods, it is ideal for imaging laterally complex subsurface structure. SeisOpt @2D works by first discretizing the model space into grids. The geophone spacing determines the grid dimensions and these can be different in horizontal and vertical directions. The travel time picks and array geometry (shot and geophone

locations, including elevation) are then read in and the algorithm samples thousands of models before settling on the one that best fits all the picks from all the shots equally well. In this process, velocity values for each grid point are determined thus allowing for lateral and vertical velocity variations.

It is crucial to understand how lateral heterogeneity affects all the Vs30 values we obtain, and ultimately, the ground motions recorded at each station. These 2D velocity sections will assist in determining whether site conditions may have played a role in controlling the extreme ground motions observed at the closest stations to the rupture aside from the directivity and source effects reported by Anderson *et al.* (2009).

Results

This project was funded to measure the characteristics of twelve ground-motion recording sites in the near-filed region of the Mogul 2008 earthquake swarm towards calibration of the sources of ground-motion data for prior and future earthquakes. During this project Optim SDS measured the twelve sites using both the refraction microtremor technique and standard P-wave refraction tomography from 5 August 2011 through to 9 August 2011. Refraction microtremor data were processed and modeled by Optim and SDS. The twelve 1D velocity profiles for each station are shown in the Appendix 1. After analysis of the data from each site summary values such as average velocities to 10-, 30-, 50-, and 100-meter depths, denoted Vs10, Vs30, Vs50, and Vs100, respectively, were computed by arithmetic slowness averaging. These results are given in Table 1. The data collected during the surveys were interpreted independently by two groups. The first interpretation was done by Optim SDS, while the second was done by Dr. Louie and students at the UNR Seismological Lab. After comparison of the results, we found the Optim results are more representative of the data, and are retained for this project.

Towards examining for evidence of lateral heterogeneity, Optim has developed a method in which a series of 1-D velocity sounding along each array was them preformed using the Refraction microtremor method using subsets of instruments to characterize lateral changes in shear-wave velocity with depth (Sirles *et al.*, 2009) beneath the survey site. These soundings were then interpolated to obtain a 2D structural representation of shear-wave velocities. In essence, the 2D image is comprised from a moving array of instruments. These lateral shear-wave interpretations are aided by the accompanying 2D P-wave velocity structure determined using conventional refraction tomography. Both the 2D shear-wave and P-wave velocity structure at each location are displayed in Appendix 2 and are available, along with the ReMi data at http://shake.seismo.unr.edu:8081/lv/share/Aasha/G11AP20022_Pancha. Some of these sites may be crossed by local faults. Approximate locations of known and inferred faults are shown in Figure 3.

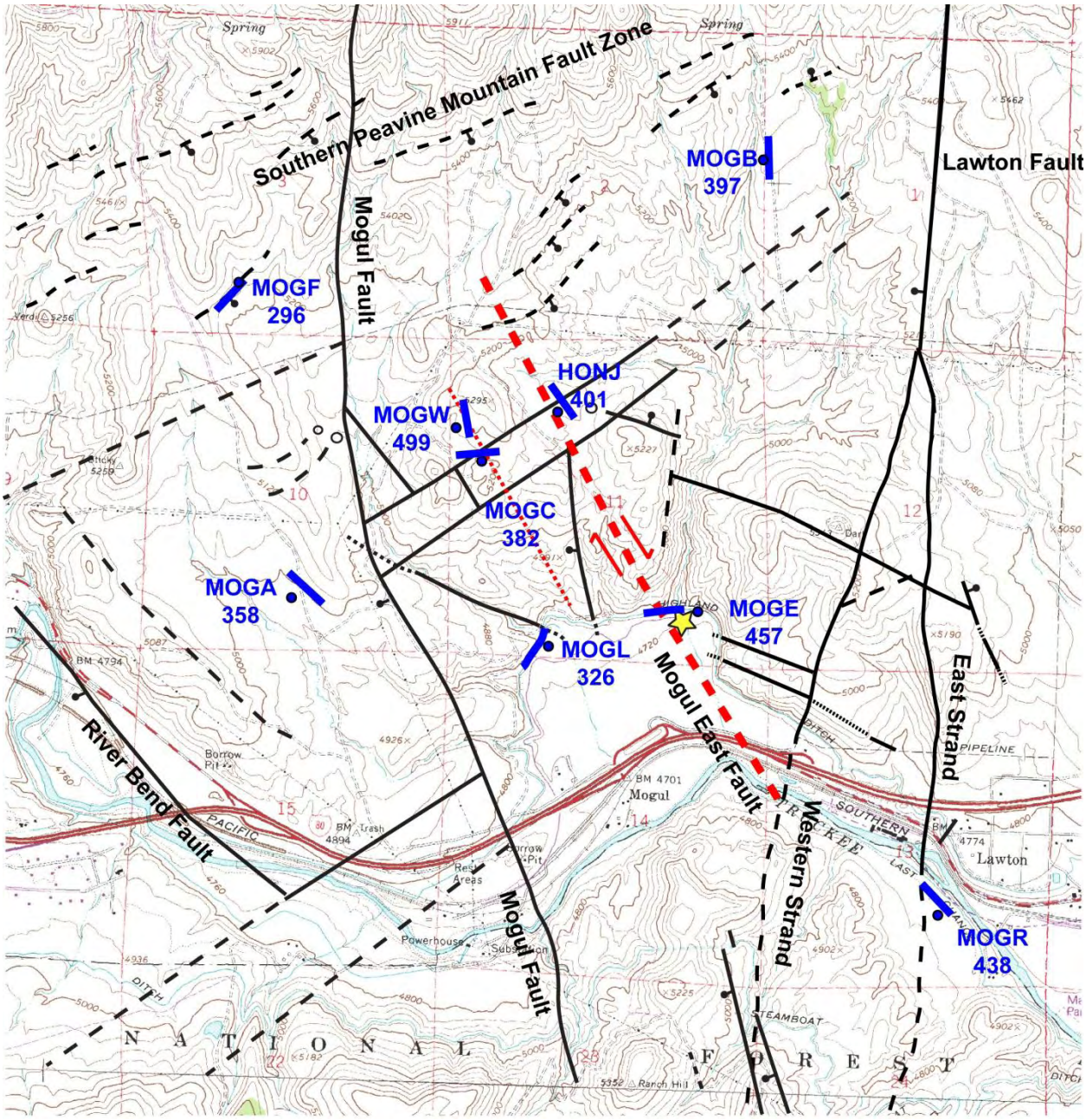

Figure 3: Map showing the location of the seismic stations (blue dots, labeled) and the relative location of the refraction lines deployed to measure near surface shear-wave and P-wave velocities. Also labeled are the Vs30 values associated with each location. The yellow star marks the location of the 26 April 2008 mainshock event. Black lines (solid and dotted) show the location of faults from published and unpublished work compiled by Craig DePolo (DePolo, 2008). The thick, solid red dashed line is the upper part of the moment magnitude 5 earthquake rupture (named the "Mogul east fault"). The alignment of red dots shows the early trend of seismicity, is called the western strand of the Mogul east fault.

Table 1: Summary of seismic station location, measurement array locations (NAD27), and our resulting average velocities to 10-, 30-, 50-, and 100-meter depths, denoted Vs10, Vs30, Vs50, and Vs100, respectively. The Refraction/Remi array location is defined by the first and last geophone.

Station Name	Station Lat	Station Long	Geophone 1 Lat	Geophone 1 Long	Geophone 24 Lat	Geophone 24 Long	Vs10, m/s	Vs30, m/s	Vs50, m/s	Vs100, m/s
HONJ	39.5307	-119.9302	39.519257°	-119.931649°	39.520715°	-119.930691°	266	401	505	704
MOGA	39.5222	-119.9454	39.521626°	-119.924843°	39.521836°	-119.922736°	298	358	448	557
MOGB	39.5425	-119.9186	39.508458°	-119.906235°	39.509545°	-119.907853°	320	397	416	481
MOGC	39.5285	-119.9348	39.486257°	-119.959513°	39.485448°	-119.961361°	252	382	456	632
MOGD	39.4867	-119.9595	39.522879°	-119.945548°	39.522879°	-119.945548°	265	340	409	558
MOGE	39.5217	-119.9216	39.528711°	-119.936039°	39.528822°	-119.933907°	230	457	563	711
MOGF	39.5362	-119.9492	39.531111°	-119.935872°	39.529512°	-119.935303°	224	296	351	442
MOGL	39.52027	-119.93066	39.531870°	-119.930815°	39.530619°	-119.929437°	185	326	401	547
MOGN	39.5481	-119.8836	39.536208°	-119.949028°	39.535074°	-119.950575°	277	413	540	786
MOGP	39.5725	-119.9081	39.543588°	-119.918360°	39.541937°	-119.918346°	289	400	482	659
MOGR	39.5084	-119.907	39.547959°	-119.882618°	39.549615°	-119.882592°	313	438	520	697
MOGW	39.5301	-119.936	39.573579°	-119.909399°	39.572192°	-119.908256°	250	499	617	785

PART TWO: Empirical site response analysis

Data

Within the Reno area basin there are currently 18 strong-motion stations which are part of the Advanced National Seismic System (ANSS) accelerograph network operated by the Nevada Seismological Laboratory, University of Nevada, Reno (NSL) with the support of the National Earthquake Hazard Reduction Program through the U.S. Geological Survey. Site conditions at these strong motion stations have been evaluated in a previous study by Pancha *et al.* (2007). We use ground motions from the 2008 Mogul swarm (Smith *et al.*, 2008) to evaluate relative amplification at these stations and the 12 Mogul seismic stations. The operational time-periods of the Mogul stations are listed in Table 2. The Nevada Seismological Laboratory compiled the waveform database for the Mogul earthquake swarm during the summer of 2011. Work was necessary due to the amalgamation of continuous and triggered data to allow extraction of the required ground motion data from the NSL database. To ensure data quality was maintained, we selected waveforms that had S-wave phase picks already allocated by the professional analyst team at the Nevada Seismological Laboratory (NSL). It was beyond the scope of this project to manually hand pick S-wave phase data for every earthquake-station pair for inclusion in this study, especially when many of these S-wave phases were emergent.

Inspection of the data revealed that many of the ANSS basin sites either lacked a clear S-wave phase or the phase was very emergent due to the reverberation of the basin due to the localized shaking. In addition, a clear S-wave arrivals were also not always available on the near-field stations. Subsequently, the earthquake data analysts had not used these unclear S-wave phases as part of the routine location of the individual events. This background noise due to the reverberation of the basin due to the localized shaking was not prominent for the more distant sources investigated by Pancha (2007).

Mogul recording stations were equipped with a continuous velocity sensor and an accelerometer. However, the triggered accelerometers did not always record each earthquake. Instances were noted where small events triggered accelerometers, but as a consequences, missed larger events that occurred shortly thereafter. Data from the velocity sensors was utilized in these instances for this study. In some cases where both accelerometer and velocity data were available, the analysts had preferred to pick the velocity waveform due to clarity of the data in deciphering the onset of the S-wave phase. These S-wave pick times were transferred from velocity sensor data to accelerometer data when available, and the accelerometer was data used for this study. Clipped data was removed. Unfortunately, not all the Mogul recording sites had been incorporated into the earthquake database at the time of earthquake location, and therefore are not picked by the analysis team.

Selecting only those events above M=2 together with S-wave phase picks on the nominated hard rock site, RFNV resulted in 137 individual events. Inspection of this data at the rock site RFNV showed that reverberation of the Reno area basin in response to the aftershock sequence strongly dominated the background noise of the data, event at higher magnitudes. As a result, the S-wave spectral signal to noise level of the S-wave phase was not as high as anticipated. To enhance the signal to noise ratio, a 5 second S-wave window was adopted rather than the 10 second window utilized by Pancha (2007). Even with this signal enhancement, examination of signal to noise plots at RFNV for each of the 137 events show that the signal-to-noise ratio was less than one across the whole frequency spectrum for many events. Many recordings showed a signal-to-noise ratio of less than one below 2 Hz. While it was envisioned

that comparisons of the response spectra could be presented here between events 3 ≤ M ≥2, with those M ≥3, especially at low frequencies, the predominance of this background noise meant that this was not possible.

We selected 29 events for which the S-wave phase for RFNV had been picked by NSL data analysts, and for which the spectral signal to noise ratio of the 5 sec S-wave window was above two for 0.6 Hz and above. These 29 earthquakes of M ≥2.7 are listed in Table 3. The S-wave signal to noise spectra for each station were observed, and those with S-wave signal to noise ratios of less than two from 0.6 Hz to 10 Hz were eliminated. Note that ground motions from the mainshock event are not included, but are analyzed separately.

We retained accelerometer data when available, and converted the velocity data to acceleration where necessary for inclusion in the analysis. For each station with co-located velocity and accelerometer data for the 29 event listed in Table 3, comparisons were made to ensure the conversion from velocity to acceleration was accurate, and acceptable for the Mogul stations were accelerometer data was not available. Figure 4 shows an example of such comparisons for Event 20 (Table 3).

Table 2: Summary of the Mogul seismic station operation times. Dates are given as year and Julian day.

Station Name	Station On Date	Station Off Date
HONJ	2008 085	2008 210
MOGA	2008 124	2008 206
MOGB	2008 126	2008 206
MOGC	2008 122	2008 197
MOGD	2008 127	2008 207
MOGE	2008 100	2008 210
MOGF	2008 127	2008 191
MOGL	2008 063	2008 169
MOGN	2008 164	--
MOGP	2008 168	2008 198
MOGR	2008 123	2008 207
MOGW	2008 094	2008 198

Table 3: List of Earthquakes events used in this study. Events marked with an asterisk are those which were recorded at MOGE with a strong signal to noise ratio.

	Latitude	Longitude	Magnitude, Ml	Depth, km	Origin Time
1	39.5304	-119.9212	3.96	6.28	4/24/08 (115) 22:47:03
2*	39.5399	-119.9244	3.76	2.60	5/08/08 (129) 05:55:01
3*	39.5364	-119.9332	3.58	1.56	4/15/08 (106) 21:33:57
4	39.5290	-119.9281	3.51	2.14	4/26/08 (117) 07:29:20
5*	39.5300	-119.9299	3.42	1.59	4/15/08 (106) 21:32:31
6*	39.5368	-119.9165	3.42	2.37	5/15/08 (136) 13:44:48
7	39.5340	-119.9348	3.39	2.06	4/15/08 (106) 14:59:37
8*	39.5145	-119.9194	3.38	1.00	4/26/08 (117) 06:43:50
9	39.5243	-119.9321	3.35	1.40	3/08/08 (068) 10:07:00
10*	39.5203	-119.9226	3.32	3.41	4/27/08 (118) 17:49:49
11*	39.5271	-119.9262	3.30	1.44	4/25/08 (116) 17:30:10
12*	39.5232	-119.9275	3.27	2.35	4/25/08 (116) 01:00:33
13*	39.5341	-119.9322	3.20	1.46	4/15/08 (106) 21:26:35
14*	39.5150	-119.9205	3.20	4.28	4/29/08 (120) 06:01:53
15	39.5477	-119.9209	3.17	2.08	6/08/08 (160) 10:13:58
16	39.5316	-119.9360	3.15	1.66	3/27/08 (087) 03:42:14
17	39.5247	-119.9325	3.12	1.87	3/24/08 (084) 19:16:14
18	39.5470	-119.9405	3.10	5.42	11/13/08 (318) 07:42:08
19*	39.5177	-119.9219	3.08	2.64	4/21/08 (112) 19:14:10
20*	39.5469	-119.9275	3.04	3.93	5/31/08 (152) 09:09:56
21*	39.5253	-119.9315	2.96	2.39	4/24/08 (115) 22:51:06
22	39.5263	-119.9357	2.95	0.97	3/15/08 (075) 15:38:35
23	39.5516	-119.9180	2.95	1.90	5/18/08 (139) 08:44:20
24	39.5221	-119.9325	2.95	2.33	4/02/08 (093) 00:07:46
25*	39.5150	-119.9229	2.94	1.67	4/23/08 (114) 06:21:09
26*	39.5274	-119.9260	2.93	2.44	5/02/08 (123) 17:11:55
27*	39.5253	-119.9316	2.92	3.70	4/26/08 (117) 06:45:07
28*	39.5149	-119.9206	2.92	4.23	4/24/08 (115) 23:51:48
29	39.5089	-119.9155	2.69	2.49	5/04/08 (125) 09:22:25

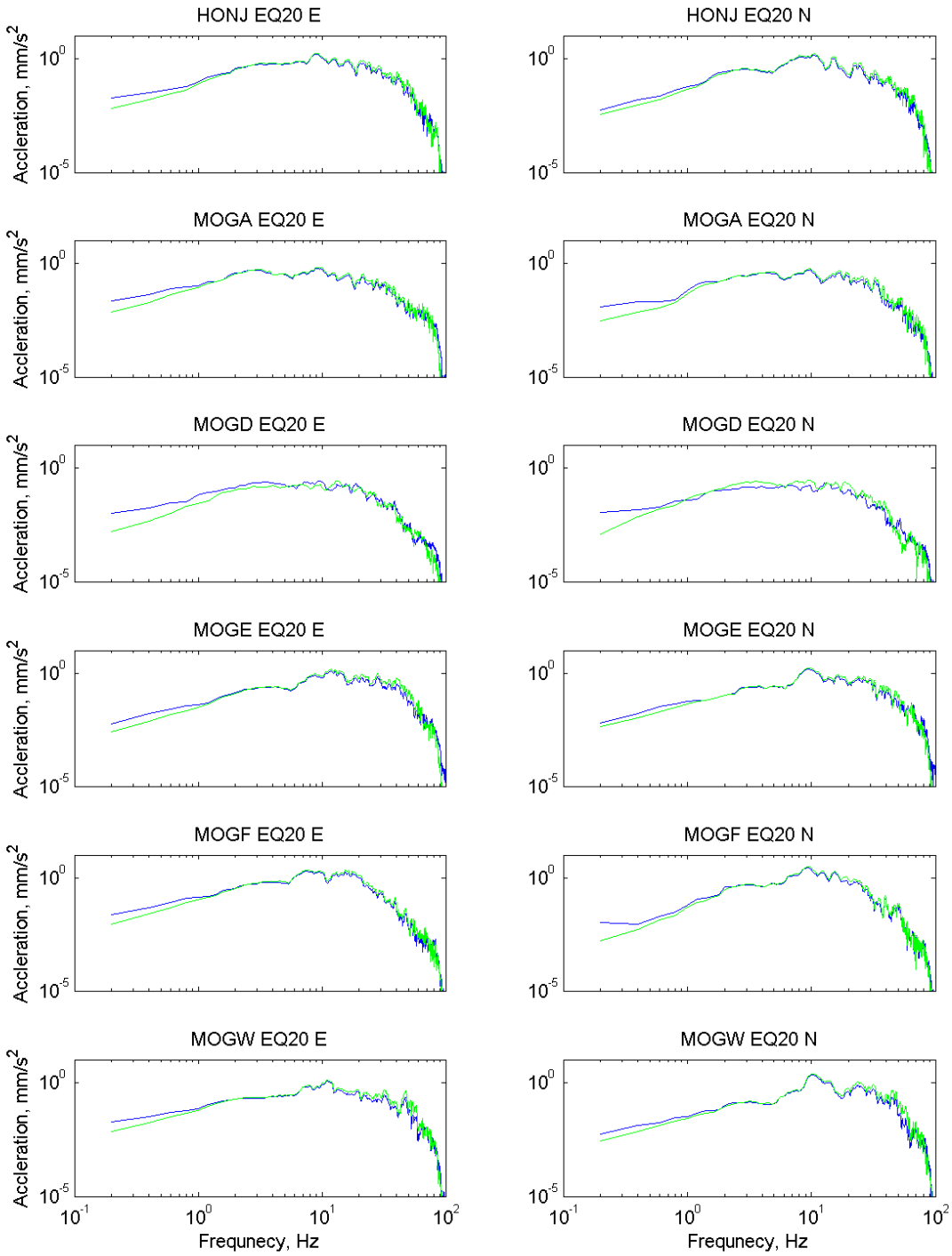

Figure 4: Comparison of S-wave spectra from the accelerometer data (blue) for Event 20 (see Table 3) with spectra obtained from the conversion of velocity sensor data to acceleration (green). Left panel shows the east component of motions while the north component is shown in the right panels.

Reference site selection

Of the ANSS stations located within the Reno area basin, three are located on volcanic bedrock: RFNV, NOAA, and SWTP (Pancha *et al.*, 2007; Bonham and Bingler, 1973; Bell and Bonham, 1987). Based on the ground motion observations presented by Pancha (2007), we select RFNV (Figure 1) as our reference rock site with respect to the ANSS stations within the basin. For the Mogul recording stations, we used MOGE for two reasons, the high velocity material beneath the site (see table 1) and the large number of events recorded on this station within the compared with other hard rock Mogul stations such as MOGW.

Soil to rock spectral ratio technique.

Site amplification at each strong motion station is estimated using the smoothed Fourier spectra, the absolute acceleration response spectra (with 5% damping), and the peak acceleration of the accelerograms. We extract 5 second S-wave windows, beginning one second before the phase arrival. A 5% cosine taper was applied before taking the Fourier transform of each of the components. The horizontal amplitude spectrum at the *i*th station for the *j*th earthquake event is defined as the root-mean-squared average of the smoothed spectra of the two horizontal components:

$$A_{ij}(f) = \sqrt{[(A_{ij}^{N}(f))^2 + (A_{ij}^{E}(f))^2]/2}\,, \qquad \text{Equation (1)}$$

where the superscripts *N* and *E* denote the orthogonal horizontal components, respectively (either north-south and east-west). Spectral smoothing of each component was achieved by an averaging routine within a 10% window about a central frequency that conserves the total energy on the spectrum. In a few instances, only one horizontal component of motion is available and Equation (1) was altered accordingly. Spectral ratios of the average horizontal spectral motion between each of the stations and the reference site were then computed. Geometric spreading effects are corrected for by normalizing the Fourier spectral ratio (FSR) by the ratio of the hypocentral distance to each site with that to the reference site. With these approximations, the soil to rock Fourier spectral ratio can be written as:

$$\mathrm{F}\,SR_{ij}(f) = \frac{A_{ij}}{A_{REF_j}} \frac{R_{ij}}{R_{REF_j}}\,, \qquad \text{Equation (2)}$$

where *A* is the average horizontal spectra as defined by Equation 1, *R* is the hypocentral distance, and subscripts *i*, *j*, and *REF* denote the *i*th soil station, *j*th event, and the reference site respectively. Site response functions for each site are then computed by taking the geometric average for all events at each frequency. We use the notation FSR for the spectral ratios of smoothed Fourier spectra.

For the ANSS stations, source effects (e.g. radiation pattern) and path effects are considered to be minimal as the sites are relatively close together compared to the hypocentral distances. However, for the Mogul stations, these effects are likely to be predominant.

Results:

<u>Relative spectral amplification within the Reno Basin</u>

Horizontal Fourier spectral ratios with respect to the rock site RFNV located at the edge of the Reno area basin are presented in Appendix 3 for the ANSS basin stations. Comparisons of these response spectra with those obtained by Pancha (2007) using regional ground motion data are presented in Figure 5. Comparisons with the relative amplification of the two horizontal components of ground motion recorded by the 26th April 2008 mainshock are also show. The response spectra obtained from ground motions of the Mogul foreshock and aftershock sequence show broad amplification functions that are mainly flat or irregular functions of frequency. Only a few stations show peaked spectra at certain frequencies, which may relate to local resonance. As discussed by Pancha (2007), basin amplification in the absence of resonance suggests lack of strong impedance contrasts between stratigraphic layers that would give resonance in the frequency band studied. The amplification response spectral shapes may also be a result of constructive and destructive wave interaction within the basin.

Comparison of the response spectra with those computed by Pancha (2007) using ground motions from regional earthquakes show similar spectral shapes for most of the stations. The relative amplification level may differ due to the smaller number of events used to calculate each response. Greatest difference in amplification levels appear at stations located along the east side of the basin at SPHI, SMRN, and most notably HVGC (see Figure 1 for locations). This observation may infer that the low amplification may be related to wave propagation into the eastern side of the basin. Such phenomena can be investigated through 3D synthetic waveform modeling. The marked difference in amplification level at HVGC may also be related to the near surface geology. Characterization of the near-surface shear-wave velocity structure of this site under NEHRP grant G09AP00051 revealed a shallow high velocity layer at 35 m depth. This sharp velocity contrast may cause trapping and local wave amplification or deamplification depending on the azimuth and angle of incidence of incoming waves.

Both the Mogul aftershock and regional ground motions show a peak in the response spectra at 5 to 10 Hz at UNRX, with similar amplification level. Similar amplification level between the two estimates is also observed at the NOAA rock site, however, the spectra developed using ground motions from the Mogul aftershock sequence shows a distinct peak at 2 to 5 Hz. Once again, this may be related to the direction of the incoming waves and the trapping of waves in the near-surface material. This site was also characterized under NEHRP grant G09AP00051, and revealed rock velocities below 100 m and relatively much slower material above.

Peaks on the response spectra at NMHS using the aftershock and region ground motions agree, both in shape and amplification level. They are also in agreement with the amplification level given by the North component of horizontal motion. Overall comparison of the response spectra obtained using the horizontal components of ground motion of the mainshock event differ in amplitude and overall spectral shape. The mainshock event was Ml=4.67, where as the events used in this study range from Ml=2.69 to Ml=3.96. Those in the study of Pancha (2007) range from Ml=3.01 to Ml=4.86 but hypocentral distances were much greater. The large size of the mainshock event and the close proximity of the event to the station locations may contribute to the differences observed. The rupture area of the mainshock event will have been larger,

contributing to radiation effects and source effects that may influence ground motions at the ANSS sites.

Previous investigation by Pancha *et al*. (2004) demonstrated a definite basin response between 0.2 to 0.6 Hz. However, as the signal to noise level was poor below 0.6 Hz, as discussed above, the basin response below 0.6 Hz was not able to be observed.

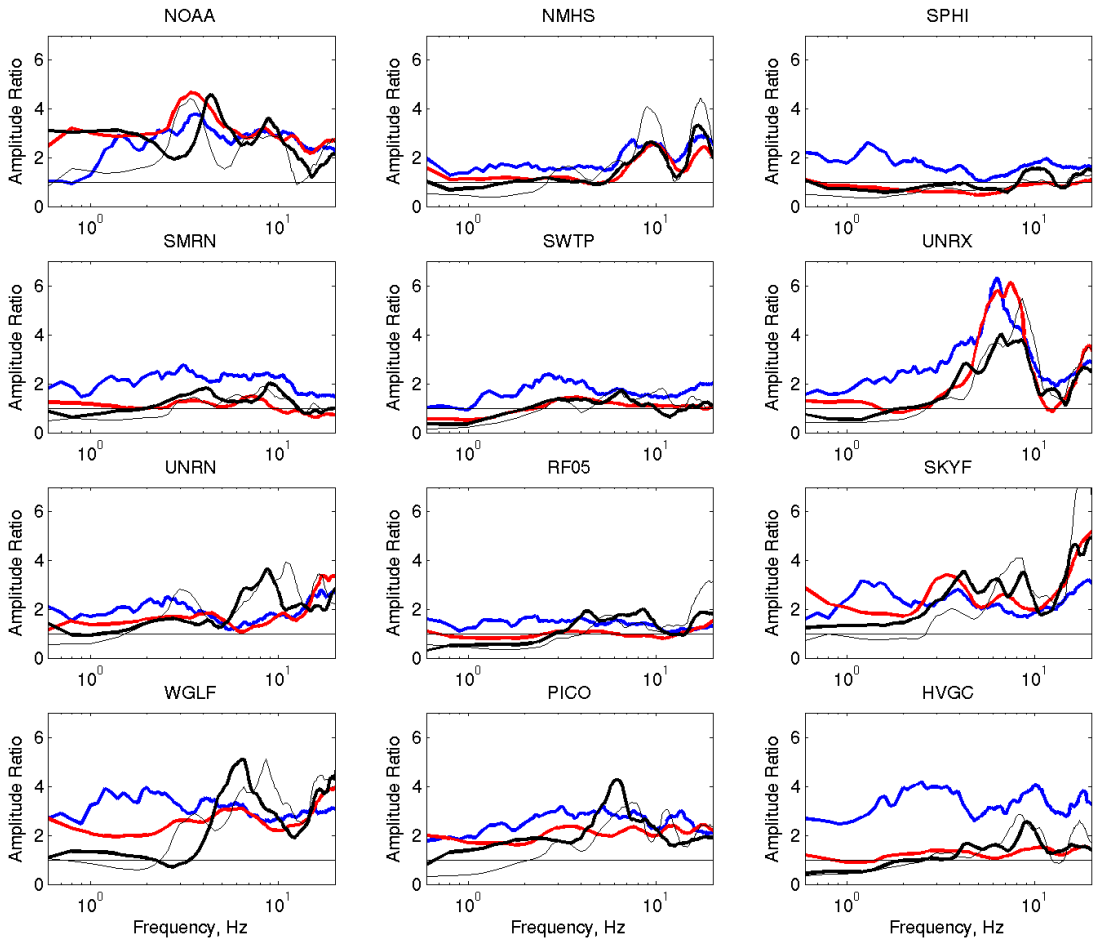

Figure 5: Average horizontal spectral response functions relative to RFNV at ANSS stations. Station locations are shown in Figure 1. Spectra computed from ground motions of the Mogul events are shown in red. Blue spectra are those determined from regional events by Pancha (2007). Relative response for the north (solid black) and east (thin black) components of motion from the Ml=4.67 mainshock event are also shown.

Correlation of amplification with site conditions within the Reno Basin

Many studies have noted a correlation between site amplification and both Vs30 (e.g. Joyner and Fumal, 1984; Borcherdt, 1994; Harmsen, 1997; Hartzel *et al*., 1997; Wald and Mori, 2000). Here we correlate Fourier spectral ratios relative to a rock site with shallow shear-wave velocities at each of the sites within the Reno area basin. Average shallow shear wave velocities to 30m (Vs30) and 100m (Vs100) depth have been characterized for the ANSS stations located within the basin either under this study, or previous endeavors (Pancha *et al.*, 2007; G09AP00051). Amplitudes of the Fourier spectral ratio are considered at the following frequencies: 0.6, 1.0, 2.0, 3.3, 5.0, 8.0, and 10.0 Hz. These frequency values are selected to be representative of amplification variation over the reliable bandwidth of the data.

Statistical tests evaluate whether or not the independent variables Vs30 and Vs100 are effective in predicting the measured amplification level. Results are presented in Table 4. Based on the null hypothesis that amplification is independent of the independent variable, the error reduction due to a least squares fit to the data is then evaluated. The significance level of the error reduction is assessed by comparison of the variances through the F probability distribution (Hoel, 1971; Kirkpatrick, 1974; Blæsild and Granfeldt, 2003). A full description of the method is given by Pancha *et al.* (2007).

Least squares lines to the mean amplification values are given in Table 4 and the data is illustrated in Appendix 4 and 5 for V30 and Vs100 respectively. Data for each station, in addition to mean amplification values, show that the slope of the regression is significantly different from zero. These results demonstrate that for the Reno area basin, amplification has a dependence on shallow shear wave velocity. The statistical confidence that the correlations are significant is smaller than the desired 95% level, but for all cases, the significance is greater than 55% (Table 4). The relative amplification at the NOAA station is notably higher than the other stations for frequencies from 1 to 5 Hz. This increase in relative amplification is apparent from Appendix 3.3 showing the amplification ratio for NOAA relative to RFNV.

Relative spectral amplification observed at the Mogul stations

To assess spectral amplification at the Mogul stations it was inappropriate to use RFNV as a reference site as the station was much further from the locality from the Mogul stations. Local path effects would not be eliminated from the spectral ratio presented in equation 2. More importantly, the ground motion recordings at the Mogul stations will also contain source effects and directivity effects. Aware of these issues, we used the database developed to extract events with S-picks recorded on RFNV to investigate relative spectral variations at the Mogul stations. As mentioned above, we used MOGE as a reference site for these stations. Events used to computed spectral amplification with respect to MOGE are marked with an asterisk in Table 3.

Figure 6 displays the resultant response functions for Mogul stations. As this is only a preliminary investigation using only events listed in Table 3, very few spectra are shown. However, as see from the plots for HONJ and MOGL, the spectral response are variable with ground motions from Event 25 (HONJ and MOGL) and Event 13 (MOGL) producing much higher amplification levels. Both of these events are shallow and have comparable magnitudes. Event 11 also has a similar depth and magnitude as Events 13 and 25 but did not produce high amplification at these sites. These preliminary plots illustrate that the ground motion spectra at

the Mogul sites are complex due to near-source effects, directivity, source location, focal mechanism, in addition to site effects and non-linearity. It was beyond the scope of this project to investigate or remove these effects to obtain the site response functions.

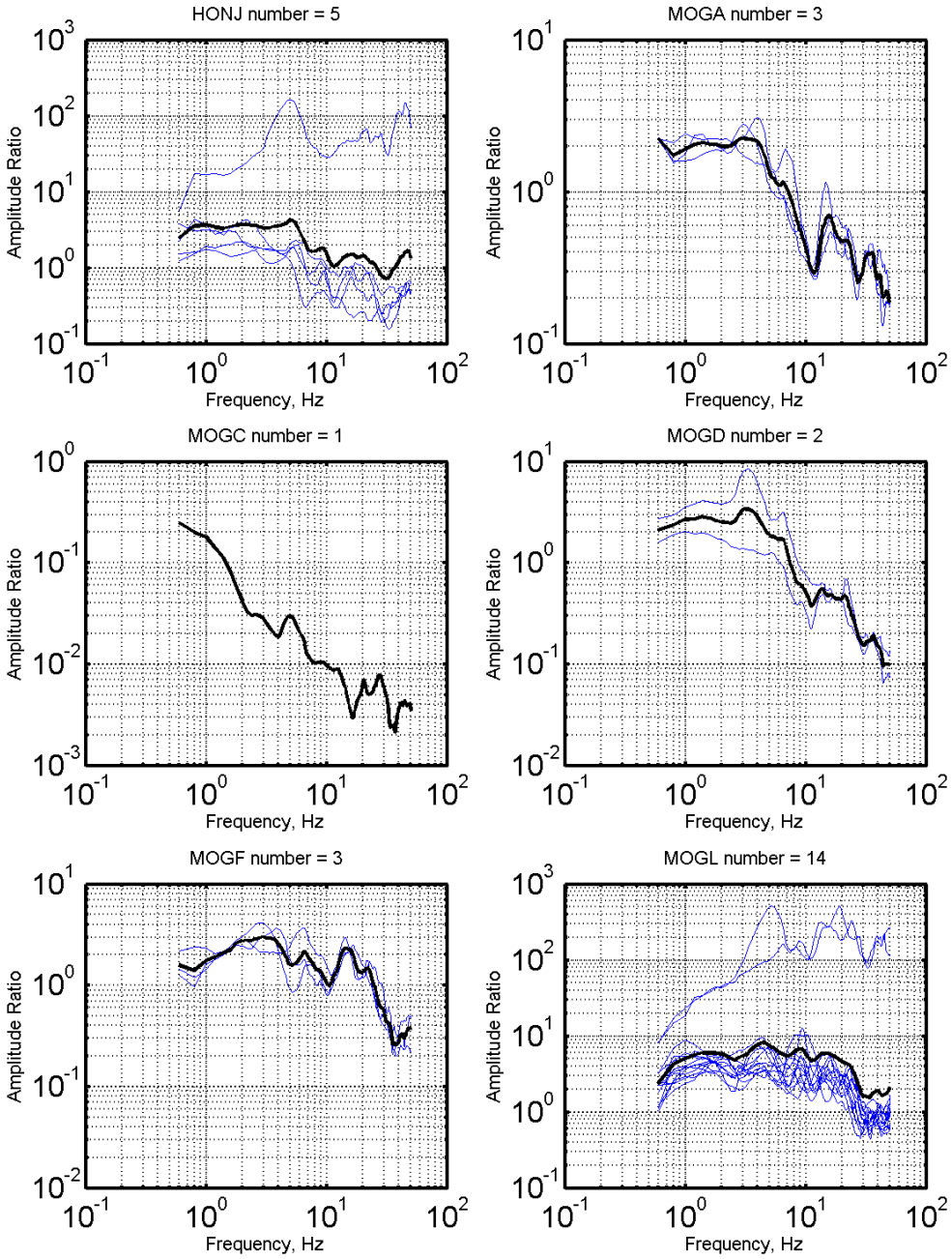

Figure 6: Horizontal spectral response functions relative to MOGE at the Mogul stations for earthquake events of the Mogul sequence. The geometric mean is shown as a heavy black line.

Table 4: Correlation of amplification values with Vs30 and Vs100.

Frequency	Independent Variable	Intercept	Gradient	Mean	cov_int	cov_grad	Variance of fit	Variance of independent data	σ_μ¶	F-Test#
0.6	Vs30	0.4248	-0.5294	0.0909	0.2113	0.4948	0.024135797	0.034972366	0.1554	72.67%
1.0	Vs30	0.3521	-0.4397	0.0747	0.2223	0.5205	0.030103638	0.038701513	0.1735	65.78%
2.0	Vs30	0.1840	-0.1550	0.0862	0.1858	0.4350	0.024253702	0.027031635	0.1557	56.79%
3.3	Vs30	0.4284	-0.3347	0.2173	0.2575	0.6029	0.044662905	0.051912433	0.2113	59.49%
5.0	Vs30	0.3417	-0.2816	0.1640	0.2958	0.6927	0.060952203	0.068528768	0.2469	57.35%
8.0	Vs30	0.5453	-0.5347	0.2080	0.2544	0.5956	0.038463447	0.050673612	0.1961	67.25%
10.0	Vs30	0.4269	-0.3892	0.1814	0.2007	0.4700	0.024716871	0.031546733	0.1572	65.34%
0.6	Vs100	0.3917	-0.4479	0.0909	0.1459	0.2915	0.022385247	0.034972366	0.1496	76.60%
1.0	Vs100	0.3260	-0.3742	0.0747	0.1535	0.3067	0.028814723	0.038701513	0.1697	68.38%
2.0l	Vs100	0.1267	-0.0603	0.0862	0.1283	0.2563	0.024773186	0.027031635	0.1574	55.40%
3.3	Vs100	0.2880	-0.1052	0.2173	0.1777	0.3552	0.047372828	0.051912433	0.2177	55.68%
5.0	Vs100	0.2449	-0.1204	0.1640	0.2042	0.4081	0.062542507	0.068528768	0.2501	55.67%
8.0	Vs100	0.4508	-0.3616	0.2080	0.1756	0.3509	0.040322246	0.050673612	0.2008	64.40%
10.0	Vs100	0.3431	-0.2407	0.1814	0.1386	0.2769	0.026260851	0.031546733	0.1621	61.59%

cov_int = covariance uncertainty of the intercept of the least squares fit.
cov_grad = covariance uncertainty of the gradient of the least squares fit.
¶ σ_μ = standard error of the mean fit.
# F-Test = F distribution confidence level. High values indicate greater reduction of variance.

Discussion

Ground motions during the 26 April 2008 Mw 5.0 Mogul, Nevada earthquake are compared with ground motion prediction equations by Anderson *et al.* (2009). The ground motion models, developed as part of the Next Generation Attenuation project, assumed Vs30 of 400m/s for the four near-field stations in operation at the time of the main event based on an average velocity inferred from Pancha *et al.* (2007). This comparison showed that peak accelerations at the four closest stations are much higher than median predictions, while peak accelerations at the 21 distant ANSS stations located in the Reno area basin are greatly over-predicted. These four stations were MOGE, MOGL, MOGW, and HONJ. Direct measurement of site conditions at each of these sites show average Vs30 values of 457 m/s MOGE, 326 m/s MOGL, 499 m/s MOGW, and 401 HONJ indicating that the assumptions by Anderson *et al.* (2009) are reasonable.

The MOGL seismic station was located along the base of the topographic slope marking the boundary of the Pliocene sediments of the Hunter Creek Sandstone with the Quaternary sediments that cover the Mogul subdivision (Bell and Garside, 1987). As described by Anderson *et al*. (2009) there is a basin edge in the vicinity of the MOGL station. The geophysical refraction array deployed in this study was located above the station in the paved Highland Ditch. Two additional refraction lines are presented in Figure 7. One is placed 10 m below the location of the seismic station on the Quaternary sediment parallel to the topographic slope, and the other is perpendicular to the original line. These additional lines were obtained to investigate the possible nature of the boundary between the Hunter Creek Sandstone and the Quaternary sediments, as well as the velocity of the Quaternary fill. The refraction results shown in Figure 8 suggest that the interface between the Sandstone and Quaternary fill is abrupt and possibly near vertical. The velocity of the Quaternary fill is much lower.

This suggesting the Quaternary sediments within the Mogul subdivision may be slower than expected. These potentially softer materials occur within the low-lying flat region of Mogul shown in Figure 3. Anderson *et al*. (2009) believe that the MOGL station is within the sedimentary rock and that a basin-edge effect is not contributing to the high ground motions. Further investigations are required to determine the location of the basin edge in the vicinity of this station, and to determine the geomorphic significance of this flat region, as well as the depth and geophysical properties Quaternary sediments within the Mogul subdivision. These data will aid interpretation as whether strong amplification due to site conditions within the Mogul subdivision contributed towards the experienced extreme ground motions

Ground motions from earthquakes of the Mogul earthquake sequence, with magnitudes from Ml=2.69 to Ml=3.96, have been used to examine the site response at the ANSS stations in the basin containing the Reno metropolitan region. Fourier spectral amplifications relative to RFNV have broadband amplifications that are typically factors of 2-3 times the reference motions, and resonances with peaks as high as 6 times the amplitude of the reference. The amplification is spatially variable. Comparisons with measured velocities show that amplification tends to be smaller as Vs30 and Vs100 increase. The statistical confidence that the correlations are significant is smaller than the desired 95% level, but in all cases, the confidence is greater than 55% (Table 4). Greatest correlation occurs at 0.6 and 1 Hz. Correlation with Vs30 and Vs100 at 0.6 Hz is significant at the 73% and 77% confidence level respectively. At 1 Hz the correlation with Vs30 and Vs100 is significant at the 67% and 68% confidence level

respectively. These results show that ground motion in the Reno area basin does have a dependence on near-surface velocities.

Comparison of the relative spectral amplification at these ANSS computed using ground motions from the Mogul earthquakes sequence with those computed using regional events (Pancha, 2007) are presented in Figure 5. While the absolute amplitudes may not match due show comparable spectral shapes. These results verify that regional ground motions can be use to obtain site response amplification functions for use in seismic hazard applications.

Figure 7: Location of the refraction and ReMi line for MOGL as well as the location of two additional refraction lines MOGL2 and MOGL3 obtained to investigate both the boundary between the Hunter Creek Sandstone and the Quaternary fill. Geophone spacing along MPGL2 was 2.438 m (8 feet) while 3.048 m (10 feet) spacing was used for MOGL3.

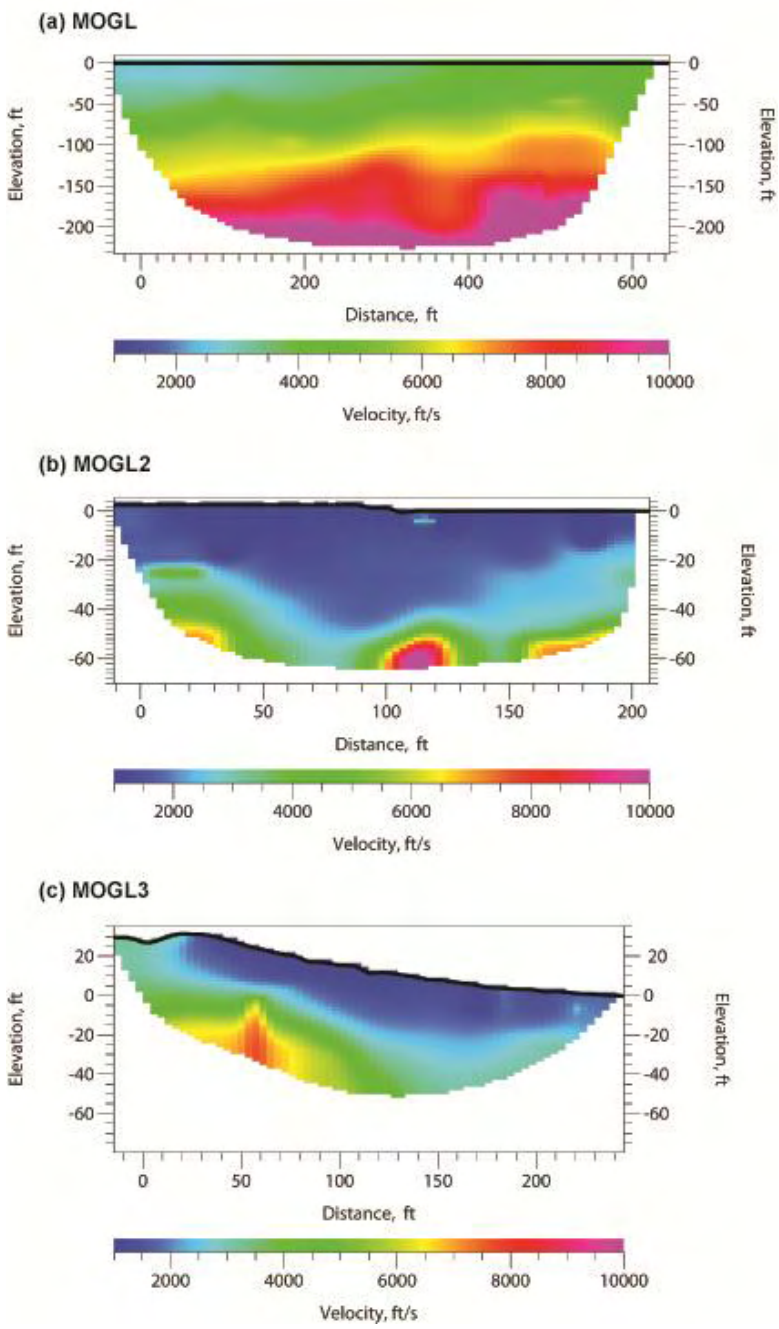

Figure 8: P-wave Refraction results for the three lines obtained at the MOGL station. Locations of these lines are shown in Figure 8.

References

Abbott, R. E., Louie J. N. (2000). Depth to bedrock using gravimetry in the Reno and Carson City, Nevada area basins, *Geophysics*, 65, 340-350.

Anderson, J. G., Tibuleac, I., Anooshehpoor, A., Biasi,G., Smith, K., and D. von Seggren (2009). Exceptional Ground Motions Recorded during the 26 April 2008 Mw 5.0 Earthquake in Mogul, Nevada, *Bull. Seismol. Soc. Amer*., 99, 3475-3486, doi: 10.1785/0120080352.

Anderson, J. G. (2010). Source and Site Characteristics of Earthquakes That Have Caused Exceptional Ground Accelerations and Velocities, *Bull. Seismol. Soc. Amer*., 100, 1-36, doi: 10.1785/0120080375.

Bell, J. W, and H. F. Bonham (1987). Vista Quadrangle Geologic Map, Nevada Bureau of Mines and Geology, Map 4Hg, 1:24,000 scale.

Bell, J. W, and L. J. Garside (1987). Verdi Quadrangle Geologic Map, Nevada Bureau of Mines and Geology, Map 4Gg, 1:24,000 scale.

BSSC: Building Seismic Safety Council, 1998, NEHRP Recommended *Provisions for Seismic Regulation for New Buildings: FEMA* 302/303, developed for the Federal Emrgency Management Agency, Washington, D. C.

Blæsild P., and J. Granfeldt (2003). *Statistics with applications in biology and geology*, Chapman and Hall/CRC, Boca Raton, pp555.

Bonham, H. F., and E. C. Bringler (1973). Reno Folio Geologic Map, Nevada Bureau of Mines and Geology, *Environmental Series*, Map 4Ag, 1:24,000 scale.

Borcherdt, R. D. (1994). Estimates of site-dependent response spectra for design (Methodology and Justification), *Earthquake Spectra*, 10, 617-654.

DePolo, C. (2008), Observations and Reported effects of the February-April 2008 Mogul-Somersett, Nevada Earthquake Sequence, Nevada Bureau of Mines and Geology report.

Harmsen, S. C. (1997). Determination of site amplification in the Los Angeles urban area from inversion of strong-motion records, *Bull. Seism. Soc. Am*., 87, 866-887.

Hartzell, S., E. Cranswick, A. D., Frankel, D. L., Carver, and M. E. Meremonte (1997). Variability of site response in the Los Angeles urban area, *Bull. Seism. Soc. Am*., 87, 1377-1400.

Hoel, P.G. (1971). *Introduction to Mathematical statistics*, Fourth Edition, John Wiley & Sons, 409 pp.

Joyner, W. B., and T. E. Fumal (1984). Use of measured shear-wave velocity for predicting geological site effects on strong-motion, *Proc. of the Eighth World Conference on Earthquake Engineering* (San Francisco), **2**, 777-783.

Kirkpatrick, E. G. (1974). *Introductory statistics and probability for engineering, science, and technology*, Prentice-Hall, New Jersey, pp 446.

Louie, John N., 2001, Faster, better: shear-wave velocity to 100 meters depth from refraction microtremor arrays, *Bull. Seismol. Soc. Amer., 91,* no. 2 (April), 347-364.

Pancha, A., J. G. Anderson, J. N. Louie, A. Anooshehpoor, and G. Biasi (2004). Data and simulation of ground motion for Reno, Nevada: *Proceedings of the 13th World Conf. on Earthquake Engineering*, Vancouver, B.C., Aug. 1-6, paper no. 3452.

Pancha, A., J. Anderson, and J. Louie (2007). Characterization of near-surface geology at strong-motion stations in the vicinity of Reno, Nevada, *Bull. Seismol. Soc. Amer*., 97, No. 6, 2096–2117, doi: 10.1785/0120060266.

Pancha, A. (2007). *Seismic Hazards in the Basin and Range province*, U.S.A., Ph.D Dissertation, University of Nevada, Reno, 382 p.

Pullammanappallil, S.K., and Louie, J.N., 1993, Inversion of seismic reflection traveltimes using a nonlinear optimization scheme: Geophysics, v. 58, p. 1607-1620.

Pullammanappallil, S.K., and Louie, J.N., 1994, A generalized simulated-annealing optimization for inversion of first arrival times: Bulletin of the Seismological Society of America, v. 84, p. 1397-1409.

Sirles, P., Z. Batchko, S. Pullammanappallil, and J. B. Shawver, 2009, Mapping top-of-rock and soft-soil Zones beneath high-traffic Areas using 2D ReMi, Proocedings of the 22nd EEGS Symposium on the Application of Geophysics to Engineering and Environmental Problems, 29 March 2009.

Smith, K., D. von Seggern, D. dePolo, J. Anderson, G. Biasi, and R. Anooshehpoor (2008). Seismicity of the 2008 Mogul–Somersett west Reno, Nevada, earthquake sequence (Abstract S53C-02), *Eos Trans. Am. Geophys. Union*, **89**, no. 53 (Fall Meet. Suppl.), S53C-02.

Stephenson, W. J., J. N. Louie, S. Pullammanappallil, R. A. Williams, and J. K. Odum, 2005, Blind shear-wave velocity comparison of ReMi and MASW results with boreholes to 200 m in Santa Clara Valley: Implications for earthquake ground motion assessment: *Bull. Seismol. Soc. Amer.*, **95**, 2506-2516, doi: 10.1785/0120040240.

Thelen, Weston A., Matthew Clark, Christopher T. Lopez, Chris Loughner, Hyunmee Park, James B. Scott, Shane B. Smith, Bob Greschke, and John N. Louie (2006). A transect of 200 shallow shear velocity profiles across the Los Angeles Basin, *Bull. Seismol. Soc. Amer*., 96, no. 3 (June), pp. 1055-1067, doi: 10.1785/0120040093.

Wald, L. A., and J. Mori (2000). Evaluating methods for estimating linear site-response amplifications in the Los Angeles region, *Bull. Seism. Soc. Am*., 90, no. 6B, S32-S42.

Acknowledgements:

This study would not be possible without data from the Nevada Seismological Laboratory (NSL), at the University of Nevada, Reno, and recorded continuously. We are indebted to Glenn Biasi who assisted with data extraction from the NSL database.

Appendix 1

Printouts of shear-velocity profiles measured by Optim SDS for 12 sites in the near-field area of the Mogul 2008 earthquake swarm, sponsored by the USGS External Research Program under contract G11AP20022. The format is the same used in the on-line archive, and was inspired by Prof. B. Luke of UNLV. Data fields are delimited by return and whitespace characters. The raw data values output by SeisOpt® ReMiTM are given but do not represent true precision, which is limited to one meter and one meter per second at best. Open-source software reading this format is at www.seismo.unr.edu/vs/archive/getv30/.

Site name: HONJ, Mogul seismic recording station
Lat/long: 39.5307/-119.9302
Lat/long ReMi line start and finish: 39.519257°/-119.931649°; 39.520715°/-119.930691°
Average velocity to 30 m, m/s: 401
Date: 05/08/2011 (dd/mm/yyyy)
Performed by: Optim SDS.
Type of measurements: ReMi
Depth of measurements: 100 m
Function stepped (y or n): yes
Posted by: Aasha Pancha 09/11/2011 (dd/mm/yyyy)

Depth(m)	Vs(m/s)
0	149.628
1.5544	149.628
1.5544	194.289
3.74886	194.289
3.74886	393.545
11.4294	393.545
11.4294	479.431
25.1448	479.431
25.1448	850.224
59.8446	850.224
59.8446	1277.74
100.579	1277.74

Site name: MOGA, Mogul seismic recording station
Lat/long: 39.5222/-119.9454
Lat/long ReMi line start and finish: 39.521626°/-119.924843° 39.521836°/-119.922736°
Average velocity to 30 m, m/s: 358
Date: 05/08/2011 (dd/mm/yyyy)
Performed by: Optim SDS.
Type of measurements: ReMi
Depth of measurements: 150 m
Function stepped (y or n): yes
Posted by: Aasha Pancha 09/11/2011 (dd/mm/yyyy)

Depth(m)	Vs(m/s)

0	84.3545
0.73148	84.3545
0.73148	149.628
1.41725	149.628
1.41725	709.606
5.7	709.606
5.7	300.788
16.6	300.788
16.6	441.641
28.4136	441.641
28.4136	735.123
102.75	735.123
102.75	1085.91
139.875	1085.91
139.875	1518.9
150	1518.9

Site name: MOGB, Mogul seismic recording station
Lat/long: 39.5425/-119.9186
Lat/long ReMi line start and finish: 39.508458°/-119.906235°; 39.509545°/-119.907853°
Average velocity to 30 m, m/s: 397
Date: 09/08/2011 (dd/mm/yyyy)
Performed by: Optim SDS.
Type of measurements: ReMi
Depth of measurements: 100 m
Function stepped (y or n): yes
Posted by: Aasha Pancha 09/11/2011 (dd/mm/yyyy)

Depth(m)	Vs(m/s)
0	203.468
2.05	203.468
2.05	352.319
7.7	352.319
7.7	448.993
79.5	448.993
79.5	929.083
100	929.083

Site name: MOGC, Mogul seismic recording station
Lat/long: 39.5285/-119.9348
Lat/long ReMi line start and finish: 39.486257°/-119.959513° 39.485448°/-119.961361°
Average velocity to 30 m, m/s: 382
Date: 05/08/2011 (dd/mm/yyyy)
Performed by: Optim SDS.
Type of measurements: ReMi

Depth of measurements: 100 m
Function stepped (y or n): yes
Posted by: Aasha Pancha 09/11/2011 (dd/mm/yyyy)

Depth(m)	Vs(m/s)
0	140.828
1.6	140.828
1.6	264.094
3.80981	264.094
3.80981	311.094
10.25	311.094
10.25	513.87
38.5	513.87
38.5	805.798
68.75	805.798
68.75	1238.66
100	1238.66

Site name: MOGD, Mogul seismic recording station
Lat/long: 39.4867/-119.9595
Lat/long ReMi line start and finish: 39.522879°/-119.945548° 39.522879°/-119.945548°
Average velocity to 30 m, m/s: 340
Date: 06/08/2011 (dd/mm/yyyy)
Performed by: Optim SDS.
Type of measurements: ReMi
Depth of measurements: 100 m
Function stepped (y or n): yes
Posted by: Aasha Pancha 09/11/2011 (dd/mm/yyyy)

Depth(m)	Vs(m/s)
0	208.949
2.8	208.949
2.8	280.313
7.8	280.313
7.8	341.946
20.1158	341.946
20.1158	462.254
39.25	462.254
39.25	783.11
86	783.11
86	1269.58
100	1269.58

Site name: MOGE, Mogul seismic recording station
Lat/long: 39.5217/-119.9216
Lat/long ReMi line start and finish: 39.528711°/-119.936039° 39.528822°/-119.933907°

Average velocity to 30 m, m/s: 457
Date: 09/08/2011 (dd/mm/yyyy)
Performed by: Optim SDS.
Type of measurements: ReMi
Depth of measurements: 100 m
Function stepped (y or n): yes
Posted by: Aasha Pancha 09/11/2011 (dd/mm/yyyy)

Depth(m)	Vs(m/s)
0	170.582
1.1	170.582
1.1	194.289
6.95	194.289
6.95	411.745
9.6	411.745
9.6	883.11
25.25	883.11
25.25	883.11
90.25	883.11
90.25	1557.27
100	1557.27

Site name: MOGF, Mogul seismic recording station
Lat/long: 39.5362/-119.9492
Lat/long ReMi line start and finish: 39.531111°/-119.935872° 39.529512°/-119.935303°
Average velocity to 30 m, m/s: 296
Date: 07/08/2011 (dd/mm/yyyy)
Performed by: Optim SDS.
Type of measurements: ReMi
Depth of measurements: 100 m
Function stepped (y or n): yes
Posted by: Aasha Pancha 09/11/2011 (dd/mm/yyyy)

Depth(m)	Vs(m/s)
0	170.022
5.2	170.022
5.2	341.946
28.665	341.946
28.665	491.163
75.5	491.163
75.5	776.622
100	776.622

Site name: MOGL, Mogul seismic recording station
Lat/long: 39.52027/-119.93066
Lat/long ReMi line start and finish: 39.531870°/-119.930815° 39.530619°/-119.929437°

Average velocity to 30 m, m/s: 326
Date: 07/08/2011 (dd/mm/yyyy)
Performed by: Optim SDS.
Type of measurements: ReMi
Depth of measurements: 100 m
Function stepped (y or n): yes
Posted by: Aasha Pancha 09/11/2011 (dd/mm/yyyy)

Depth(m)	Vs(m/s)
0	176.063
9.30357	176.063
9.30357	521.365
31.6824	521.365
31.6824	630.59
55.3185	630.59
55.3185	795.414
82.9778	795.414
82.9778	1146.2
100.579	1146.2

Site name: MOGN, Mogul seismic recording station
Lat/long: 39.5481/-119.8836
Lat/long ReMi line start and finish: 39.536208°/-119.949028° 39.535074°/-119.950575°
Average velocity to 30 m, m/s: 413
Date: 07/08/2011 (dd/mm/yyyy)
Performed by: Optim SDS.
Type of measurements: ReMi
Depth of measurements: 100 m
Function stepped (y or n): yes
Posted by: Aasha Pancha 09/11/2011 (dd/mm/yyyy)

Depth(m)	Vs(m/s)
0	241.834
5.44041	241.834
5.44041	335.142
10.75	335.142
10.75	482.998
25.6477	482.998
25.6477	1042.06
50.75	1042.06
50.75	1451.66
100	1451.66

Site name: MOGP, Mogul seismic recording station
Lat/long: 39.5725/-119.9081
Lat/long ReMi line start and finish: 39.543588°/-119.918360°; 39.541937°/-119.918346°

Average velocity to 30 m, m/s: 400
Date: 07/08/2011 (dd/mm/yyyy)
Performed by: Optim SDS.
Type of measurements: ReMi
Depth of measurements: 100 m
Function stepped (y or n): yes
Posted by: Aasha Pancha 09/11/2011 (dd/mm/yyyy)

Depth(m)	Vs(m/s)
0	189.9879
1.142944	189.9879
1.142944	280.5684
6.286188	280.5684
6.286188	362.9142
12.6181	362.9142
12.6181	465.8465
23.38462	465.8465
23.38462	626.4209
37.96857	626.4209
37.96857	778.7608
63.86766	778.7608
63.86766	1070.328
85.49223	1070.328
85.49223	1424.179
100.579	1424.179

Site name: MOGR, Mogul seismic recording station
Lat/long: 39.5084/-119.907
Lat/long ReMi line start and finish: 39.547959°/-119.882618°; 39.549615°-119.882592°
Average velocity to 30 m, m/s: 438
Date: 09/08/2011 (dd/mm/yyyy)
Performed by: Optim SDS.
Type of measurements: ReMi
Depth of measurements: 100 m
Function stepped (y or n): yes
Posted by: Aasha Pancha 09/11/2011 (dd/mm/yyyy)

Depth(m)	Vs(m/s)
0	230.8725
4.9	230.8725
4.9	477.5168
23.46845	477.5168
23.46845	737.5878
50.28955	737.5878
50.28955	998.2103
91.52697	998.2103
91.52697	1502.461

100	1502.461

Site name: MOGW, Mogul seismic recording station
Lat/long: 39.5301/-119.936
Lat/long ReMi line start and finish: 39.573579°/-119.909399°; 39.572192°-119.908256°
Average velocity to 30 m, m/s: 499
Date: 05/08/2011 (dd/mm/yyyy)
Performed by: Optim SDS.
Type of measurements: ReMi
Depth of measurements: 100 m
Function stepped (y or n): yes
Posted by: Aasha Pancha 09/11/2011 (dd/mm/yyyy)

Depth(m)	Vs(m/s)
0	108.4026
1.691557	108.4026
1.691557	245.8205
4.754648	245.8205
4.754648	291.1633
7.314843	291.1633
7.314843	850.2237
10.66748	850.2237
10.66748	976.2864
72.91984	976.2864
72.91984	1184.564
100	1184.564

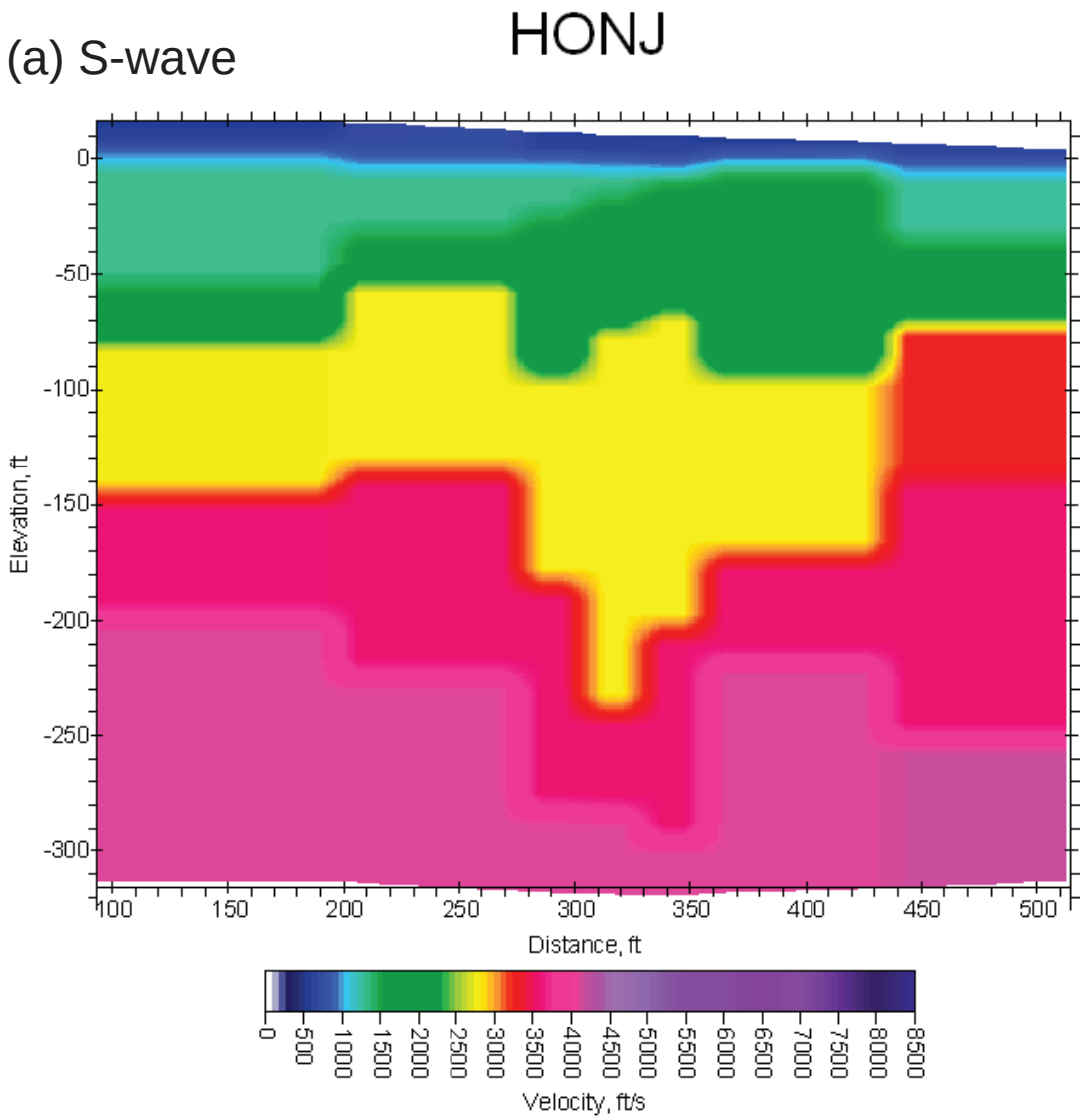

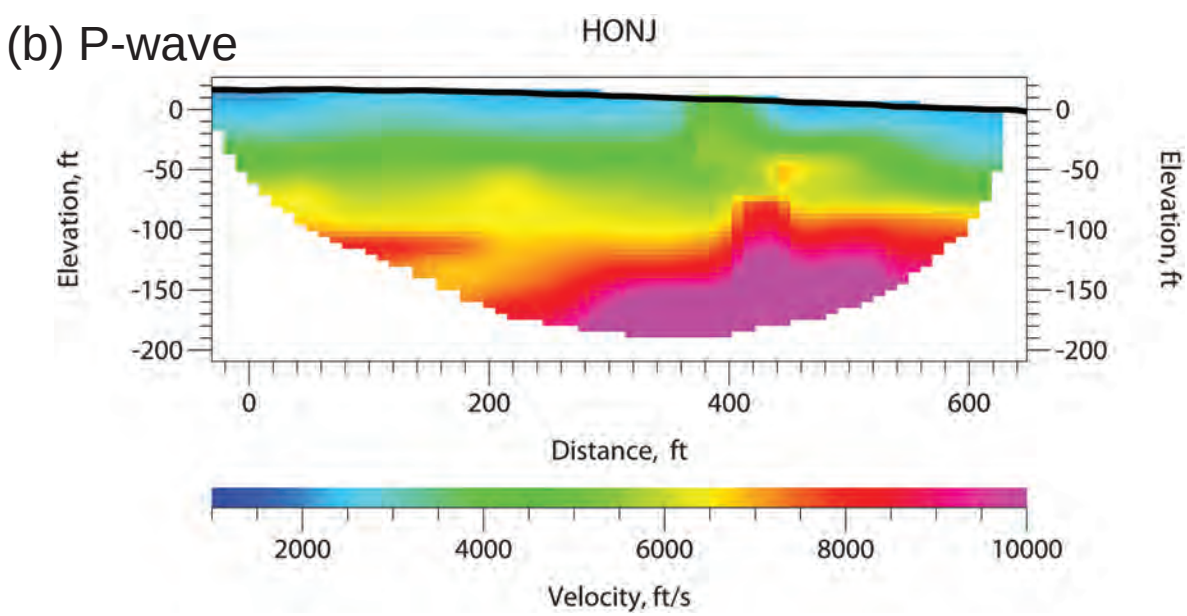

Appendix 2.1 2D velocity representations for the seismic station HONJ. Top = shear-wave velocity section from obtained from 1D ReMi soundings along the array. Bottom = P-wave refraction tomography.

(a) S-wave

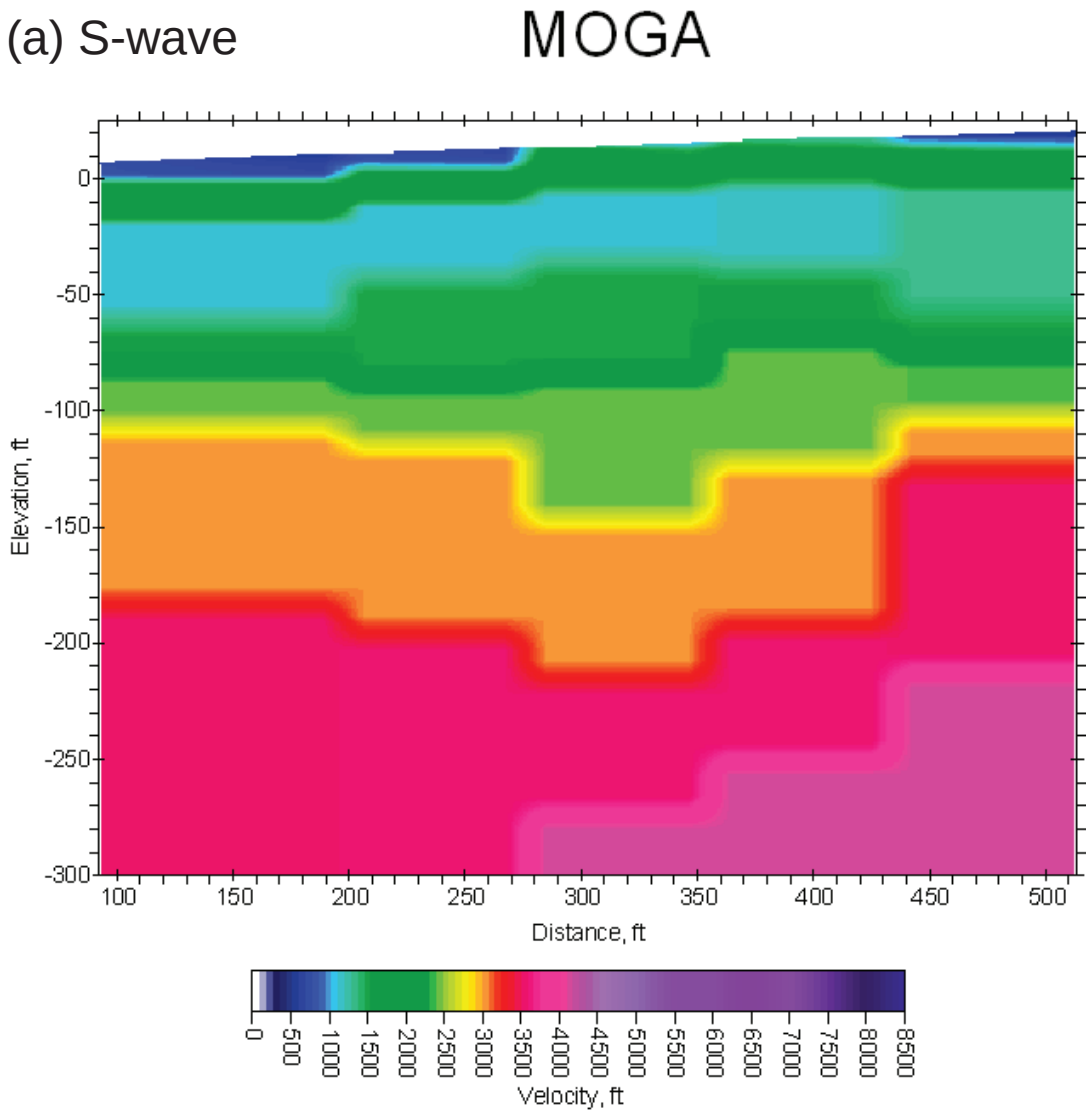

(b) P-wave

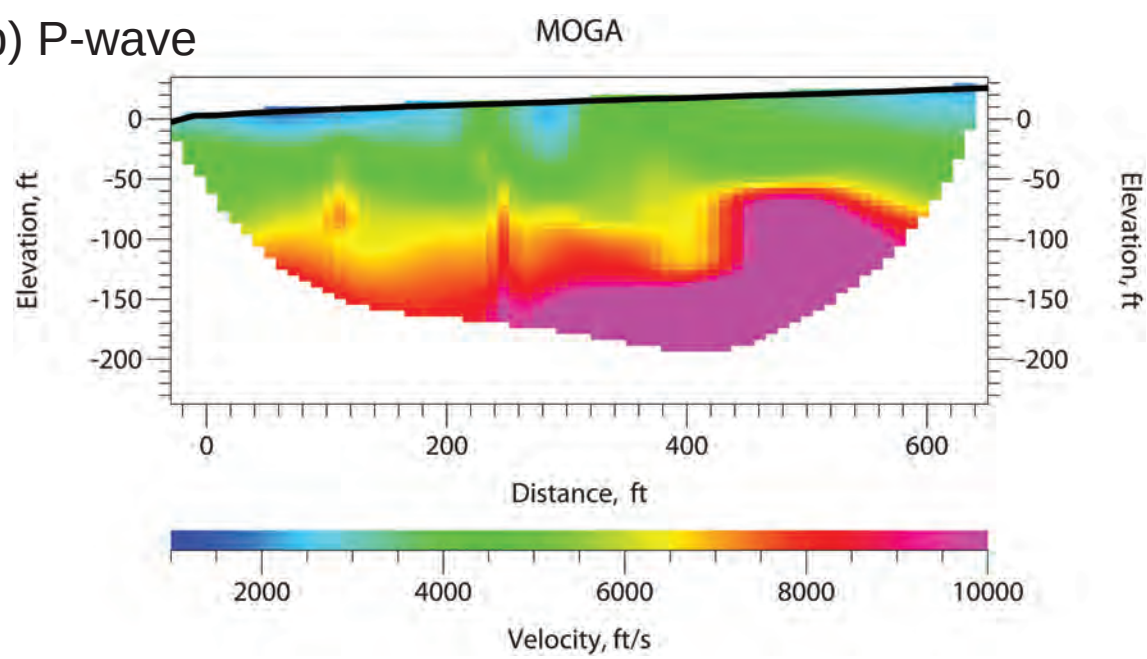

Appendix 2.2 2D velocity representations for the seismic station MOGA. Top = shear-wave velocity section from obtained from 1D ReMi soundings along the array. Bottom = P-wave refraction tomography.

(a) S-wave

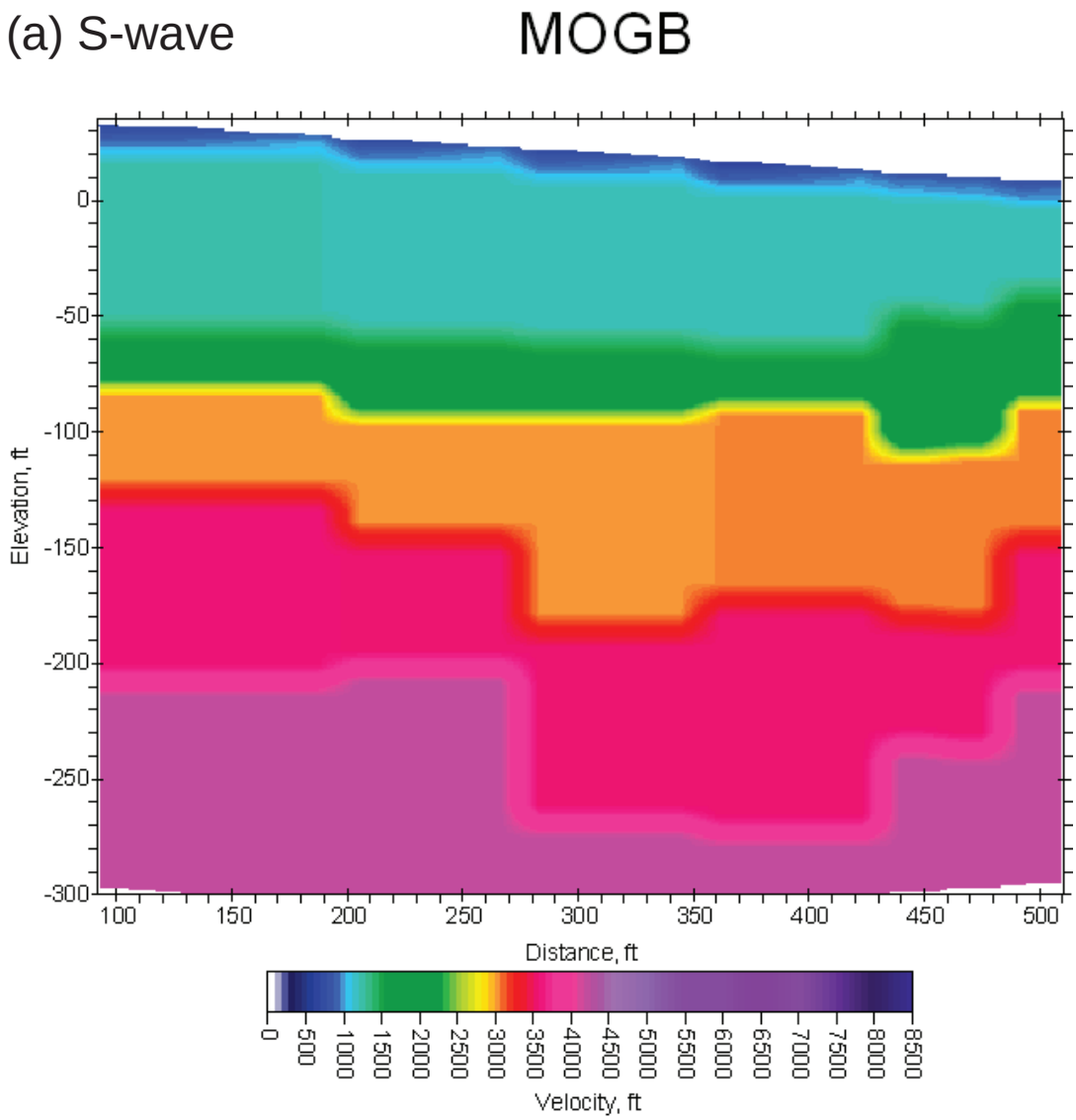

(b) P-wave

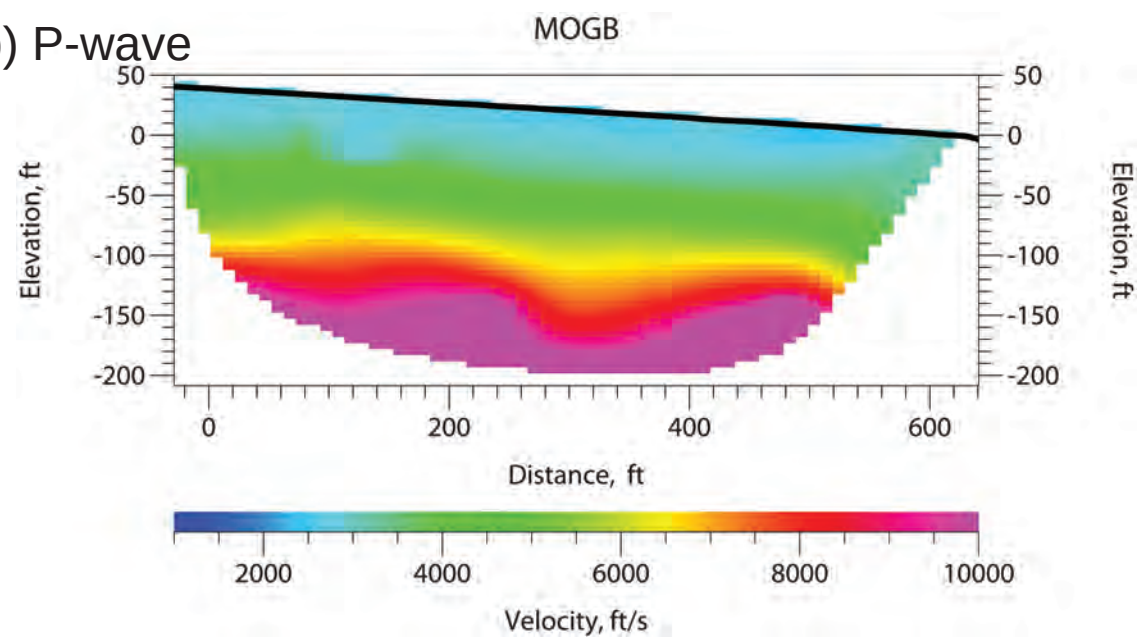

Appendix 2.3 2D velocity representations for the seismic station MOGB. Top = shear-wave velocity section from obtained from 1D ReMi soundings along the array. Bottom = P-wave refraction tomography.

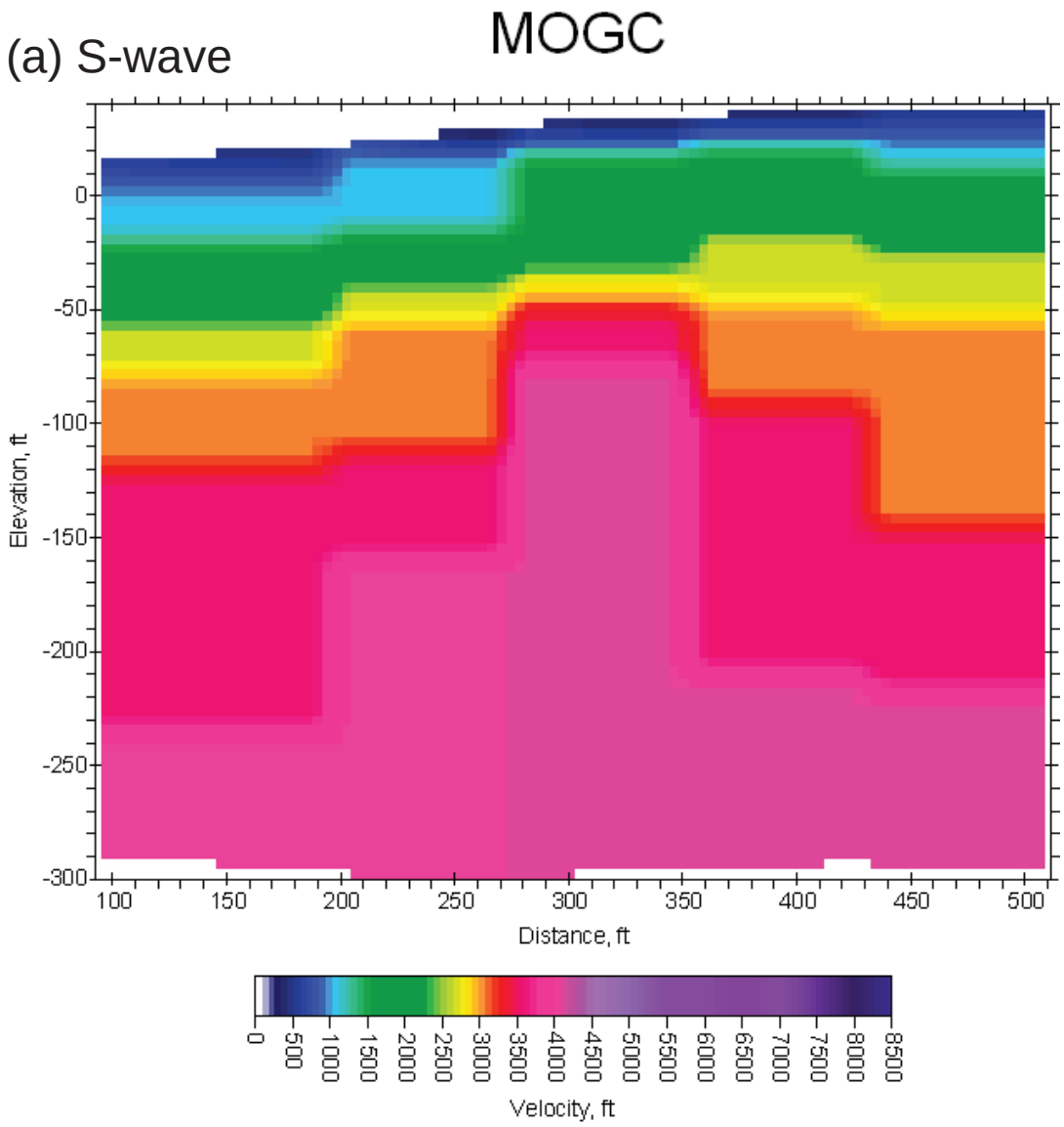

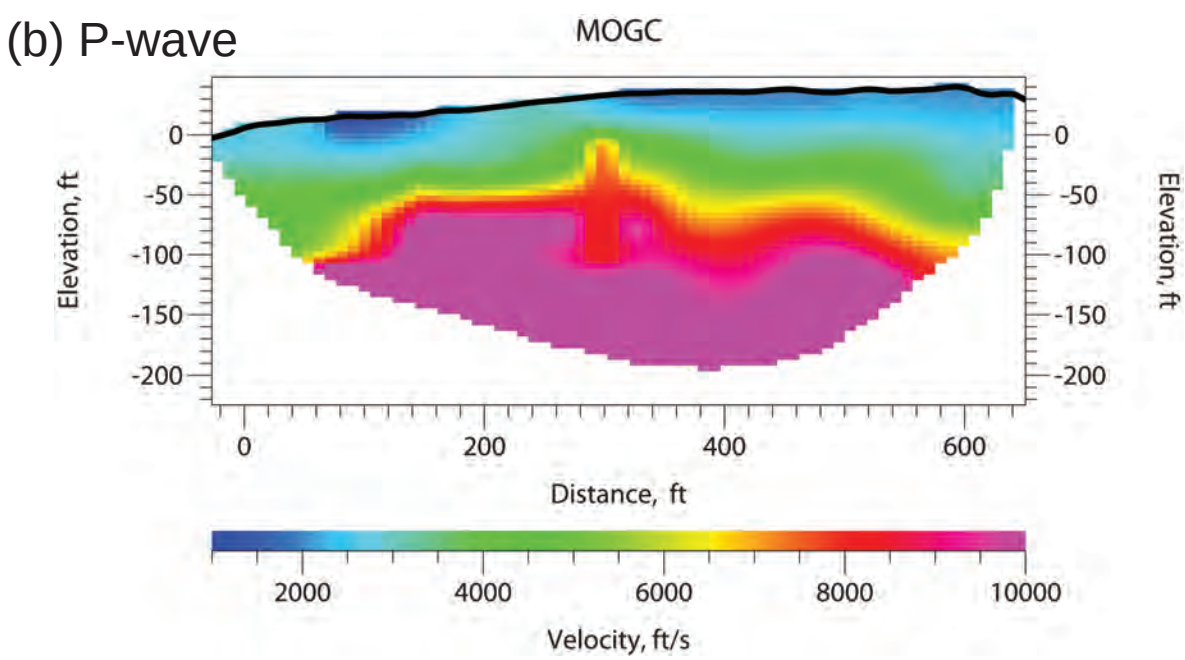

Appendix 2.4 2D velocity representations for the seismic station MOGC. Top = shear-wave velocity section from obtained from 1D ReMi soundings along the array. Bottom = P-wave refraction tomography.

(a) S-wave

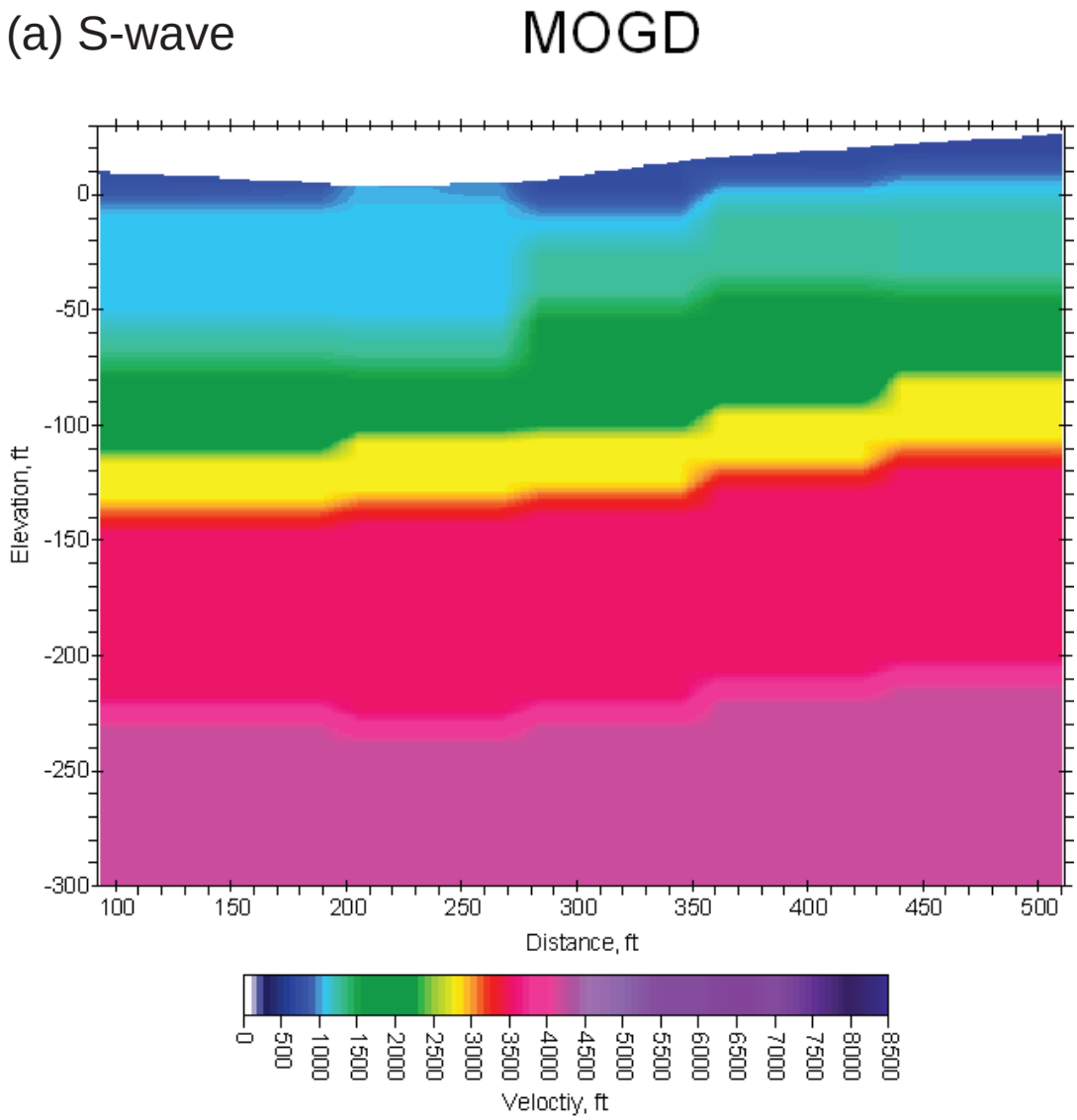

(b) P-wave

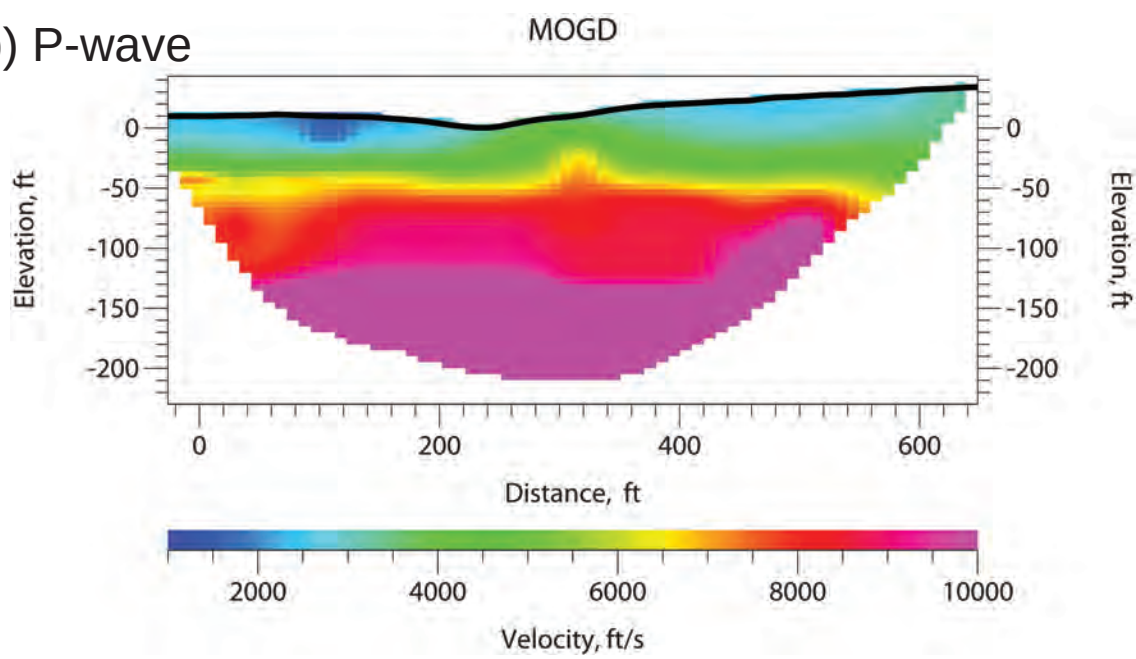

Appendix 2.5 2D velocity representations for the seismic station MOGD. Top = shear-wave velocity section from obtained from 1D ReMi soundings along the array. Bottom = P-wave refraction tomography.

(a) S-wave

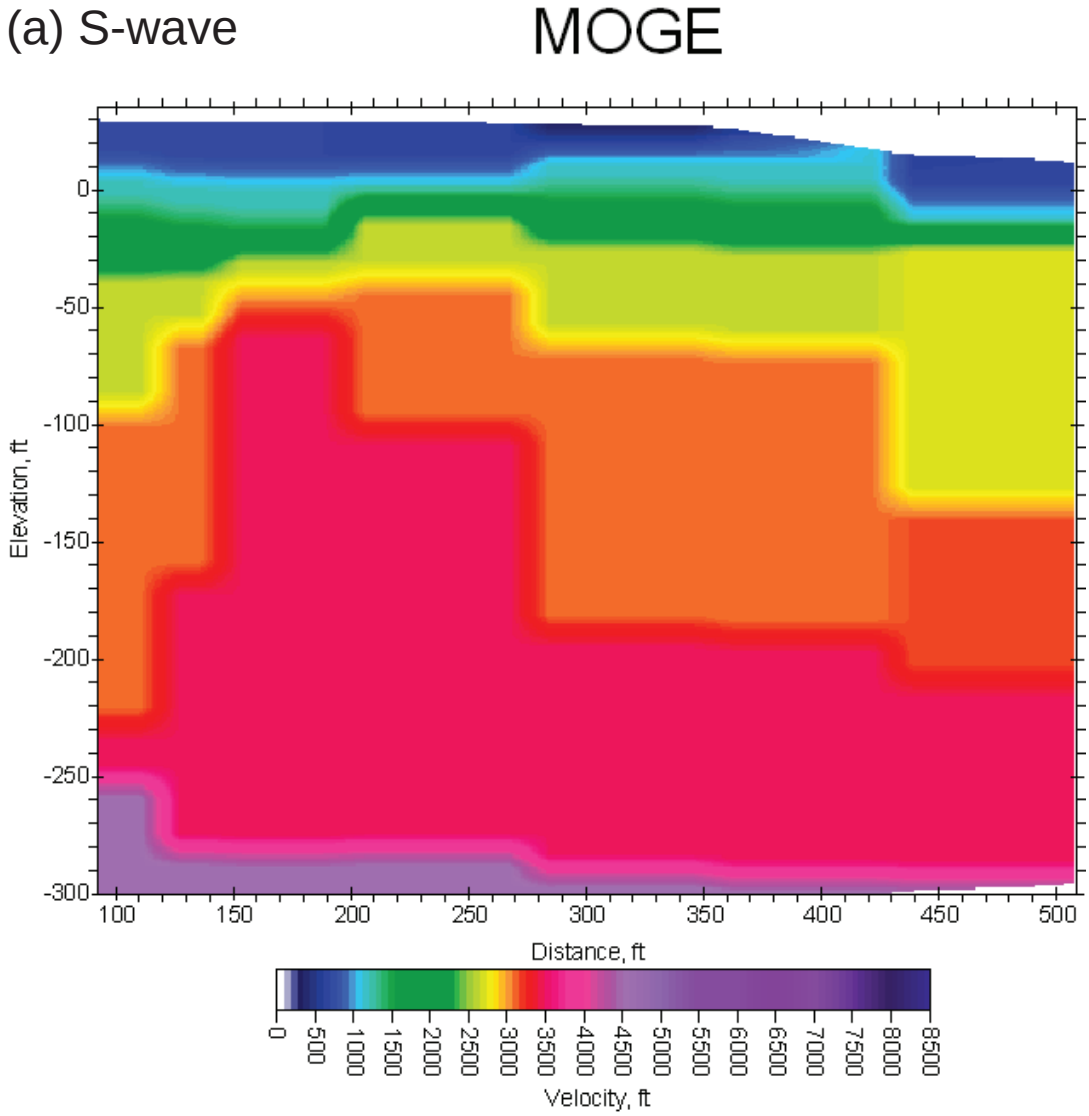

(b) P-wave

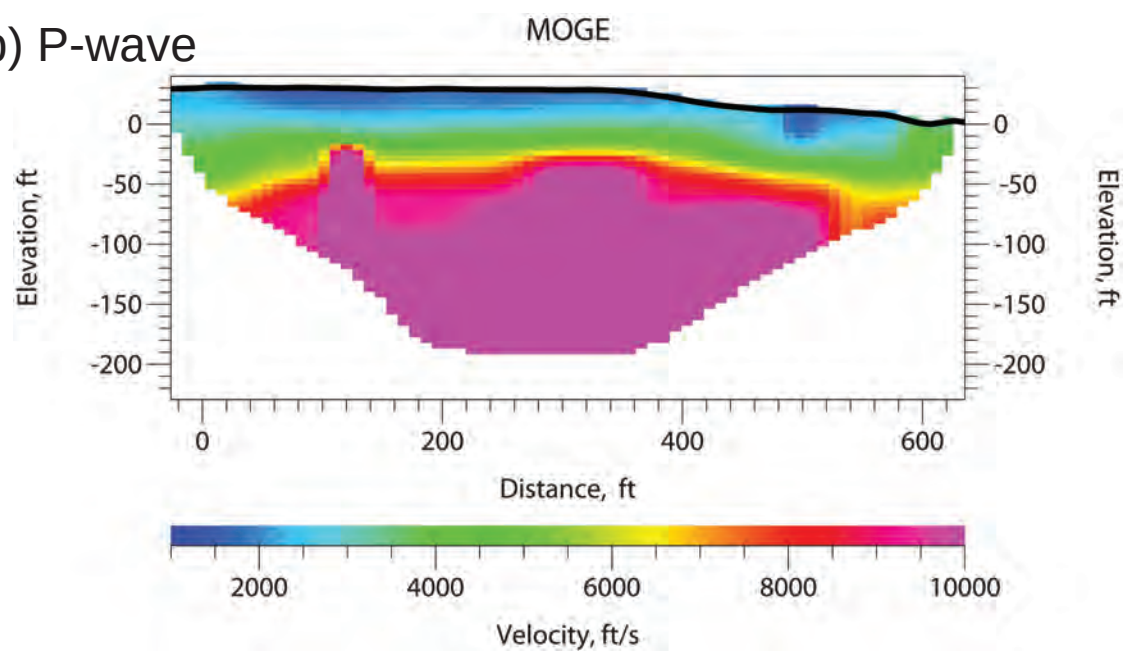

Appendix 2.6 2D velocity representations for the seismic station MOGE. Top = shear-wave velocity section from obtained from 1D ReMi soundings along the array. Bottom = P-wave refraction tomography.

(a) S-wave

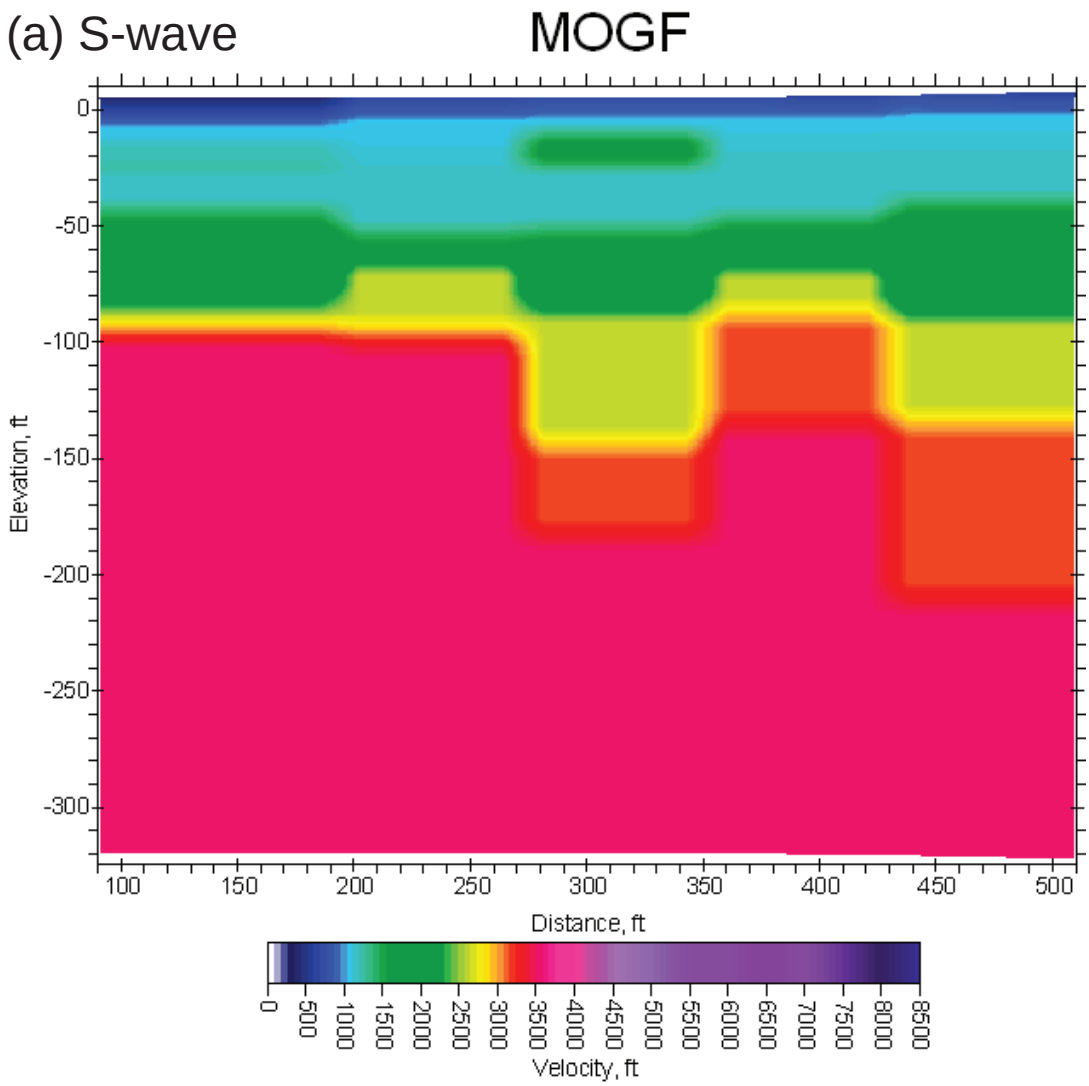

(b) P-wave

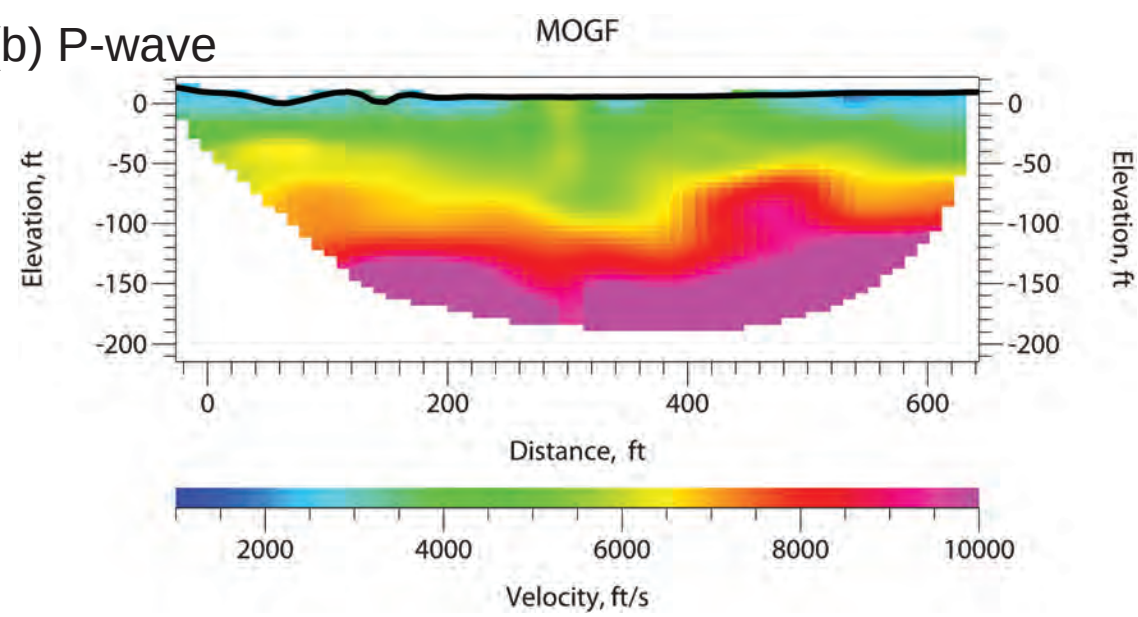

Appendix 2.7 2D velocity representations for the seismic station MOGF. Top = shear-wave velocity section from obtained from 1D ReMi soundings along the array. Bottom = P-wave refraction tomography.

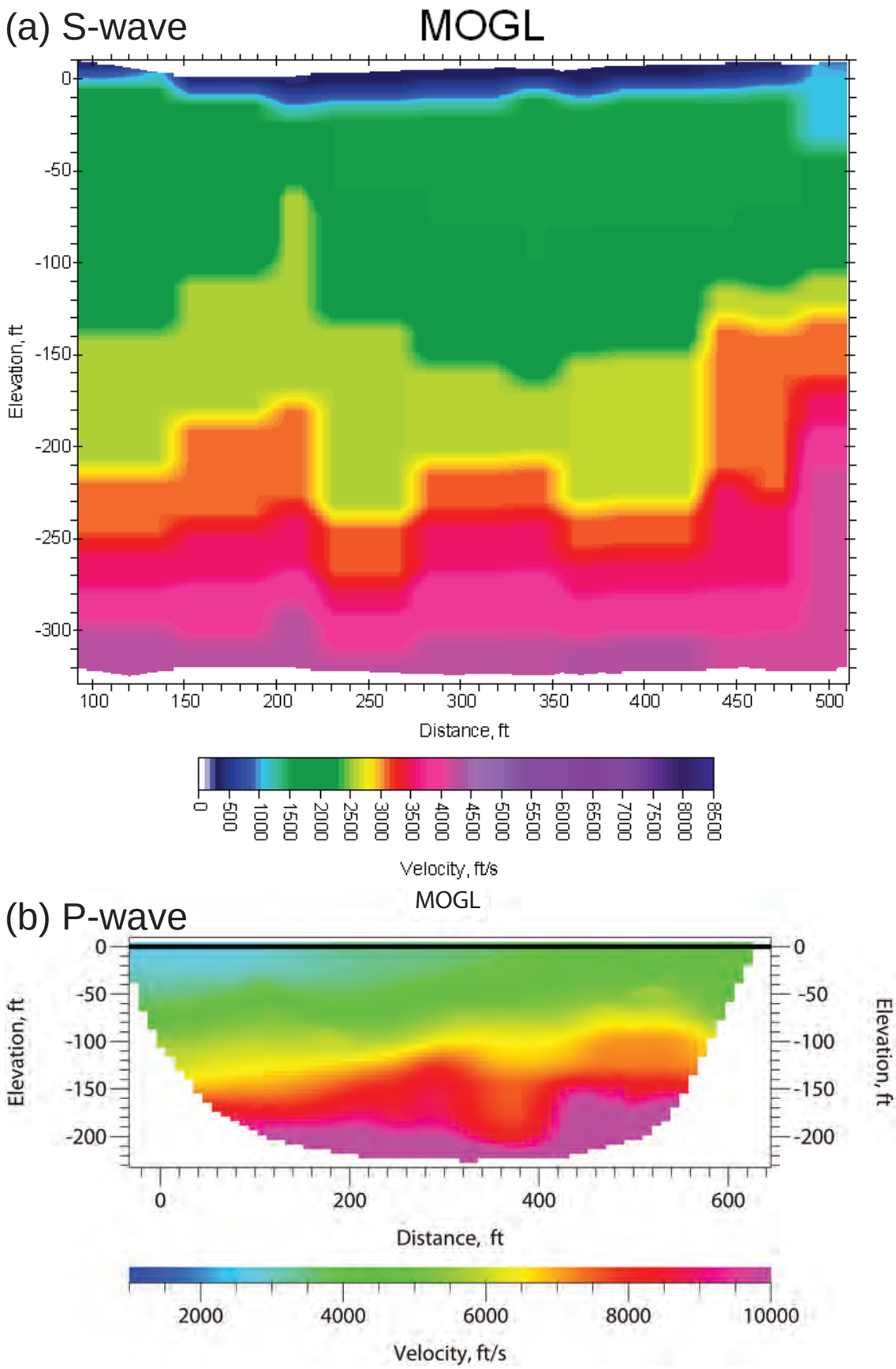

Appendix 2.8 2D velocity representations for the seismic station MOGL. Top = shear-wave velocity section from obtained from 1D ReMi soundings along the array. Bottom = P-wave refraction tomography.

(a) S-wave

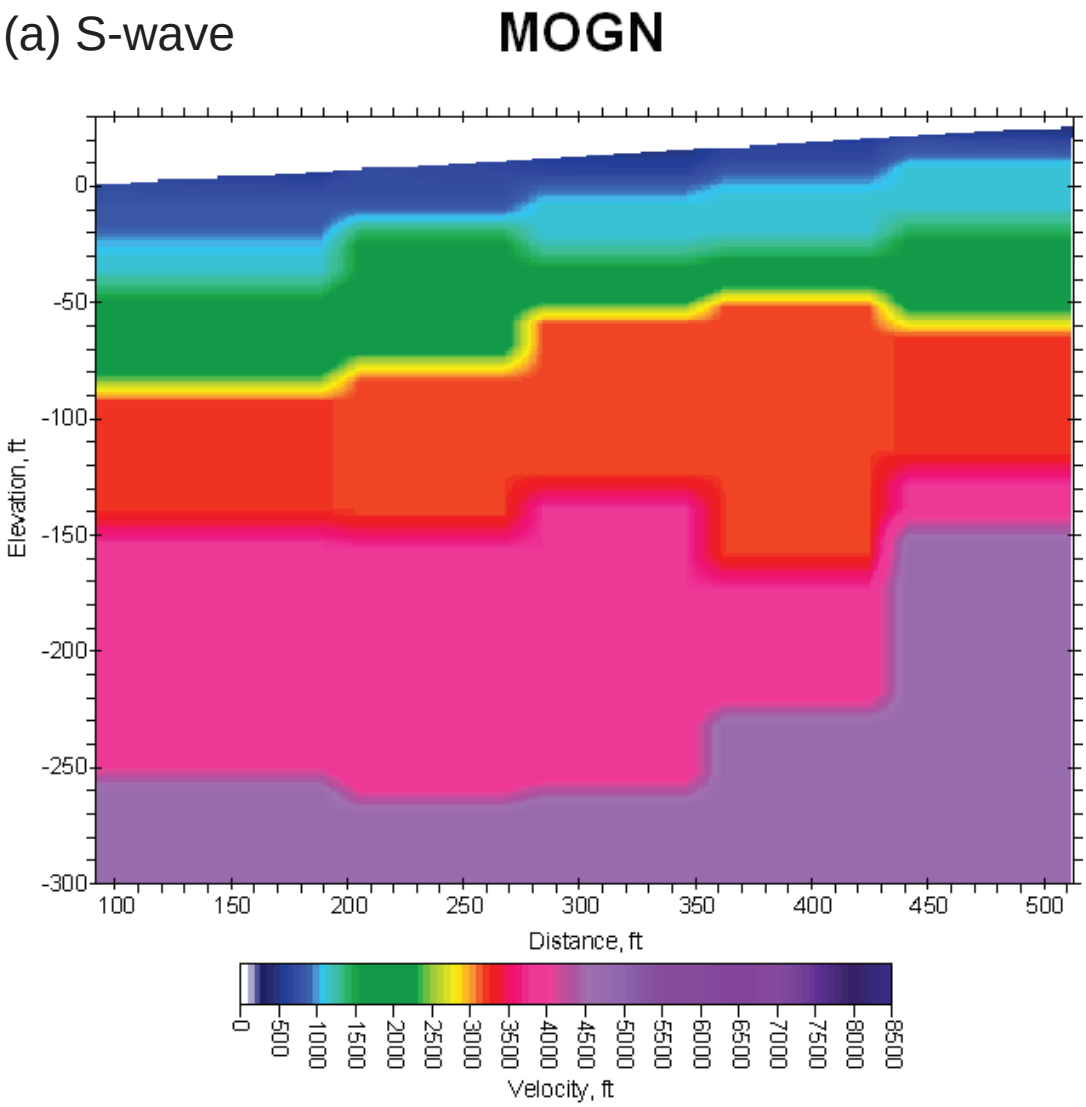

(b) P-wave

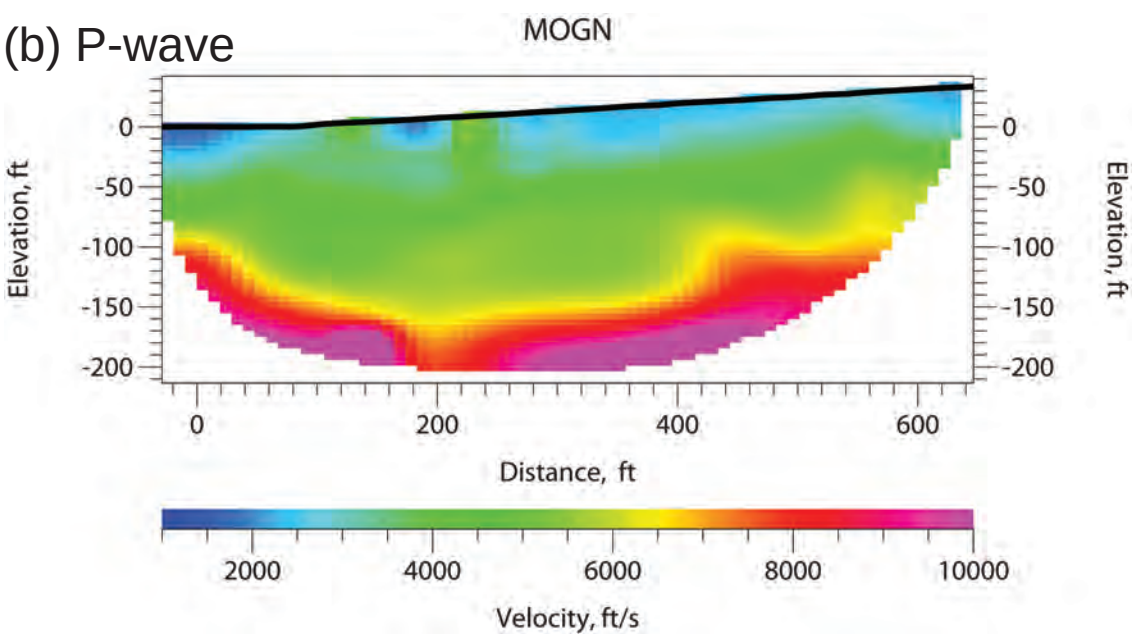

Appendix 2.9 2D velocity representations for the seismic station MOGN. Top = shear-wave velocity section from obtained from 1D ReMi soundings along the array. Bottom = P-wave refraction tomography.

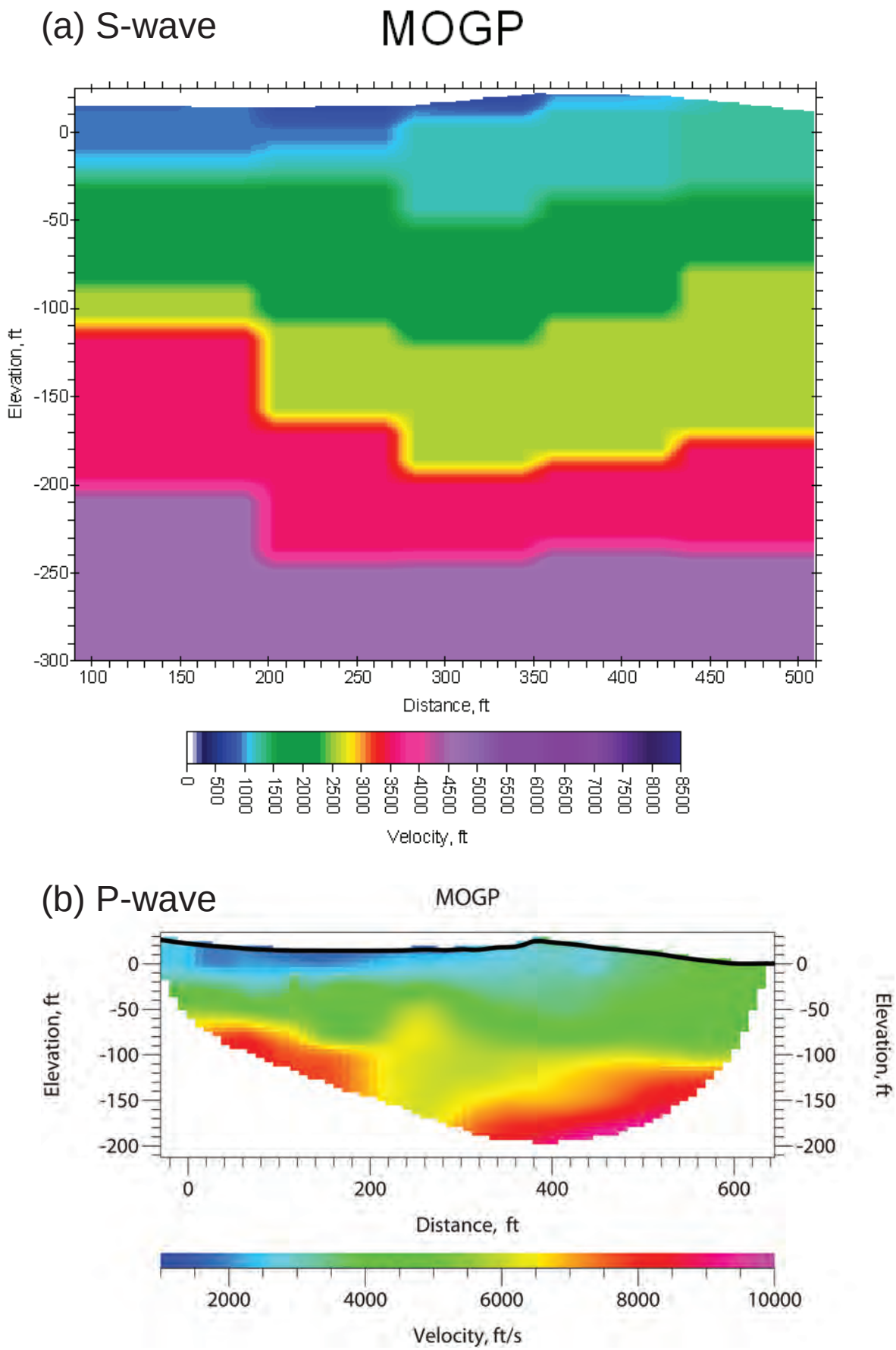

Appendix 2.10 2D velocity representations for the seismic station MOGP. Top = shear-wave velocity section from obtained from 1D ReMi soundings along the array. Bottom = P-wave refraction tomography.

(a) S-wave

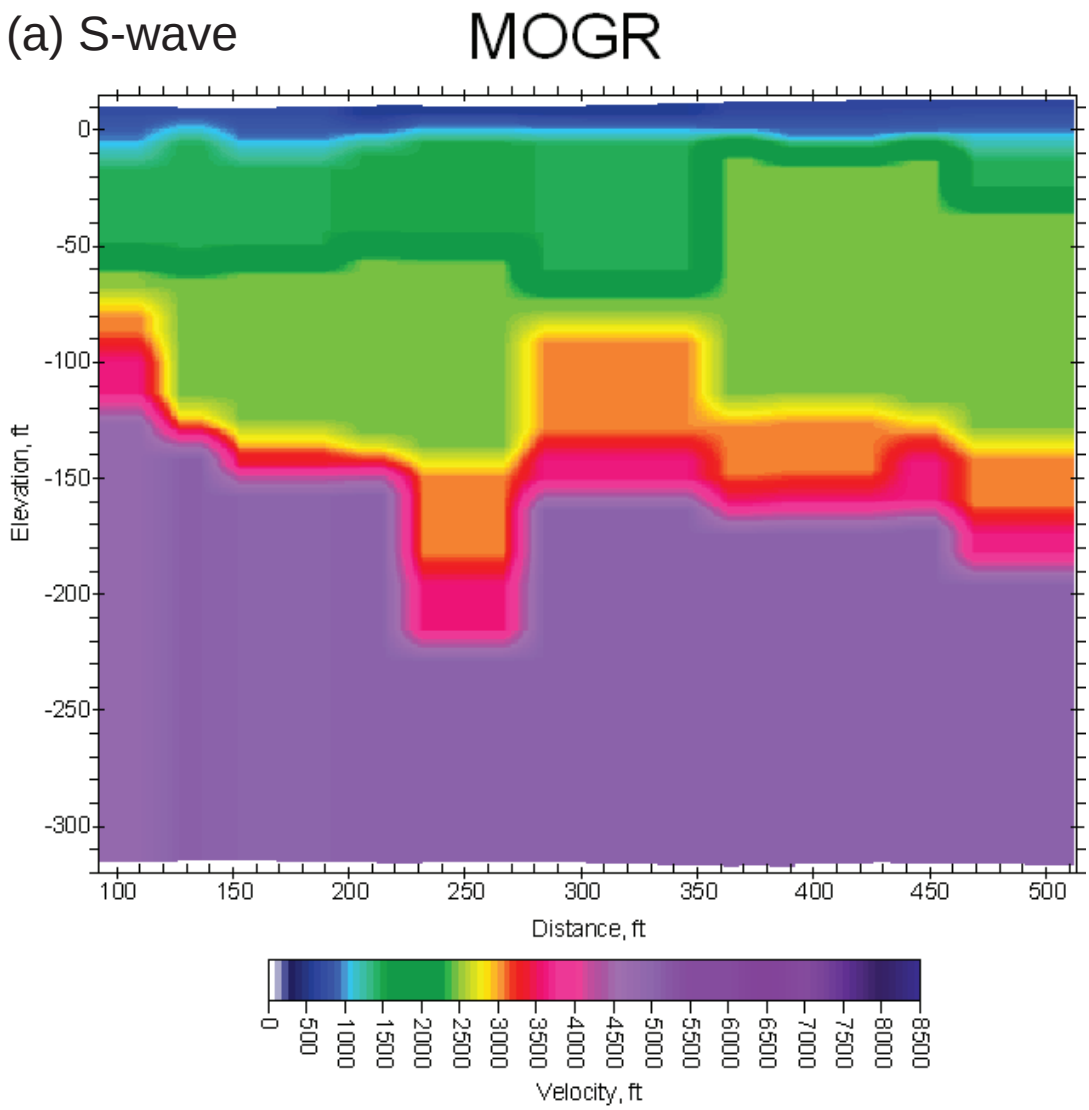

(b) P-wave

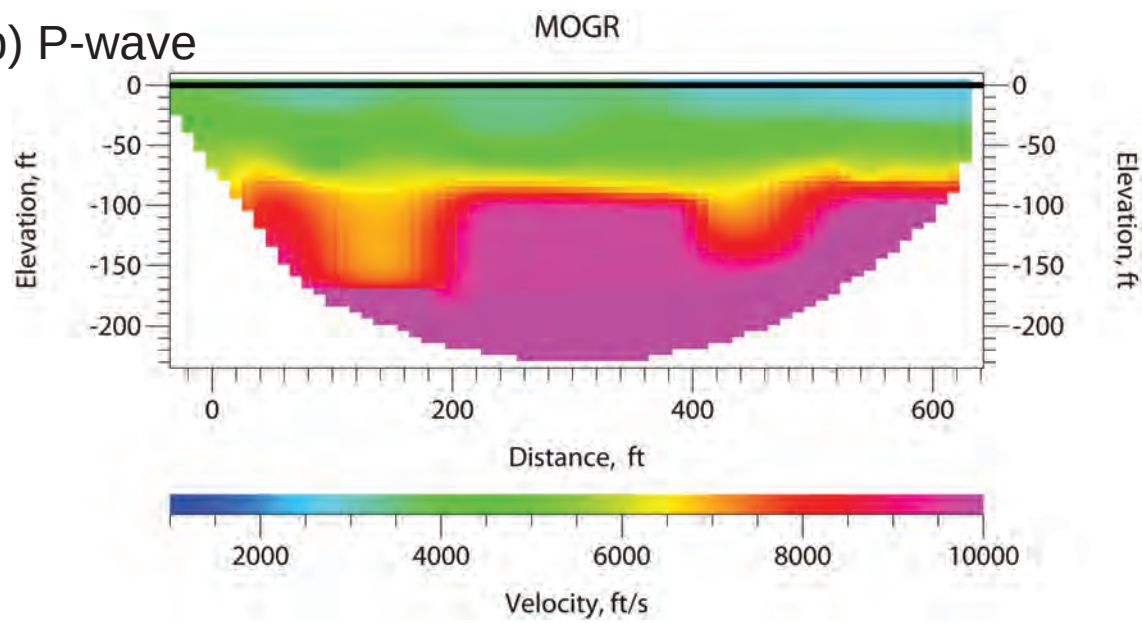

Appendix 2.11 2D velocity representations for the seismic station MOGR. Top = shear-wave velocity section from obtained from 1D ReMi soundings along the array. Bottom = P-wave refraction tomography.

(a) S-wave

MOGW

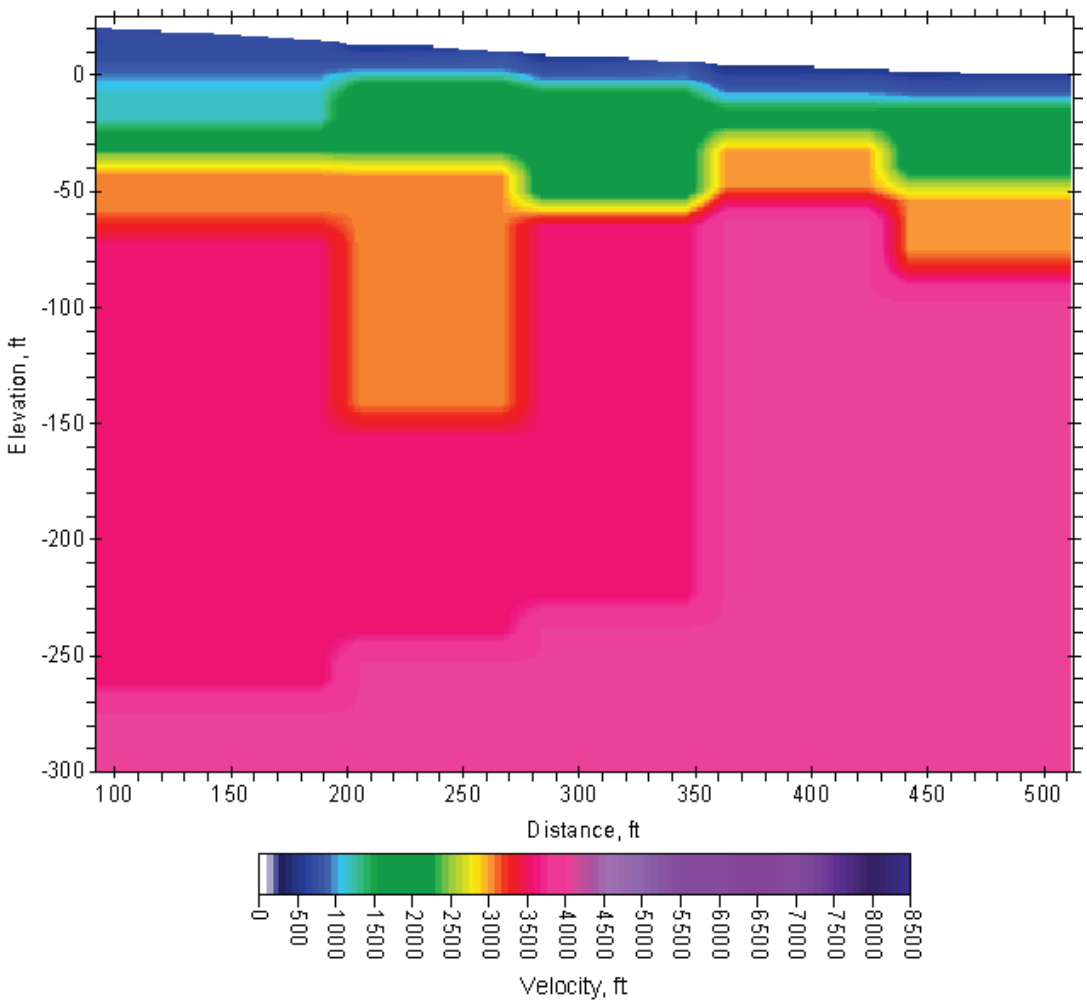

(b) P-wave

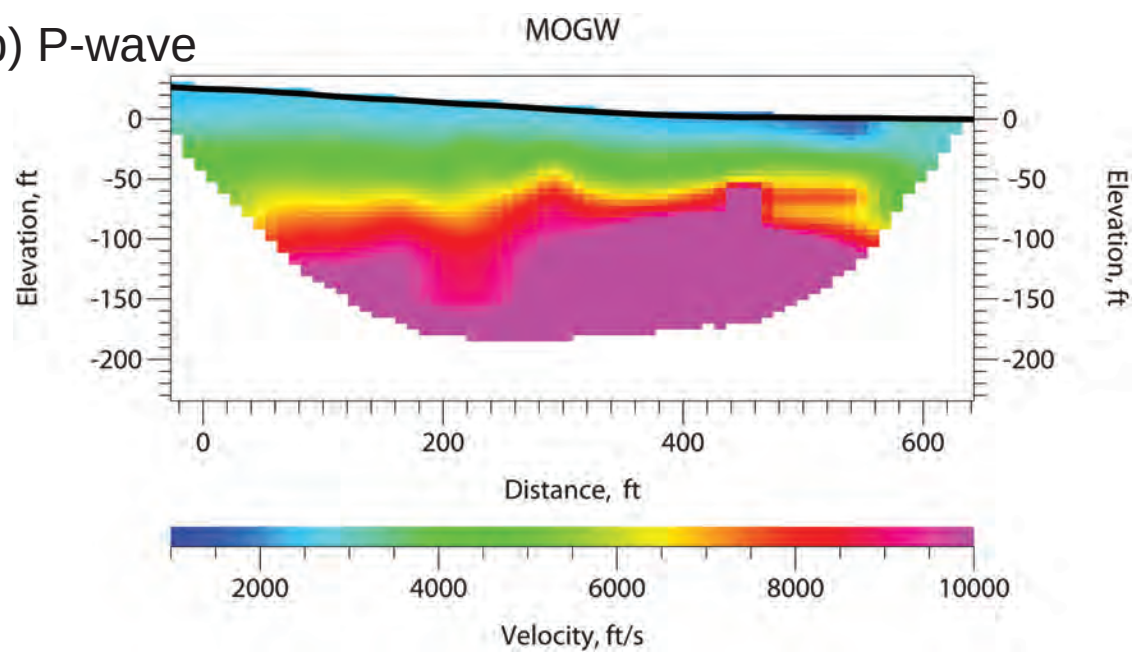

Appendix 2.12 2D velocity representations for the seismic station MOGW. Top = shear-wave velocity section from obtained from 1D ReMi soundings along the array. Bottom = P-wave refraction tomography.

Appendix 3.1: Horizontal spectral ratios with respect to the reference site RFNV for the station HVGC. The top plot shows the amplification level on a log scale while the bottom plots illustrates the amplification level on a linear scale. The number of events used in the analysis is given in the title of each plot.

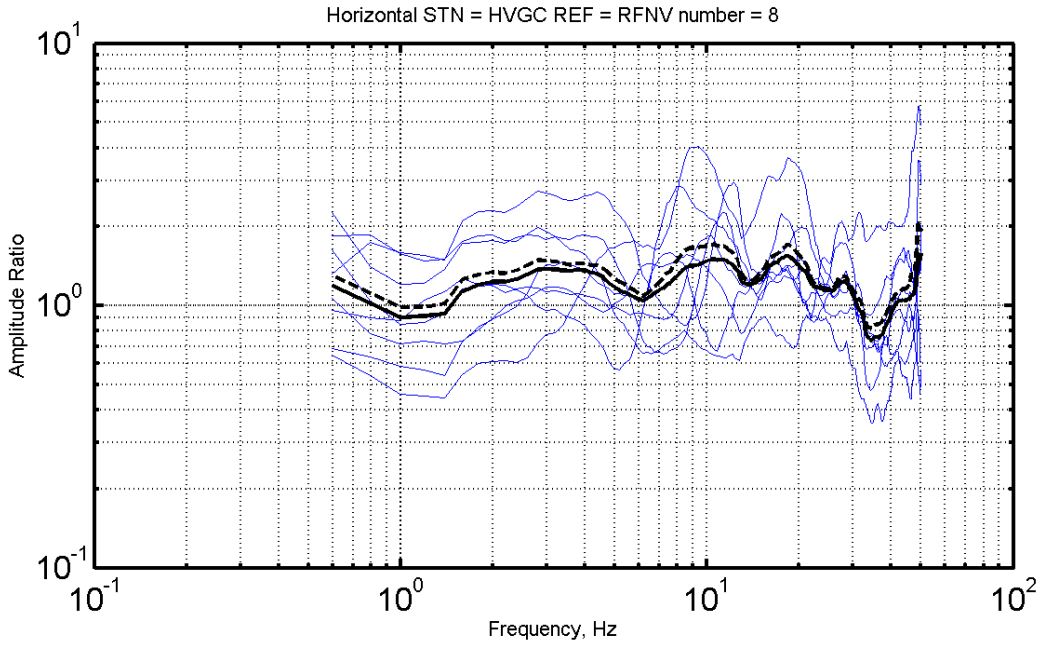

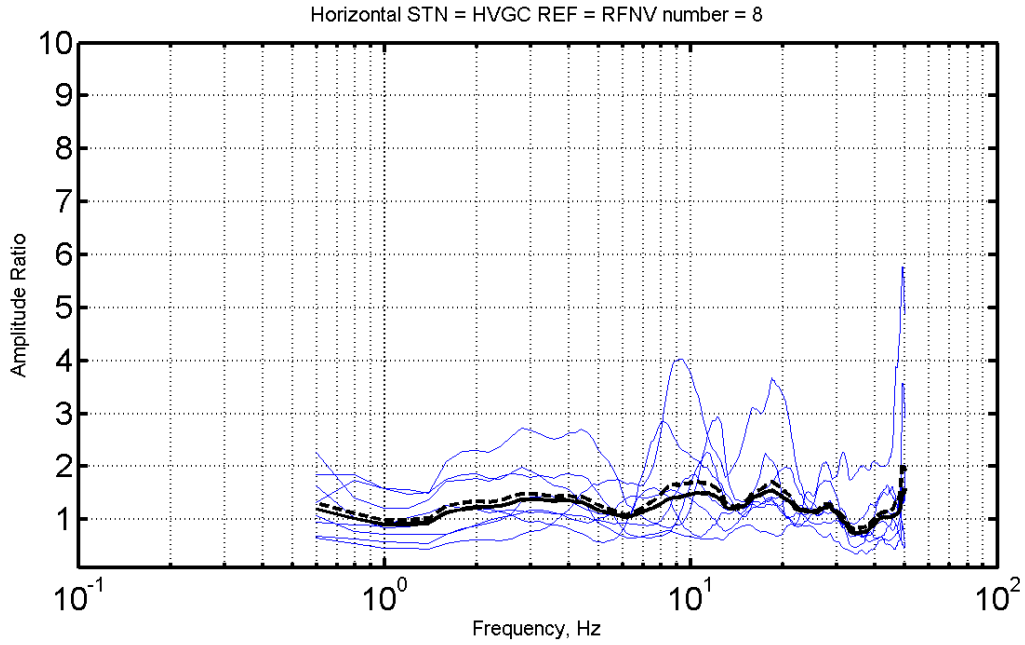

Appendix 3.2: Horizontal spectral ratios with respect to the reference site RFNV for the station NMHS. The top plot shows the amplification level on a log scale while the bottom plots illustrates the amplification level on a linear scale. The number of events used in the analysis is given in the title of each plot.

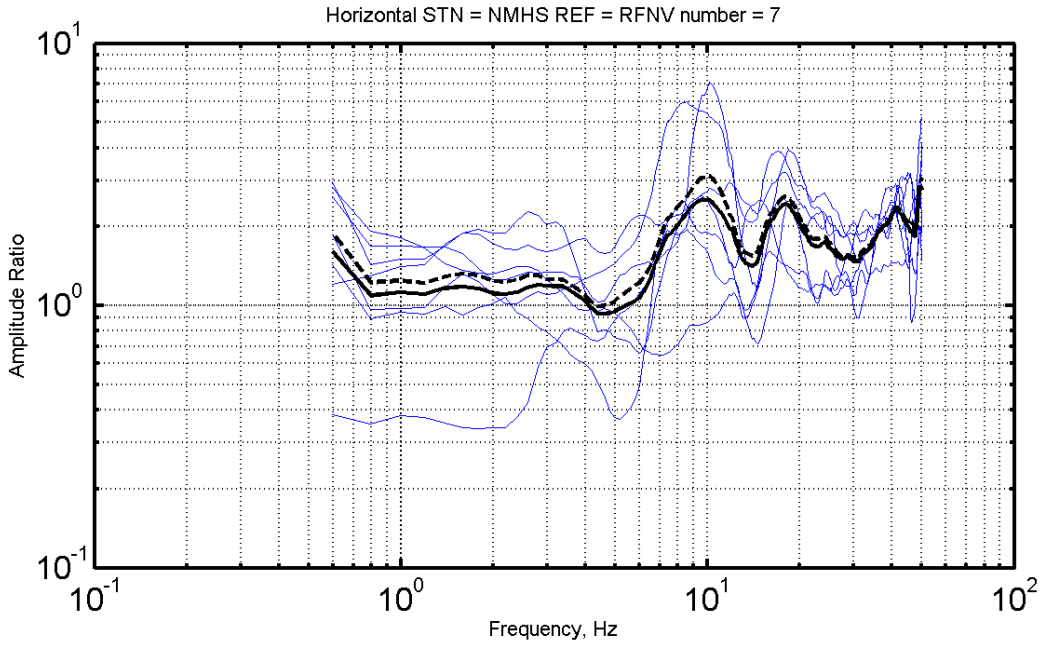

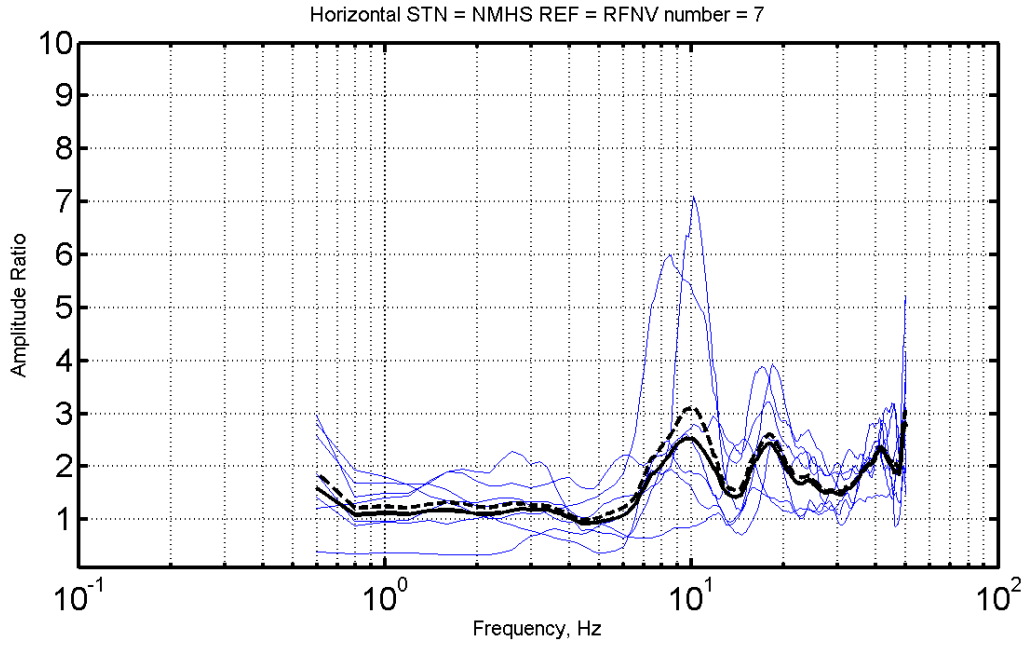

Appendix 3.3: Horizontal spectral ratios with respect to the reference site RFNV for the station NOAA. The top plot shows the amplification level on a log scale while the bottom plots illustrates the amplification level on a linear scale. The number of events used in the analysis is given in the title of each plot.

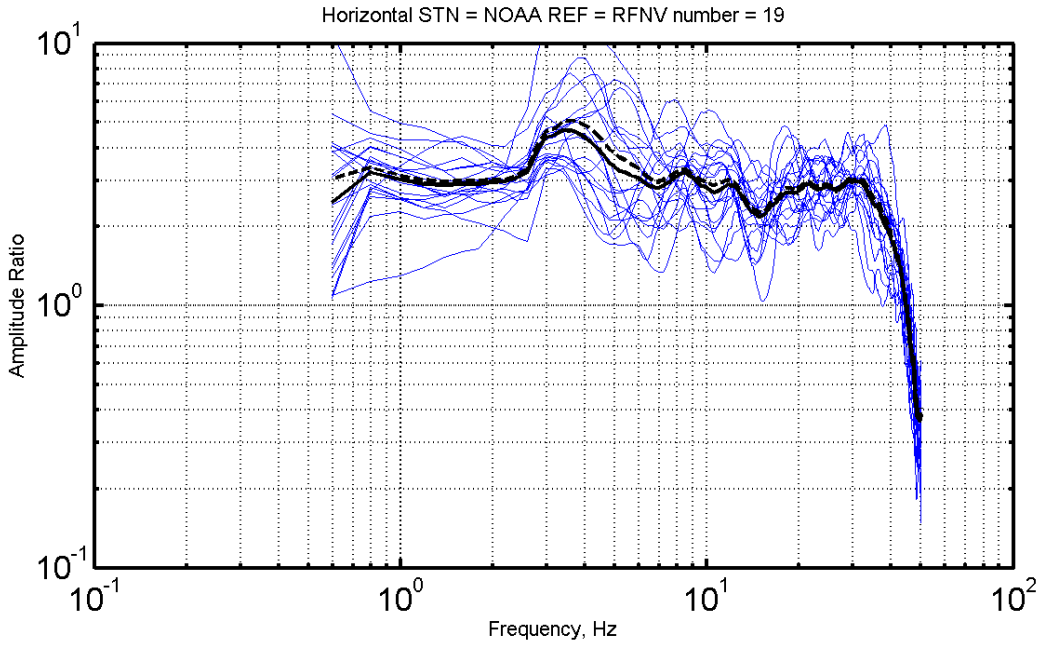

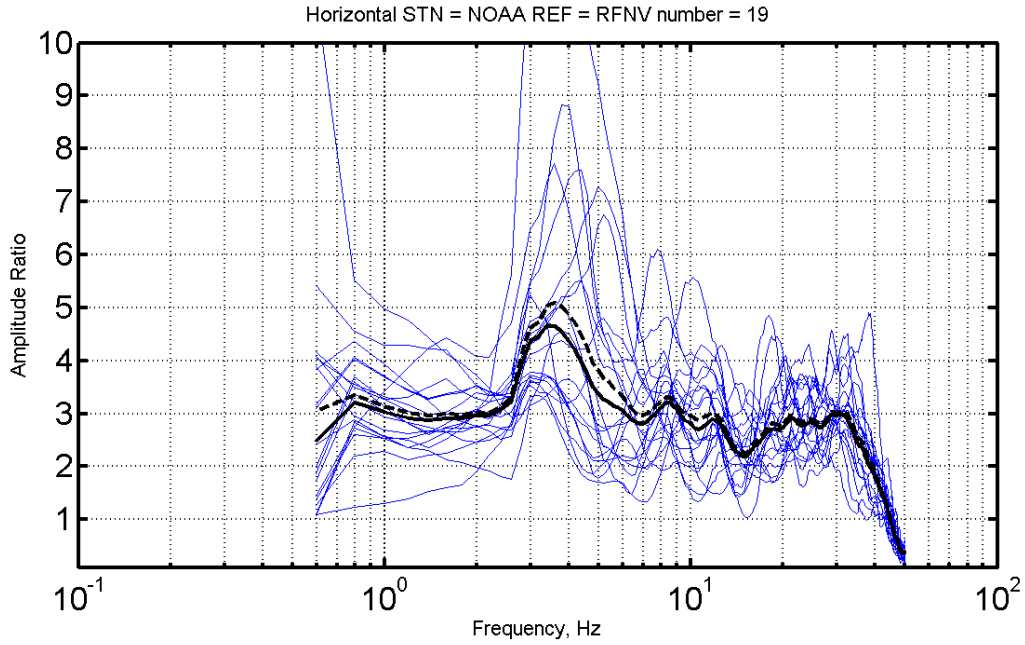

Appendix 3.4: Horizontal spectral ratios with respect to the reference site RFNV for the station PICO. The top plot shows the amplification level on a log scale while the bottom plots illustrates the amplification level on a linear scale. The number of events used in the analysis is given in the title of each plot.

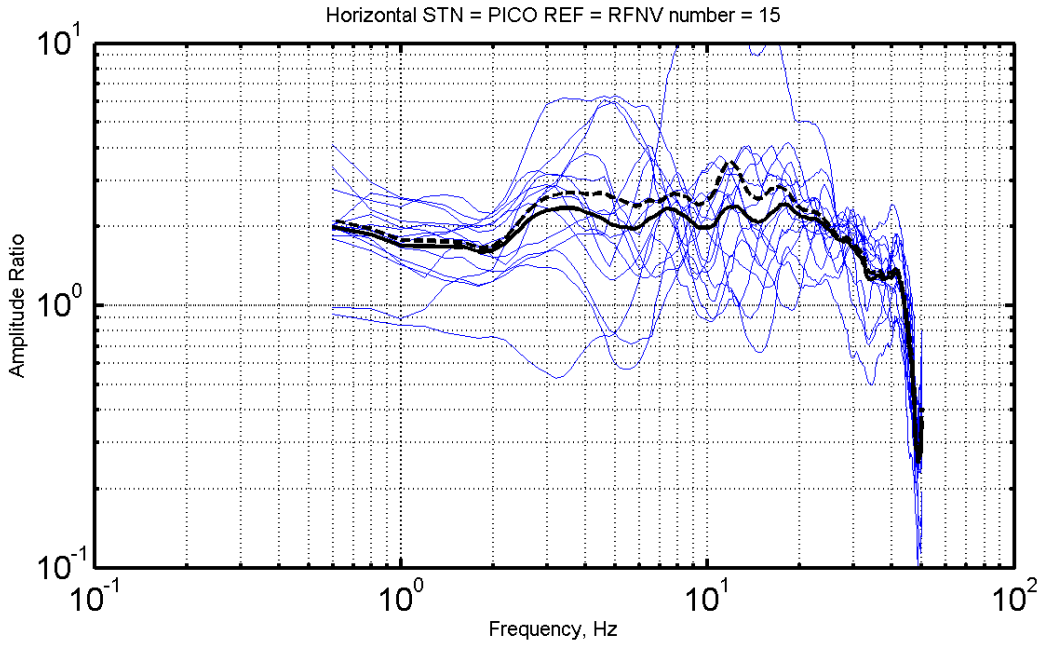

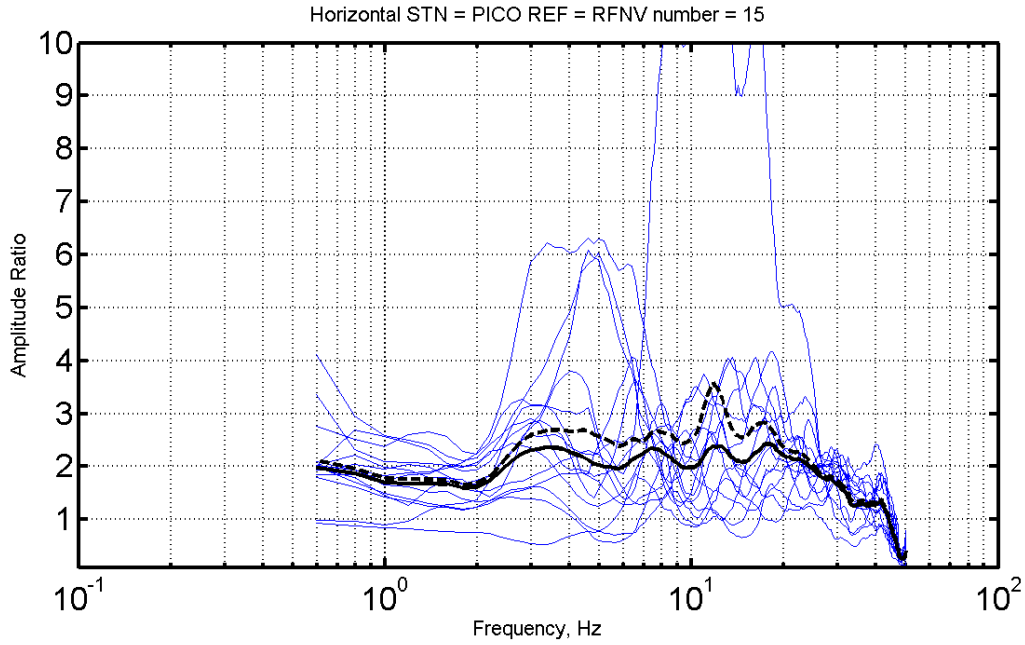

Appendix 3.5: Horizontal spectral ratios with respect to the reference site RFNV for the station RF05. The top plot shows the amplification level on a log scale while the bottom plots illustrates the amplification level on a linear scale. The number of events used in the analysis is given in the title of each plot.

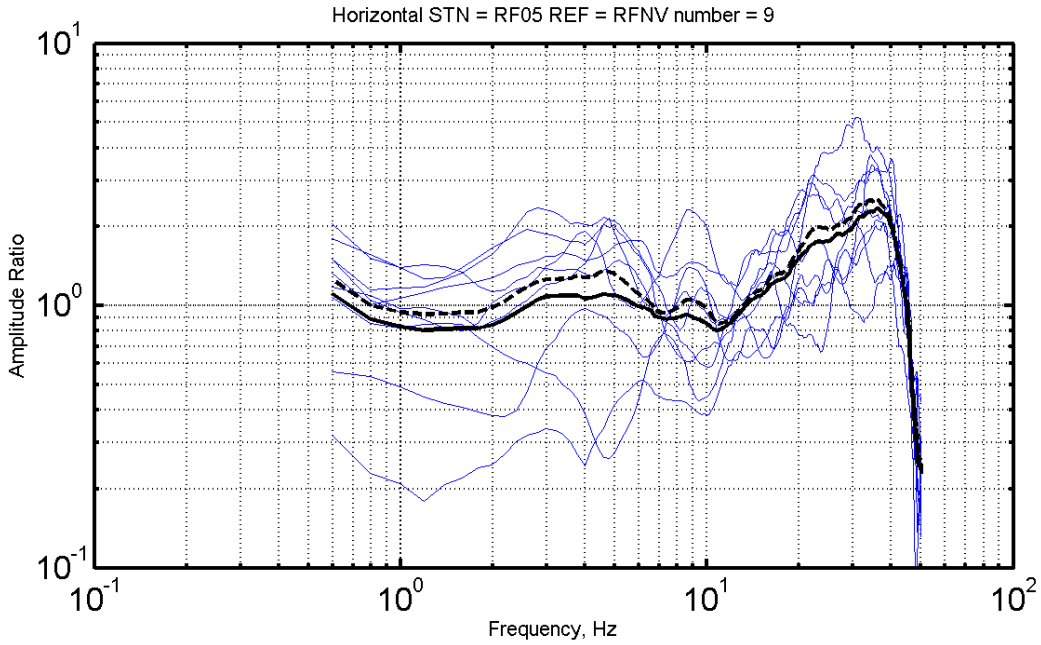

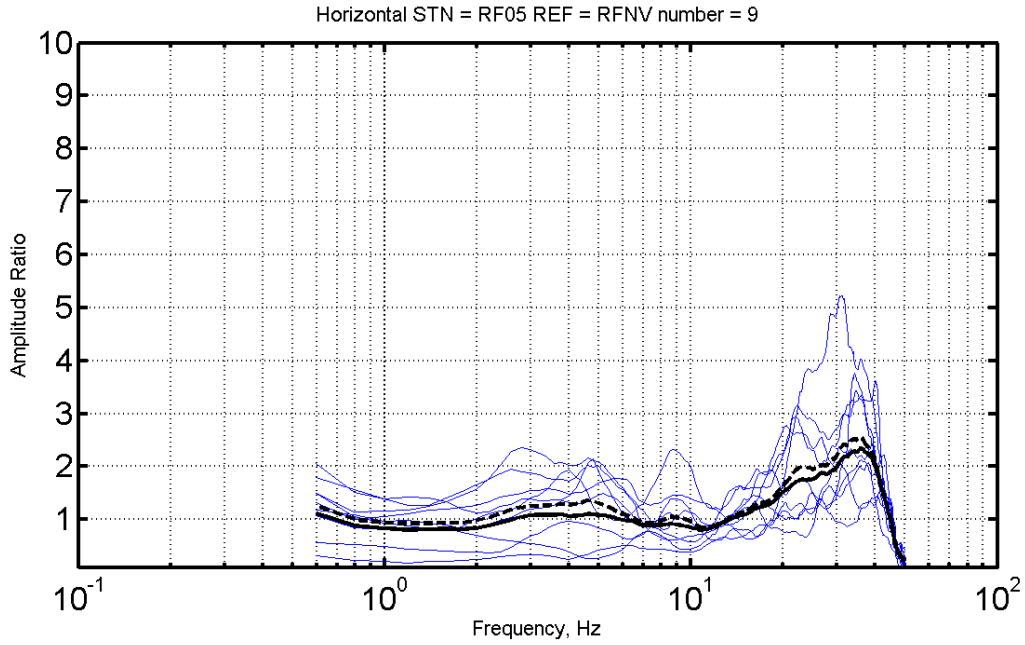

Appendix 3.6: Horizontal spectral ratios with respect to the reference site RFNV for the station SKYF. The top plot shows the amplification level on a log scale while the bottom plots illustrates the amplification level on a linear scale. The number of events used in the analysis is given in the title of each plot.

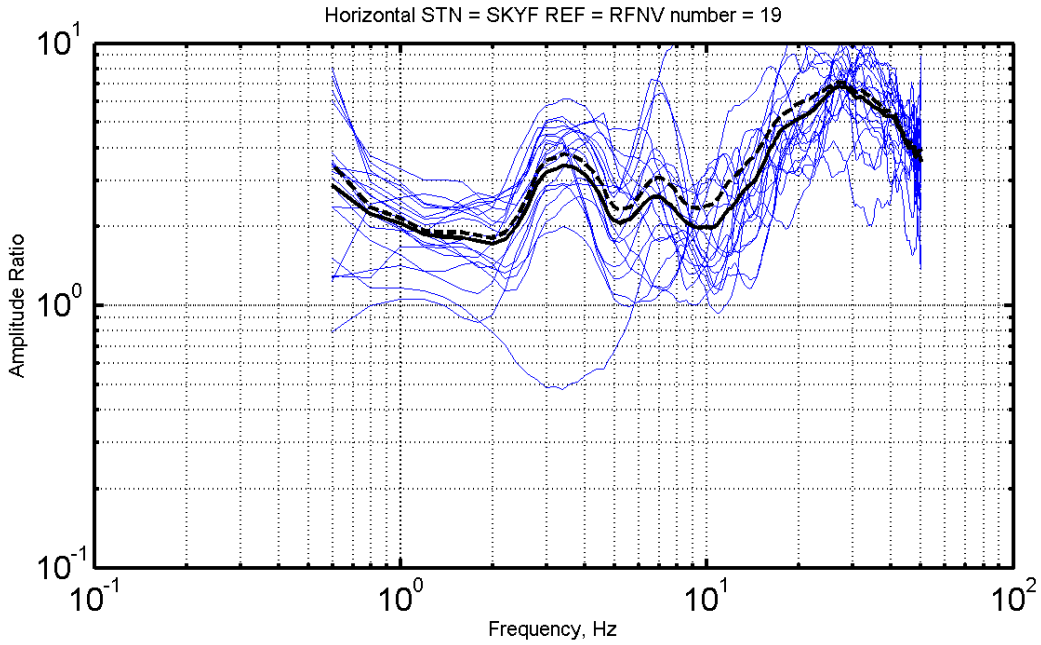

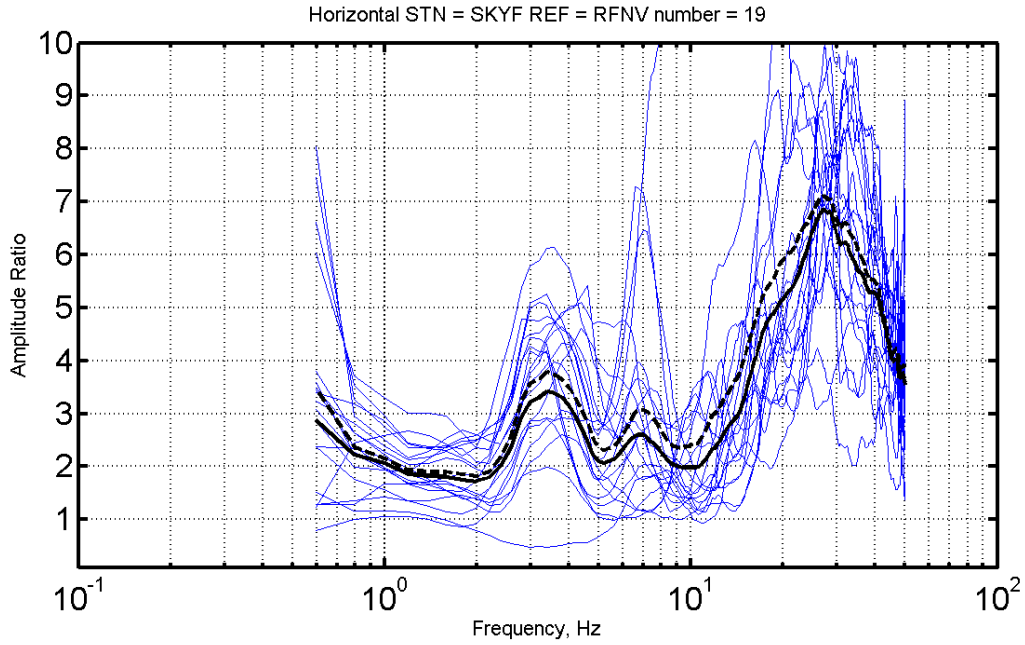

Appendix 3.7: Horizontal spectral ratios with respect to the reference site RFNV for the station SMRN. The top plot shows the amplification level on a log scale while the bottom plots illustrates the amplification level on a linear scale. The number of events used in the analysis is given in the title of each plot.

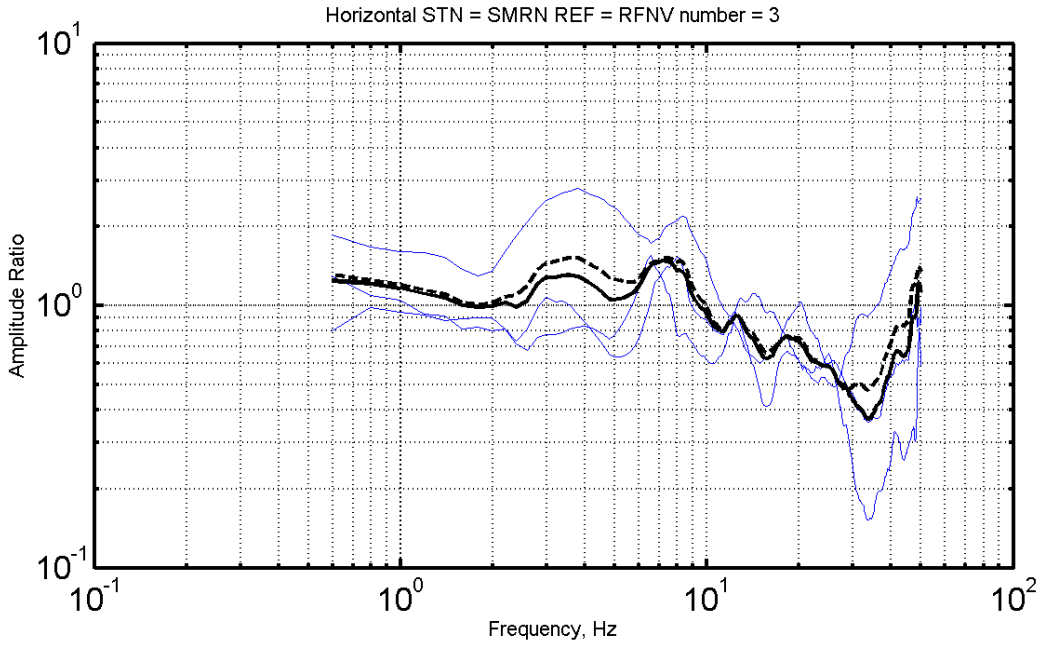

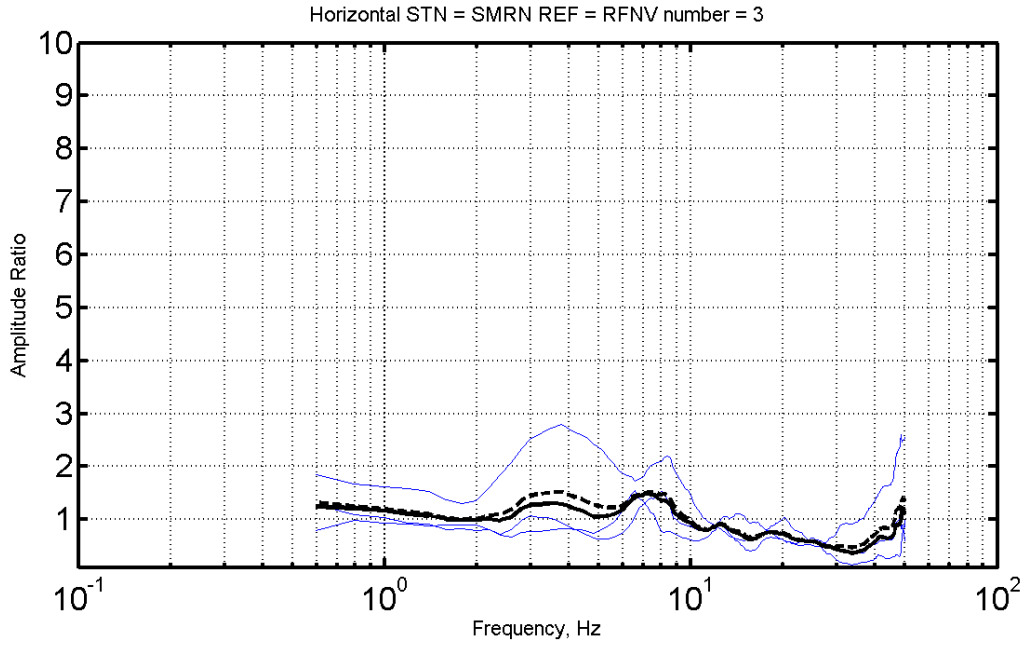

Appendix 3.8: Horizontal spectral ratios with respect to the reference site RFNV for the station SPHI. The top plot shows the amplification level on a log scale while the bottom plots illustrates the amplification level on a linear scale. The number of events used in the analysis is given in the title of each plot.

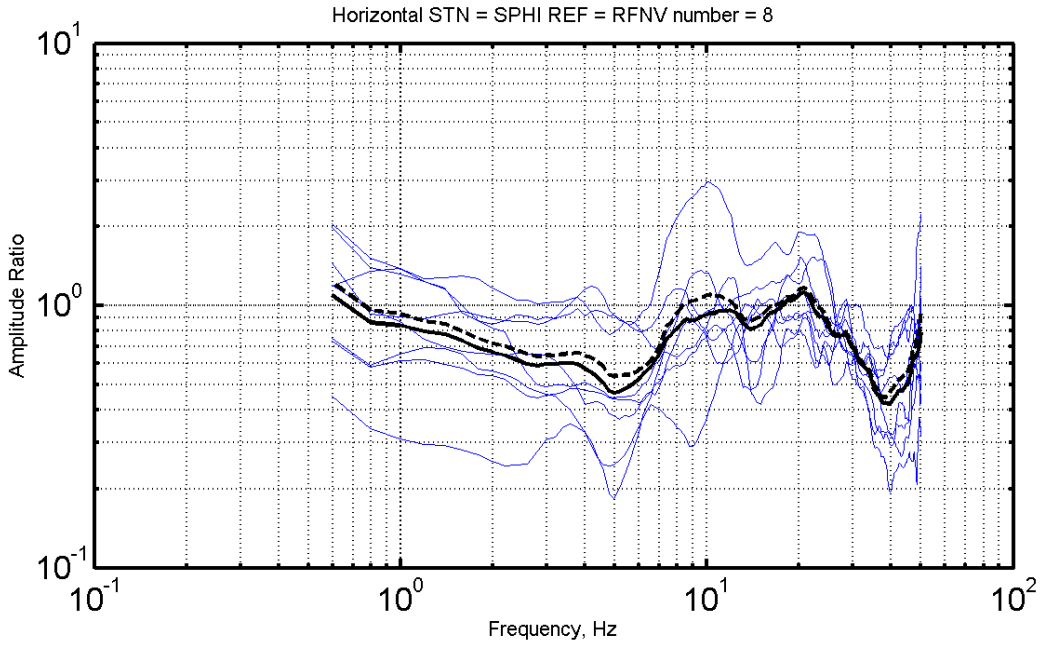

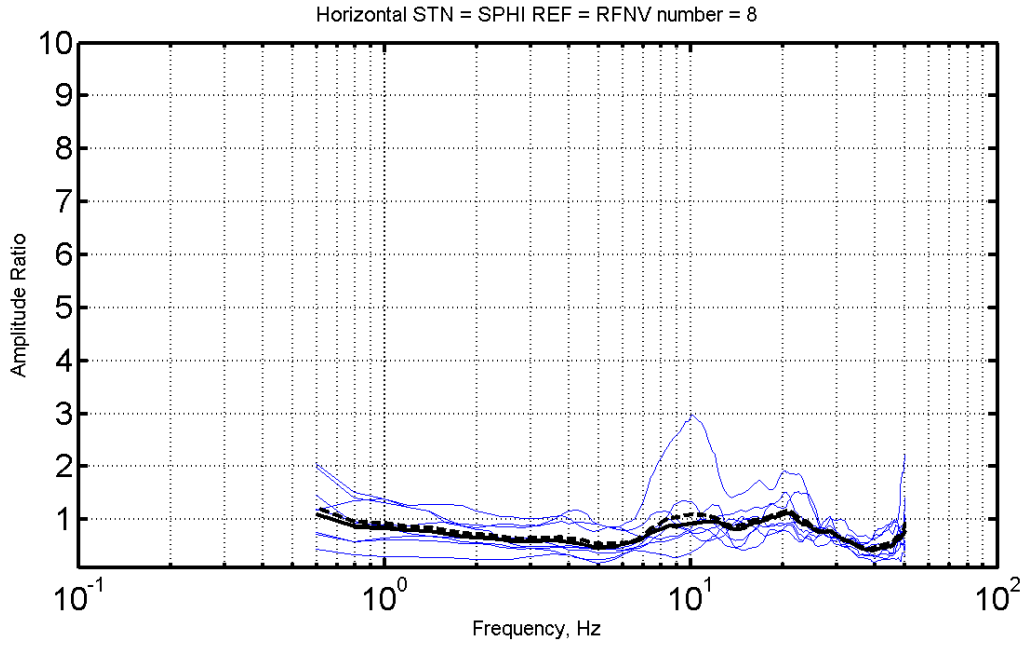

Appendix 3.9: Horizontal spectral ratios with respect to the reference site RFNV for the station SWTP. The top plot shows the amplification level on a log scale while the bottom plots illustrates the amplification level on a linear scale. The number of events used in the analysis is given in the title of each plot.

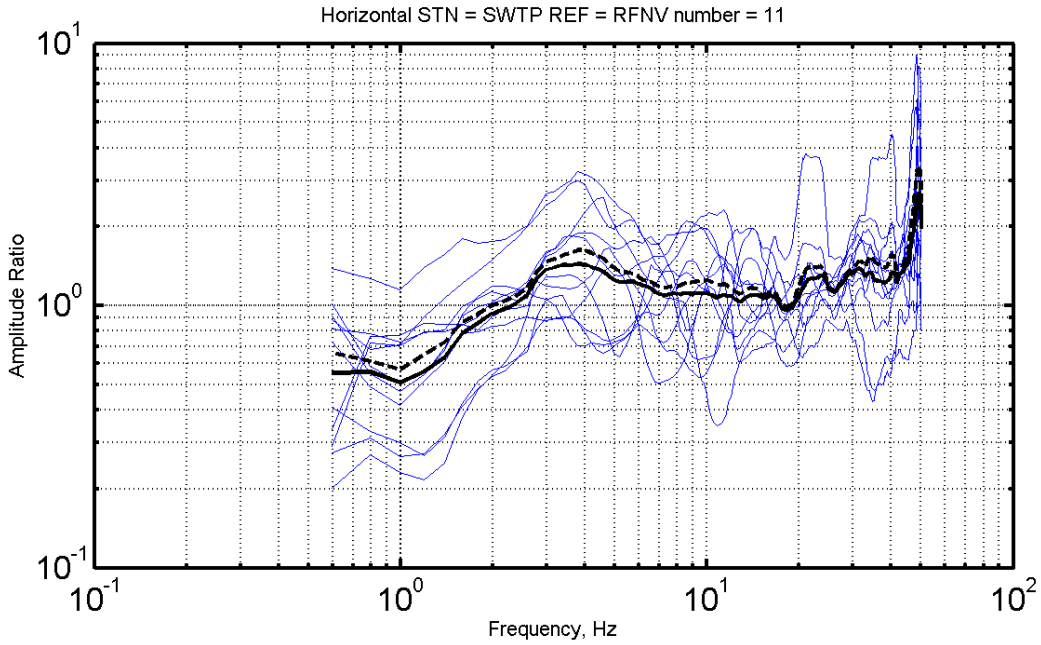

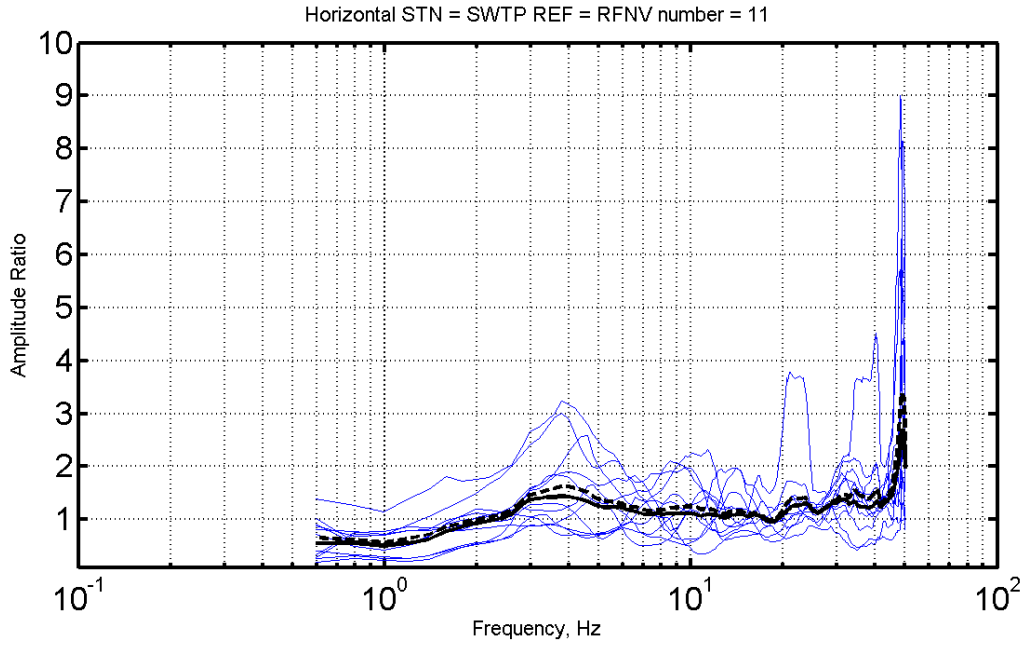

Appendix 3.10: Horizontal spectral ratios with respect to the reference site RFNV for the station UNRN. The top plot shows the amplification level on a log scale while the bottom plots illustrates the amplification level on a linear scale. The number of events used in the analysis is given in the title of each plot.

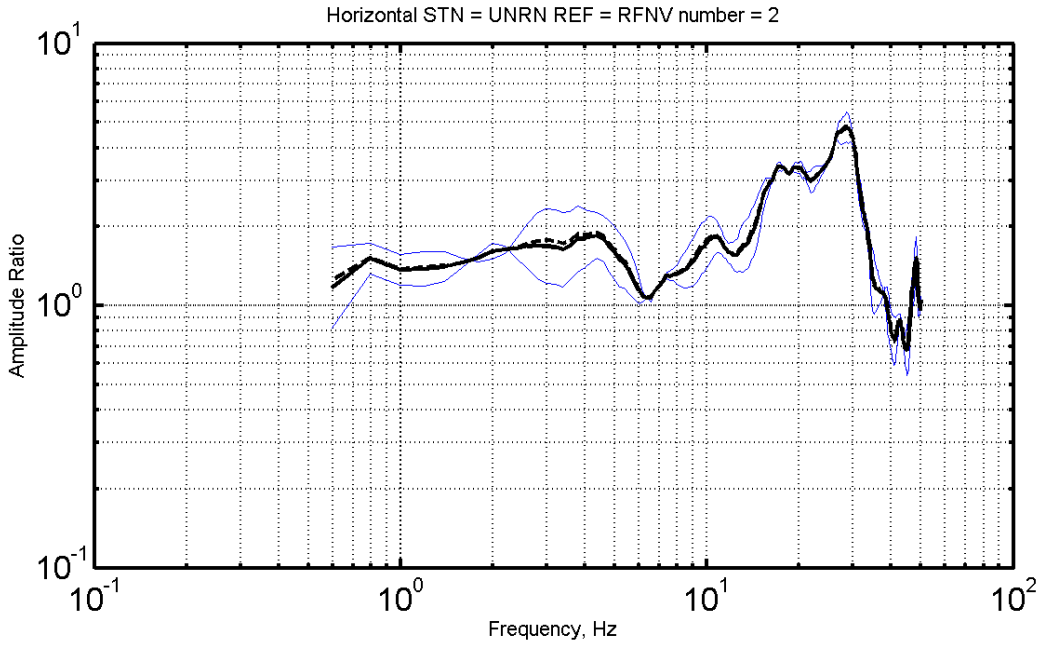

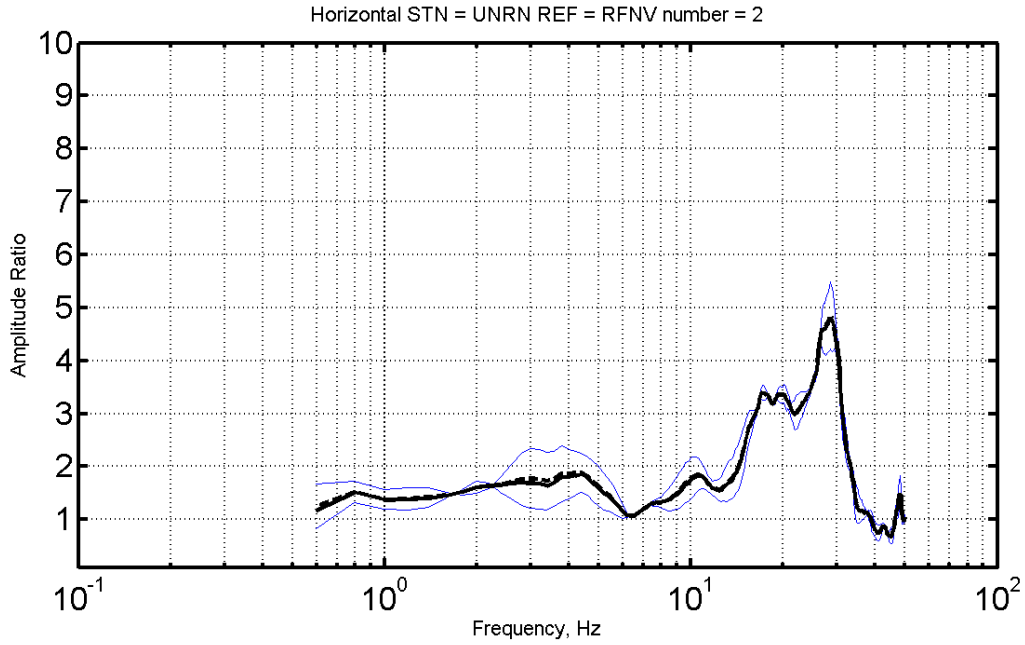

Appendix 3.11: Horizontal spectral ratios with respect to the reference site RFNV for the station UNRX. The top plot shows the amplification level on a log scale while the bottom plots illustrates the amplification level on a linear scale. The number of events used in the analysis is given in the title of each plot.

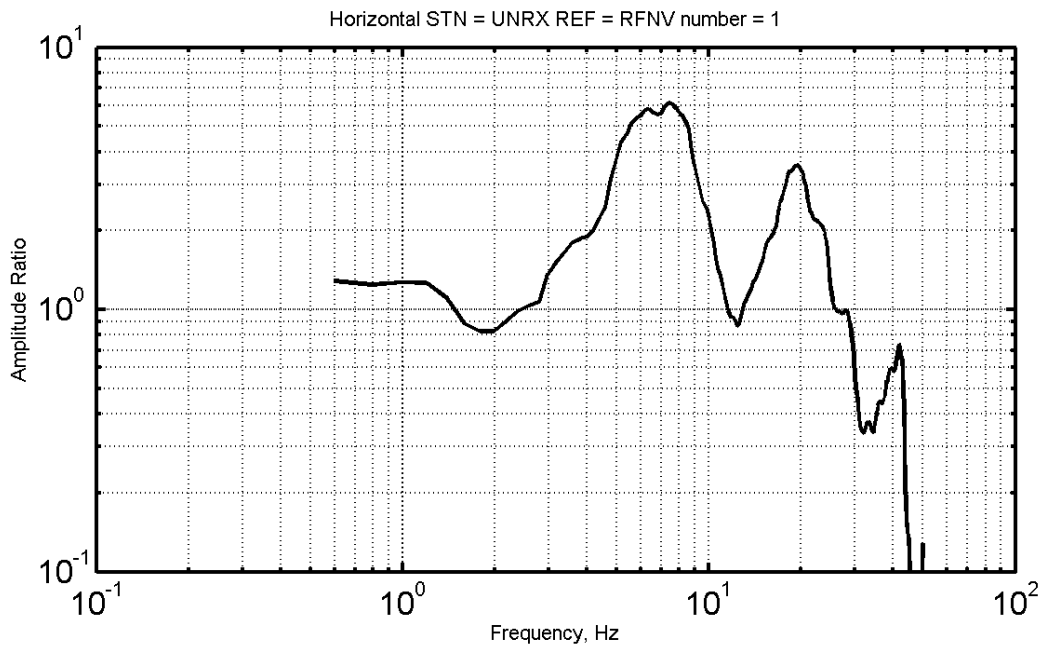

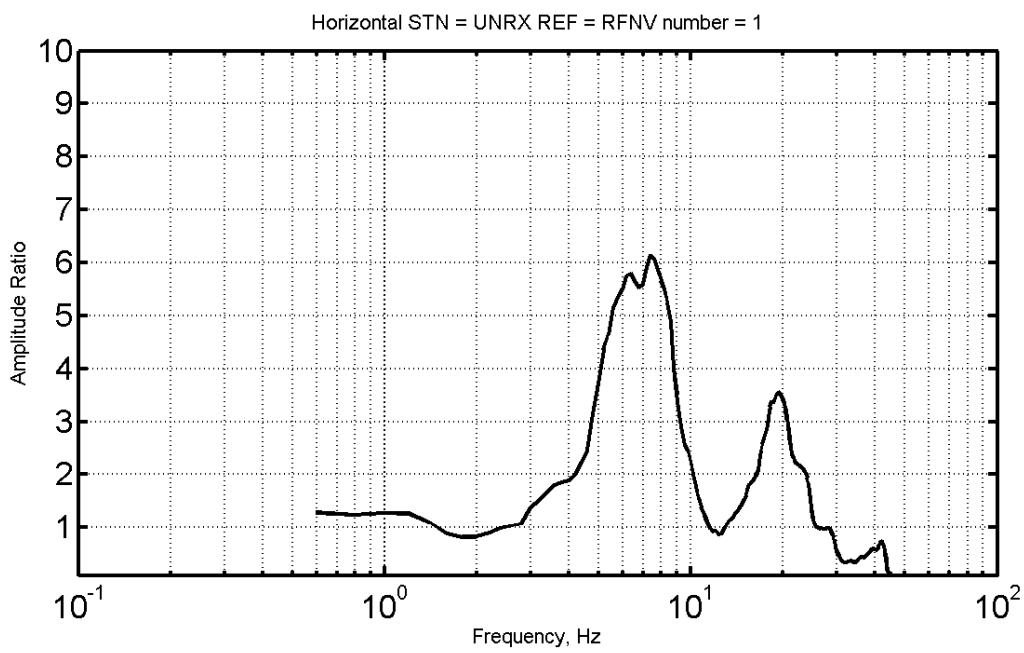

Appendix 3.12: Horizontal spectral ratios with respect to the reference site RFNV for the station WGLF. The top plot shows the amplification level on a log scale while the bottom plots illustrates the amplification level on a linear scale. The number of events used in the analysis is given in the title of each plot.

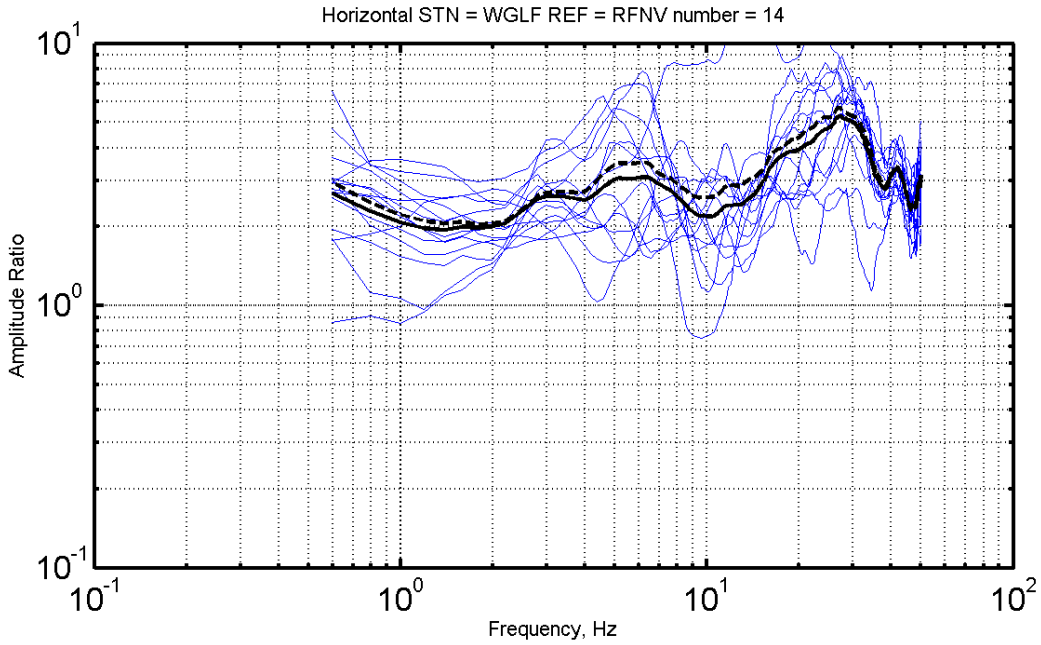

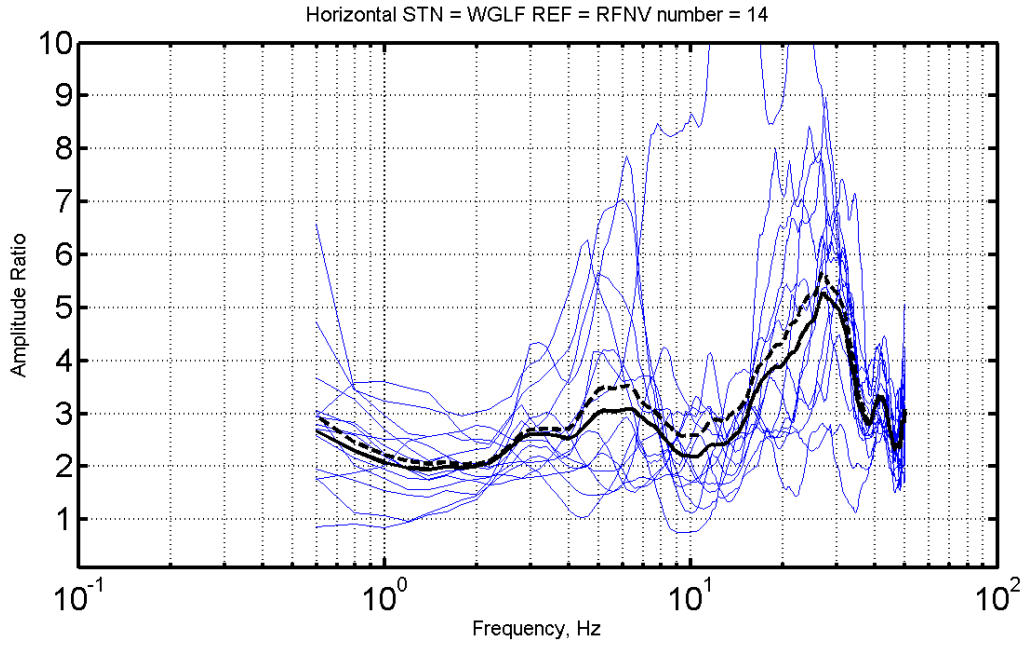

Appendix 4.1: Distance normalized spectral amplification at 0.6 Hz frequency relative to RFNV versus Vs30 for each station-earthquake pair. Data for each station is color coded. Mean amplification values along with 1 standard deviation error bars are also shown. The solid heavy black line shows the least squares fit to the mean amplification values for each station. The correlation is significant at the 73% confidence level (See Table 3).

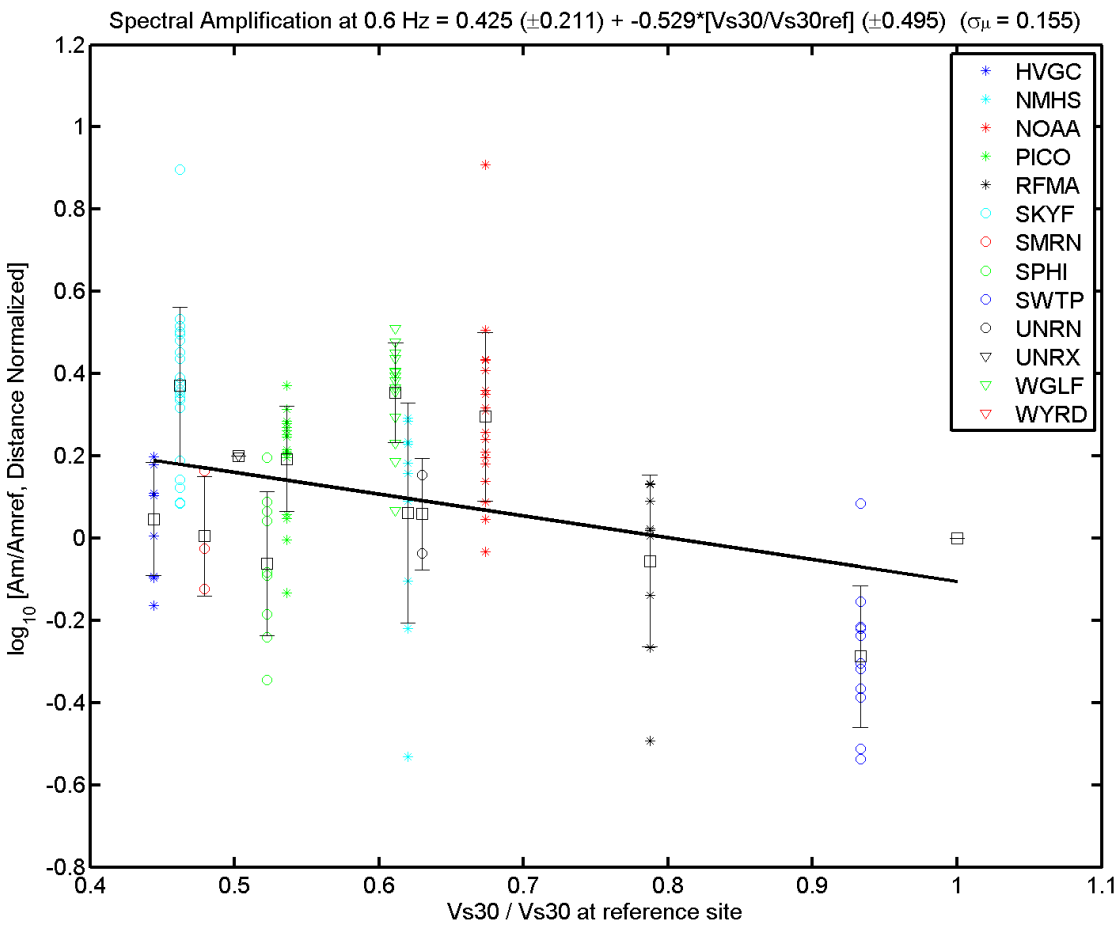

Appendix 4.2: Distance normalized spectral amplification at 1 Hz frequency relative to RFNV versus Vs30 for each station-earthquake pair. Data for each station is color coded. Mean amplification values along with 1 standard deviation error bars are also shown. The solid heavy black line shows the least squares fit to the mean amplification values for each station. The correlation is significant at the 66% confidence level (See Table 3).

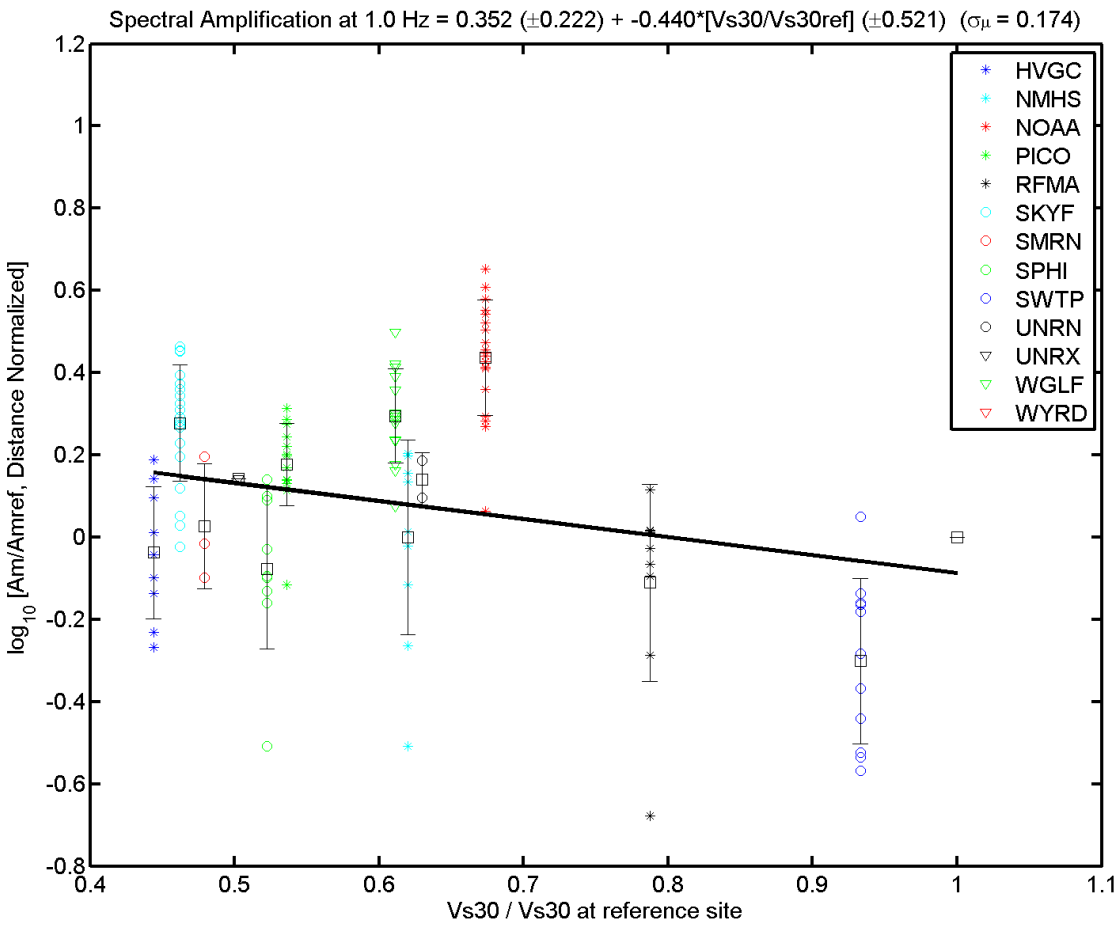

Appendix 4.3: Distance normalized spectral amplification at 2 Hz frequency relative to RFNV versus Vs30 for each station-earthquake pair. Data for each station is color coded. Mean amplification values along with 1 standard deviation error bars are also shown. The solid heavy black line shows the least squares fit to the mean amplification values for each station. The correlation is significant at the 57% confidence level (See Table 3).

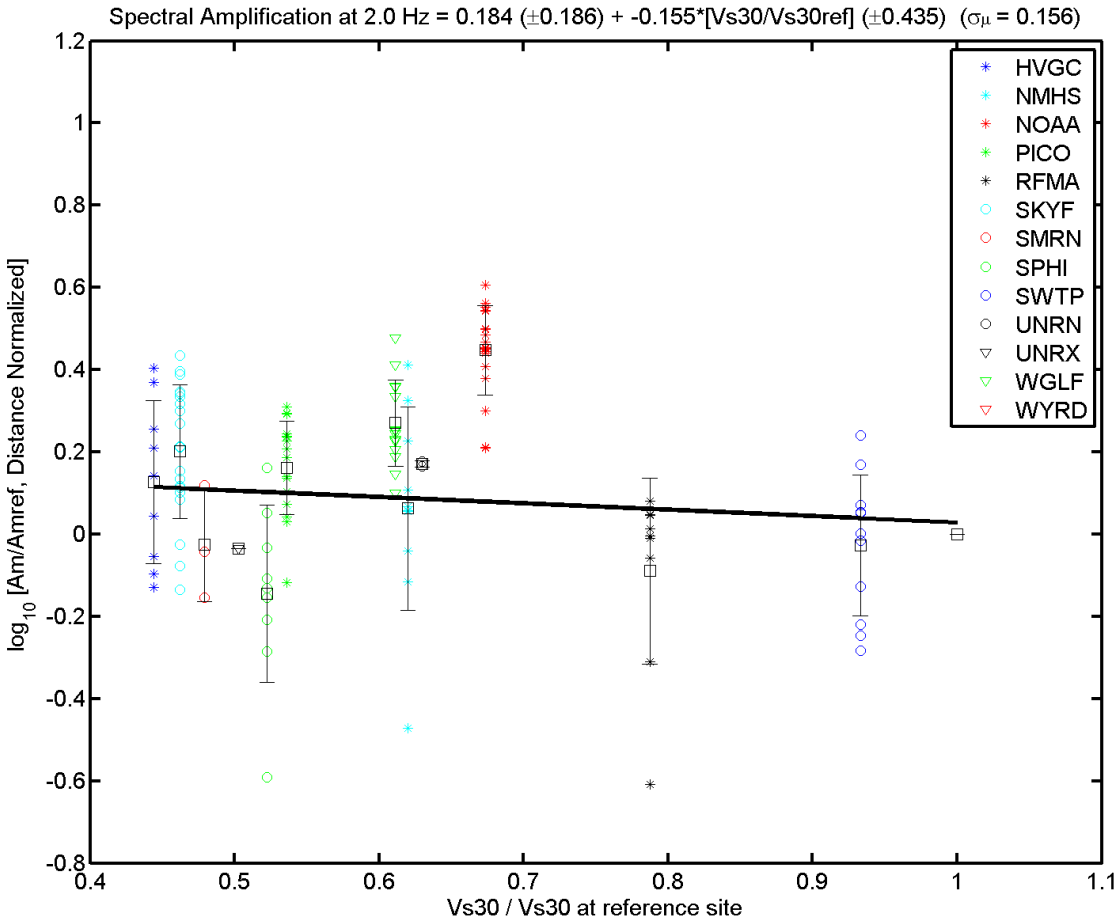

Appendix 4.4: Distance normalized spectral amplification at 3.3 Hz frequency relative to RFNV versus Vs30 for each station-earthquake pair. Data for each station is color coded. Mean amplification values along with 1 standard deviation error bars are also shown. The solid heavy black line shows the least squares fit to the mean amplification values for each station. The correlation is significant at the 59% confidence level (See Table 3).

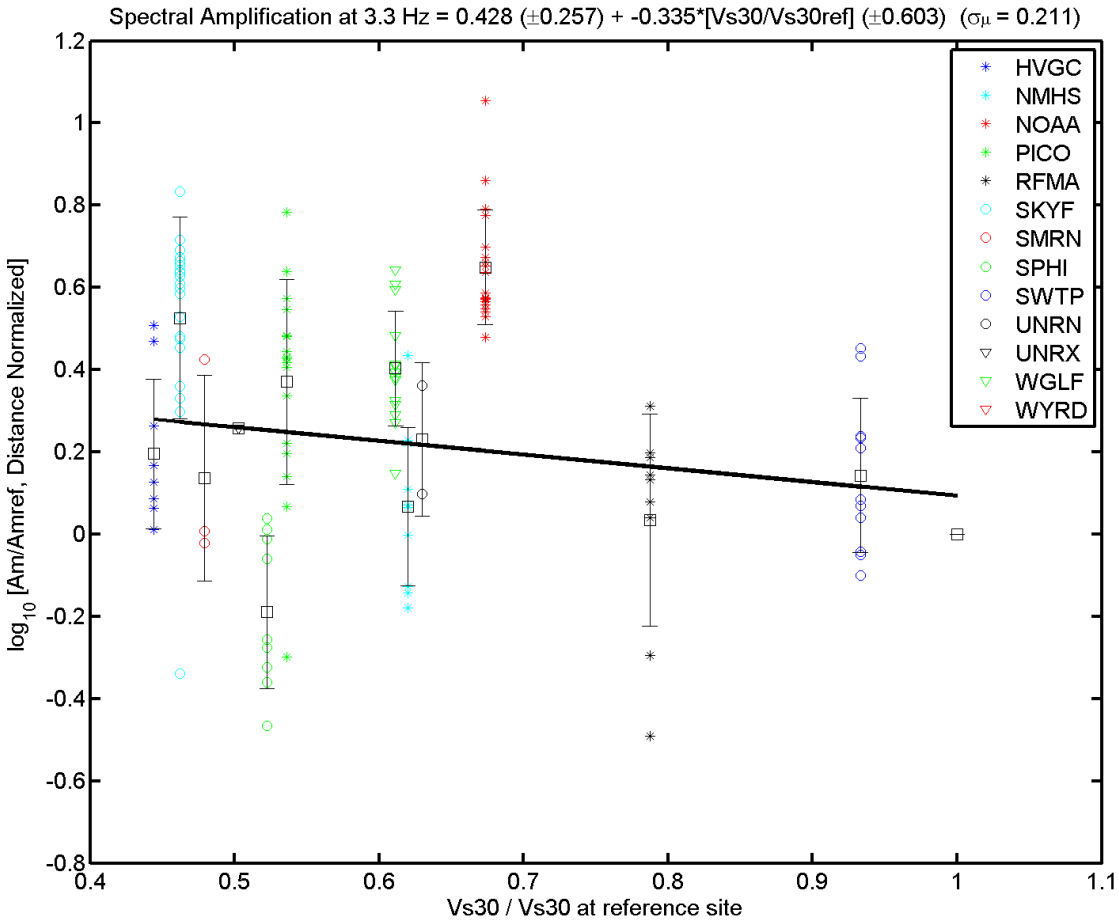

Appendix 4.5: Distance normalized spectral amplification at 5 Hz frequency relative to RFNV versus Vs30 for each station-earthquake pair. Data for each station is color coded. Mean amplification values along with 1 standard deviation error bars are also shown. The solid heavy black line shows the least squares fit to the mean amplification values for each station. The correlation is significant at the 57% confidence level (See Table 3).

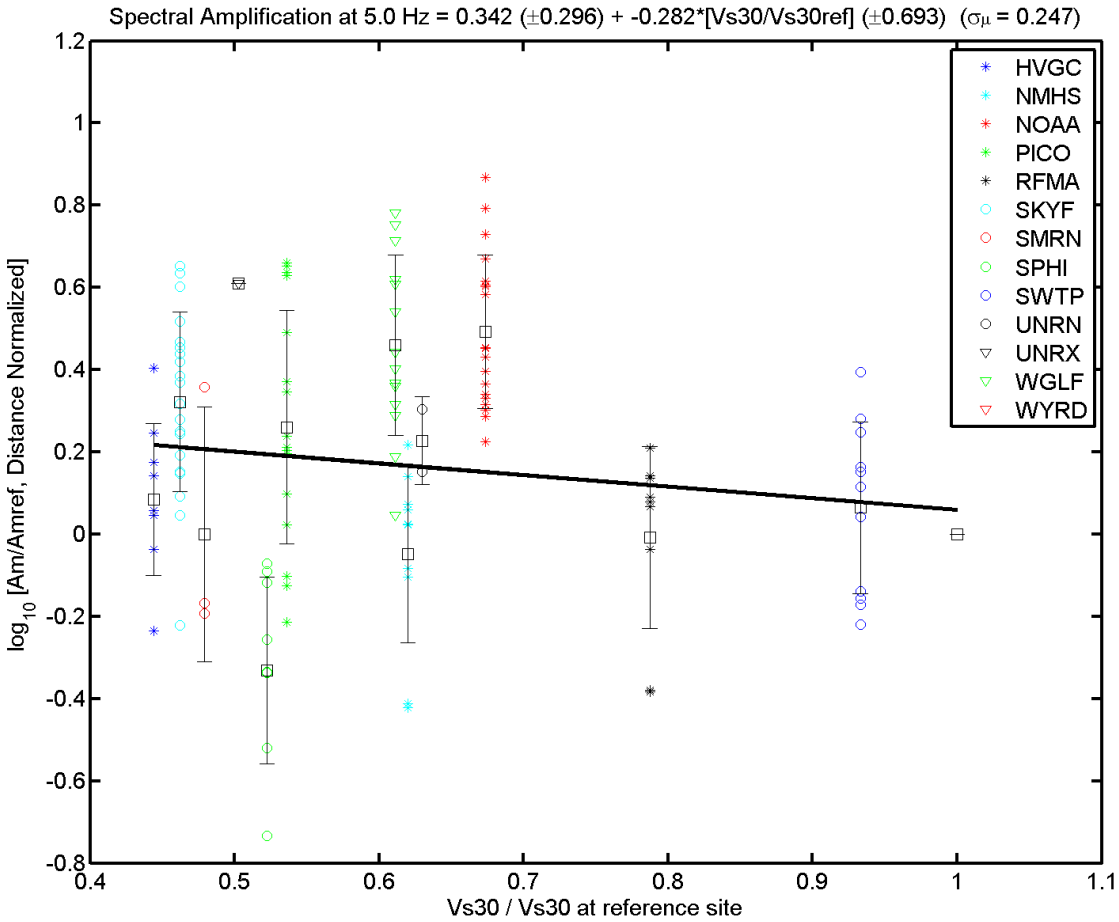

Appendix 4.6: Distance normalized spectral amplification at 8 Hz frequency relative to RFNV versus Vs30 for each station-earthquake pair. Data for each station is color coded. Mean amplification values along with 1 standard deviation error bars are also shown. The solid heavy black line shows the least squares fit to the mean amplification values for each station. The correlation is significant at the 67% confidence level (See Table 3).

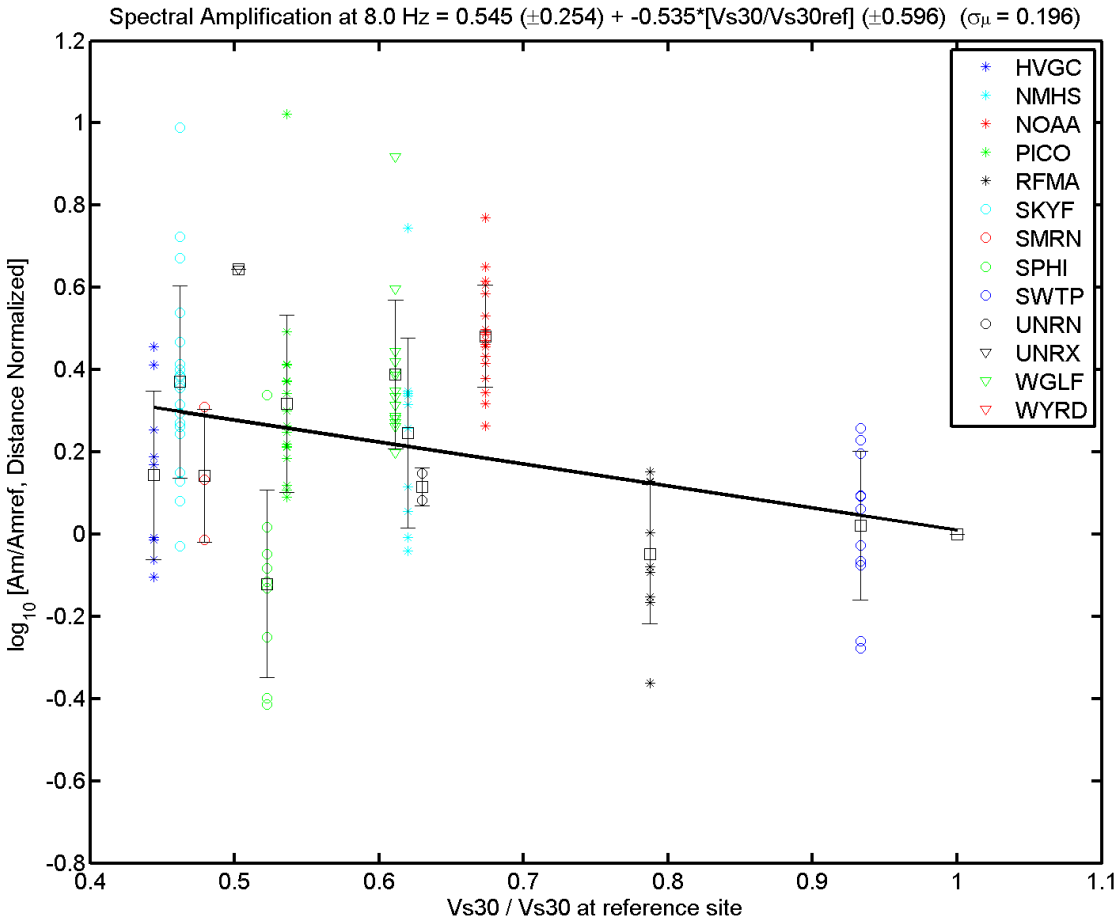

Appendix 4.7: Distance normalized spectral amplification at 10 Hz frequency relative to RFNV versus Vs30 for each station-earthquake pair. Data for each station is color coded. Mean amplification values along with 1 standard deviation error bars are also shown. The solid heavy black line shows the least squares fit to the mean amplification values for each station. The correlation is significant at the 65% confidence level (See Table 3).

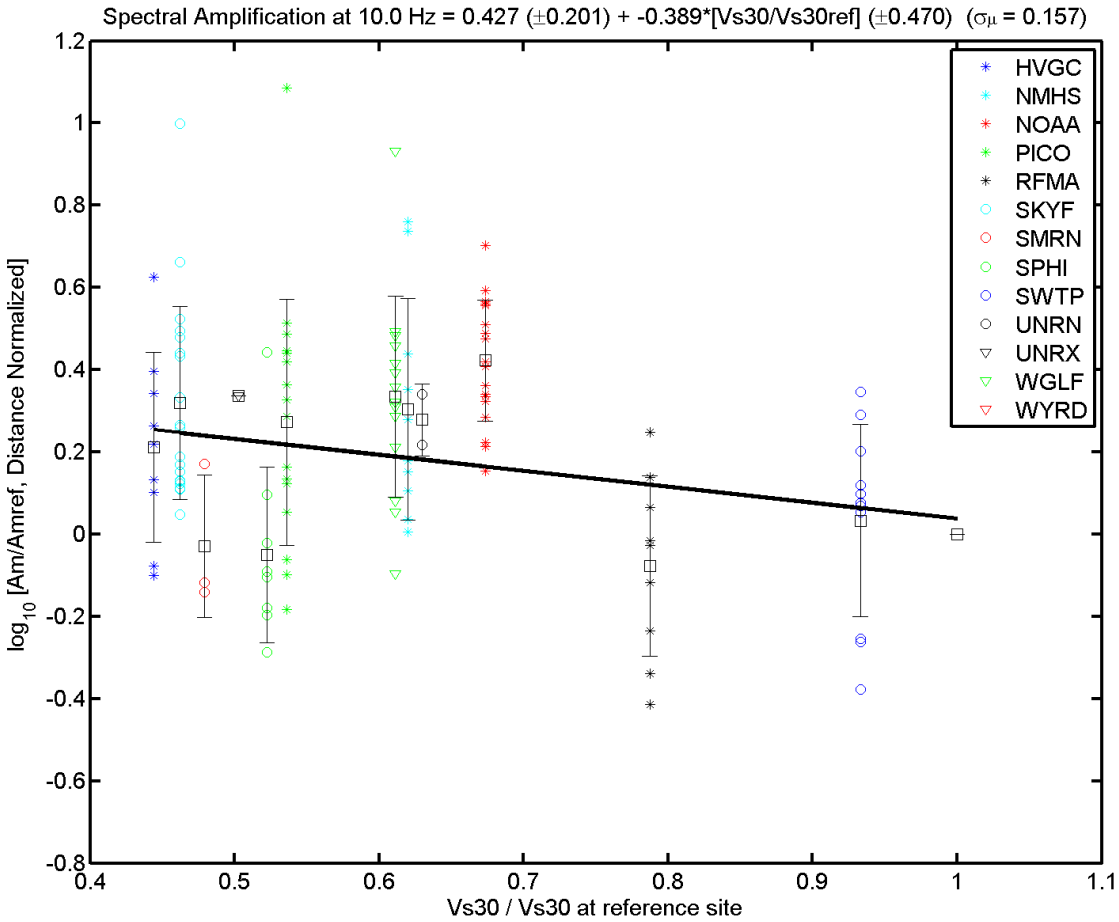

Appendix 5.1: Distance normalized spectral amplification at 0.6 Hz frequency relative to RFNV versus Vs100 for each station-earthquake pair. Data for each station is color coded. Mean amplification values along with 1 standard deviation error bars are also shown. The solid heavy black line shows the least squares fit to the mean amplification values for each station. The correlation is significant at the 77% confidence level (See Table 3).

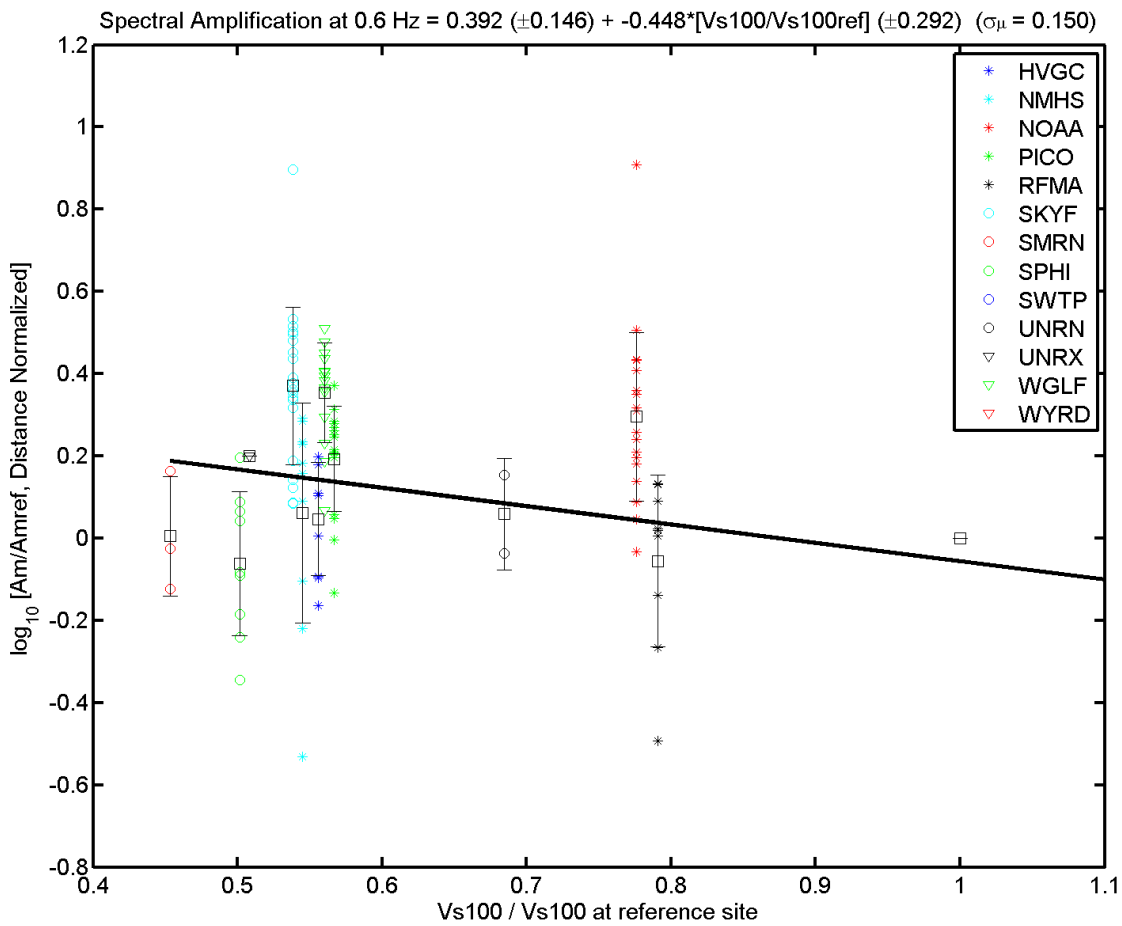

Appendix 5.2: Distance normalized spectral amplification at 1 Hz frequency relative to RFNV versus Vs100 for each station-earthquake pair. Data for each station is color coded. Mean amplification values along with 1 standard deviation error bars are also shown. The solid heavy black line shows the least squares fit to the mean amplification values for each station. The correlation is significant at the 68% confidence level (See Table 3).

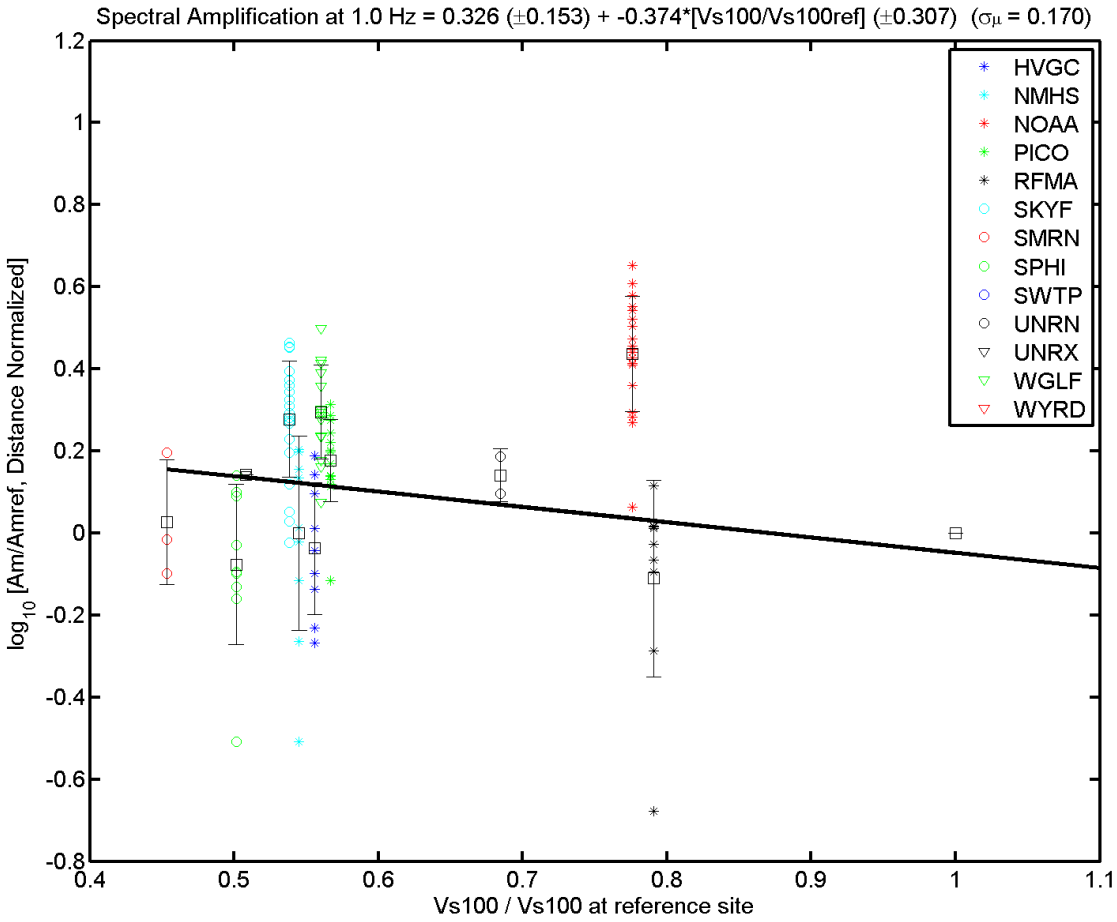

Appendix 5.3: Distance normalized spectral amplification at 2 Hz frequency relative to RFNV versus Vs100 for each station-earthquake pair. Data for each station is color coded. Mean amplification values along with 1 standard deviation error bars are also shown. The solid heavy black line shows the least squares fit to the mean amplification values for each station. The correlation is significant at the 55% confidence level (See Table 3).

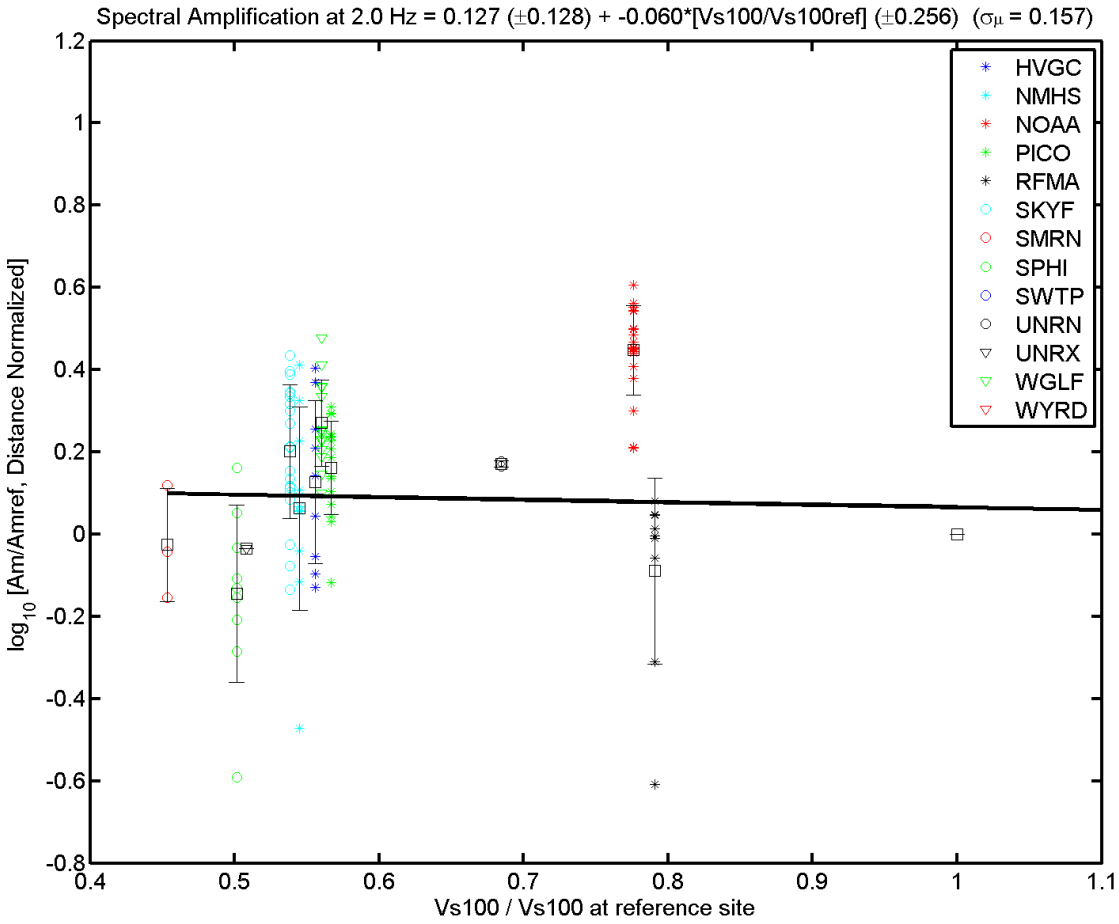

Appendix 5.4: Distance normalized spectral amplification at 3.3 Hz frequency relative to RFNV versus Vs100 for each station-earthquake pair. Data for each station is color coded. Mean amplification values along with 1 standard deviation error bars are also shown. The solid heavy black line shows the least squares fit to the mean amplification values for each station. The correlation is significant at the 56% confidence level (See Table 3).

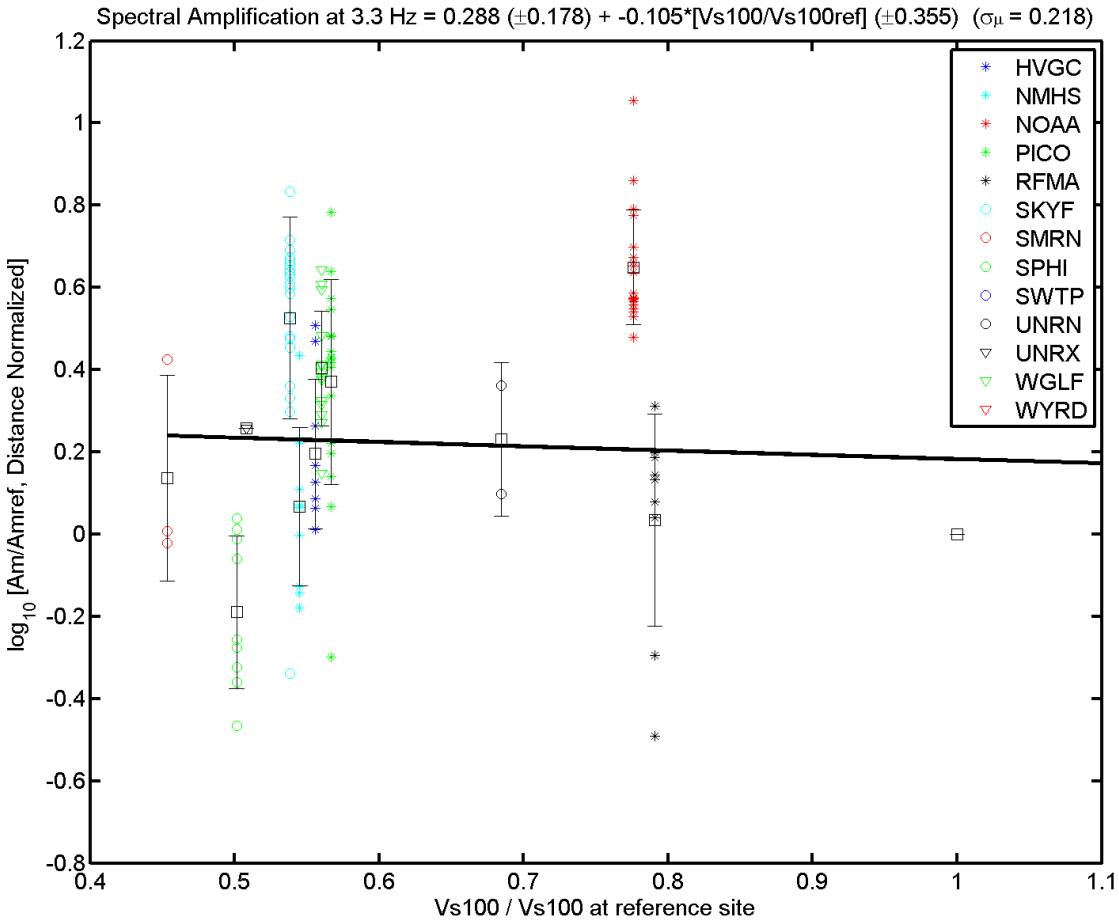

Appendix 5.5: Distance normalized spectral amplification at 5 Hz frequency relative to RFNV versus Vs100 for each station-earthquake pair. Data for each station is color coded. Mean amplification values along with 1 standard deviation error bars are also shown. The solid heavy black line shows the least squares fit to the mean amplification values for each station. The correlation is significant at the 56% confidence level (See Table 3).

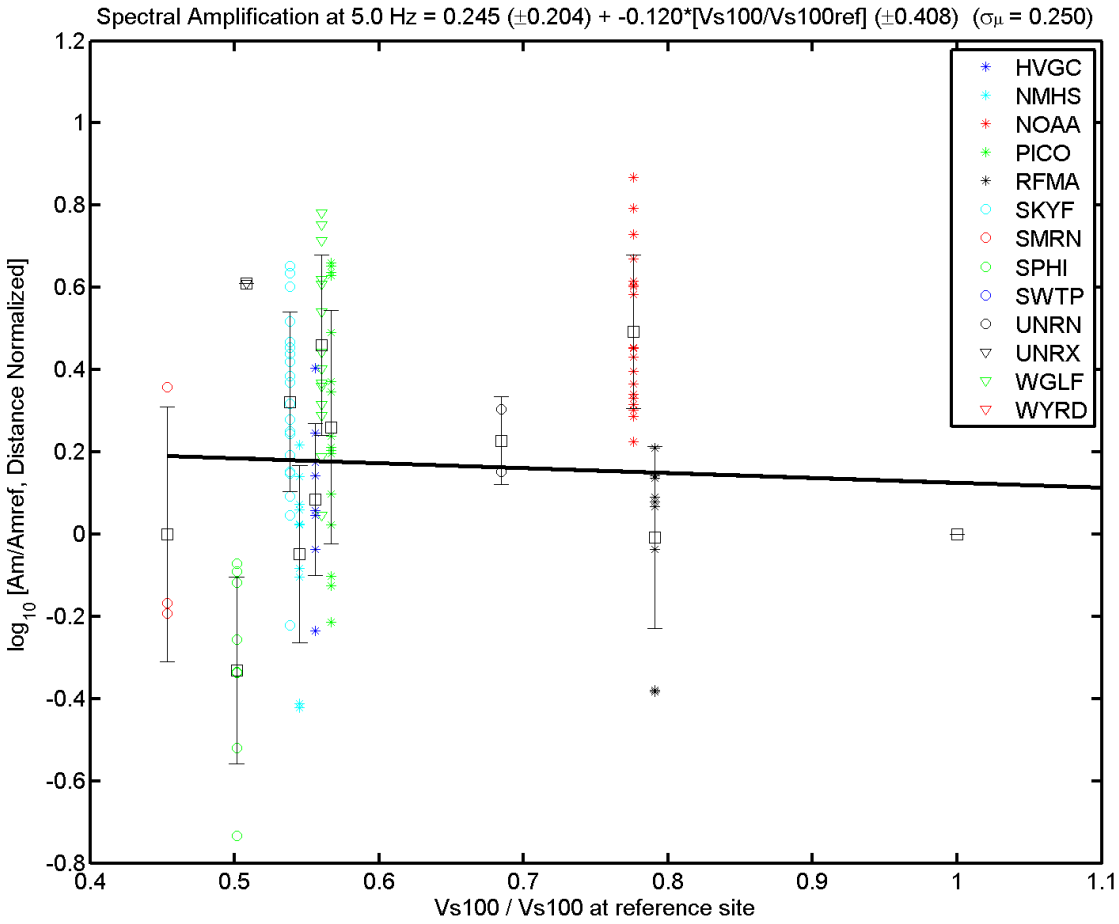

Appendix 5.6: Distance normalized spectral amplification at 8 Hz frequency relative to RFNV versus Vs100 for each station-earthquake pair. Data for each station is color coded. Mean amplification values along with 1 standard deviation error bars are also shown. The solid heavy black line shows the least squares fit to the mean amplification values for each station. The correlation is significant at the 64% confidence level (See Table 3).

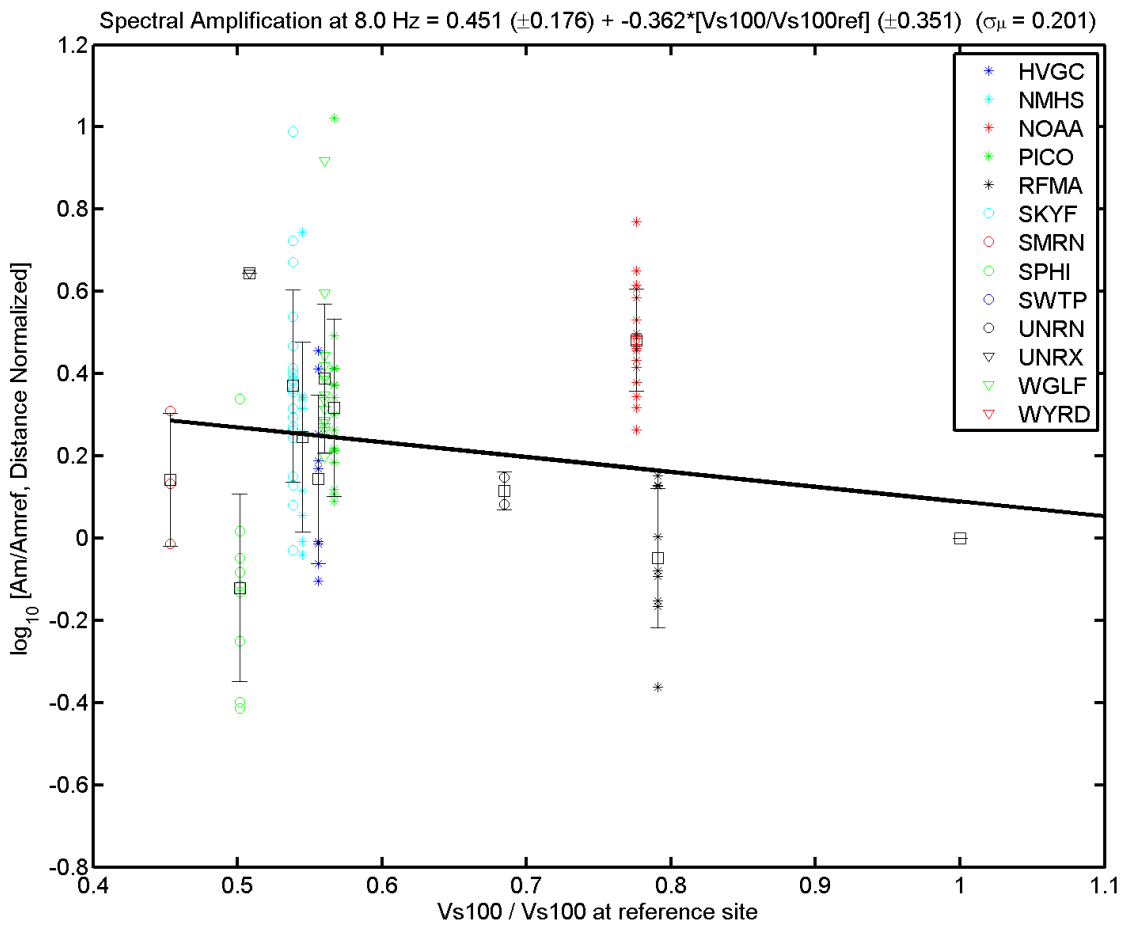
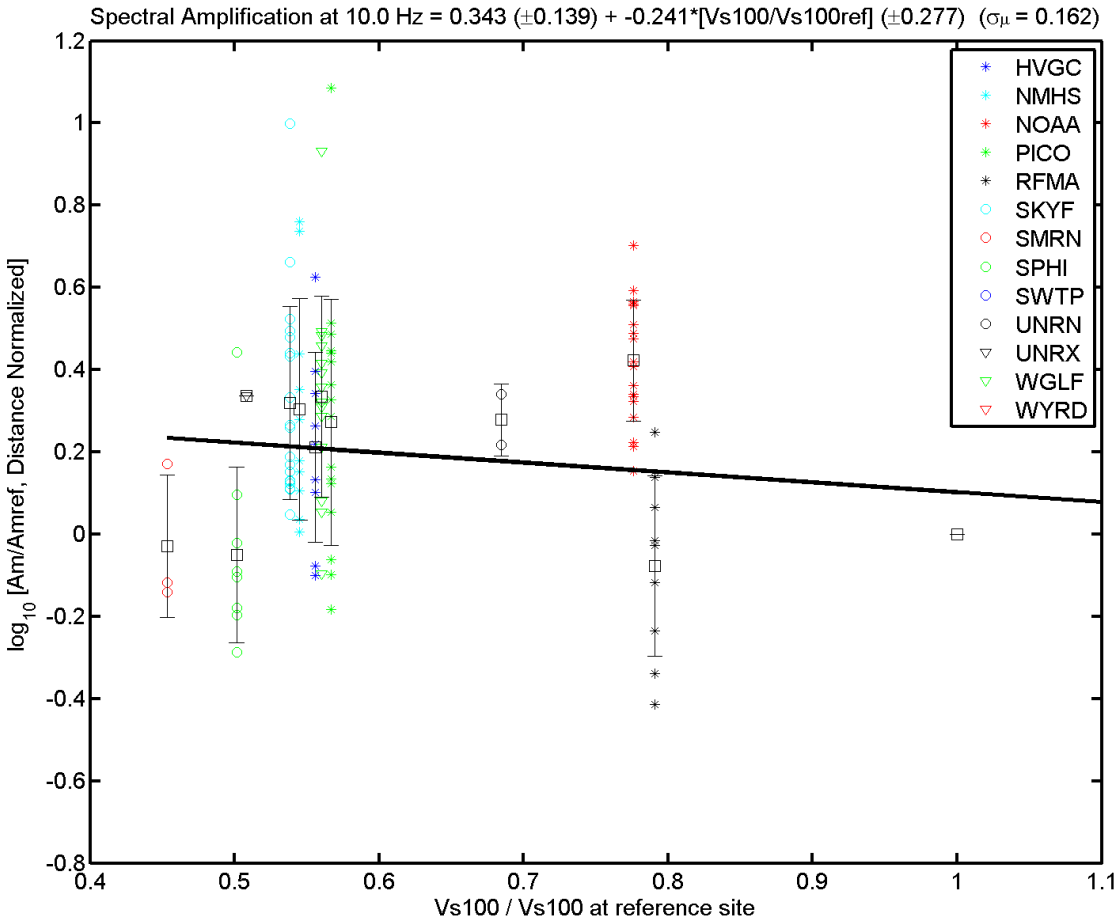
Appendix 5.7: Distance normalized spectral amplification at 10 Hz frequency relative to RFNV versus Vs100 for each station-earthquake pair. Data for each station is color coded. Mean amplification values along with 1 standard deviation error bars are also shown. The solid heavy black line shows the least squares fit to the mean amplification values for each station. The correlation is significant at the 62% confidence level (See Table 3).